

**INTERPRETATION OF AEROMAGNETIC AND LANDSAT-
ETM+ DATA OVER PART OF THE YOUNGER GRANITE
COMPLEX, NIGERIA: IMPLICATION FOR GEOTHERMAL
EXPLORATION**

BY

NWOKOCHA, KINGSLEY CHIEMELA (B. TECH., FUTO)

REG. NO: 20124764278

**A THESIS SUBMITTED TO THE POSTGRADUATE SCHOOL
FEDERAL UNIVERSITY OF TECHNOLOGY, OWERRI**

**IN PARTIAL FULFILLMENT OF THE REQUIREMENTS FOR
THE AWARD OF THE DEGREE OF MASTER OF SCIENCE
(MSC) IN GEOPHYSICS**

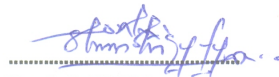
DECEMBER, 2016



Interpretation of aeromagnetic and landsat-etm+ data over part of the younger granite complex, Nigeria: Implication for geothermal exploration. By Nwokocho, K .C. is licensed under a [Creative Commons Attribution-NonCommercial-NoDerivatives 4.0 International License](https://creativecommons.org/licenses/by-nc-nd/4.0/).

CERTIFICATION

This is to certify that this work "Interpretation of Aeromagnetic and Landsat-ETM+ data over part of the Younger Granite Complex, Nigeria: implication for geothermal exploration" was carried out by NWOKOCHA, KINGSLEY CHIEMELA (20124764278) in partial fulfilment for the award of the degree of M.Sc. in Geophysics in the department of Geology of the Federal University of Technology Owerri.



Dr. A. I. OPARA
(Principal Supervisor)

22/12/2016

Date



Dr. C. N. OKEREKE
(Co-supervisor)

23-12-2016

Date



Dr. O. C. OKEKE
(Head of Department)

10/01/2017

Date



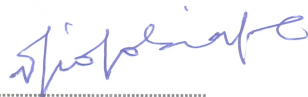
Prof. B. C. ANUSIONWU
(Dean of School of Physical Sciences)

19/1/2017

Date

Prof. (Mrs.) NNEENA N. OTI
(Dean, School of Postgraduate)

Date



Prof. VICTOR OBIANWU
(External Supervisor)

Date

DEDICATION

I dedicate this research work to God Almighty for His divine guidance and financial provision all through this study.

ACKNOWLEDGEMENTS

A special thank you goes to my magnificent supervisor, Dr. Opara, Alex I., whose persistence, meticulousness, assistance and constructive criticism contributed greatly to the success of this project. I also express my sincere gratitude to my co-supervisor, Dr. Okereke, C. N., who gave me special assistance and contributions to the success of this project.

I remain grateful to the Nigerian Geologic Survey who provided me with aeromagnetic and Landsat data. Also, in writing this report, i am indebted to many authors for ideas and materials.

I salute my parents Mr and Mrs Nwokocha, E. C. whose words of encouragement plus financial, and spiritual counsels provided the bedrock towards completing this research work. I will not forget my very special friends and course mates Chris, Collins, Kingsley, Ikechukwu and Muze, just to mention a few who in one way or the other influenced me for good. I remain grateful and thankful to all.

TABLE OF CONTENTS

Title page	i
Dedication	ii
Certification	iii
Acknowledgements	iv
Abstract	v
Table of Contents	vi
List of Tables	x
List of Figures	xi
 CHAPTER ONE: INTRODUCTION	
1.1 Background Information	1
1.2 Statement of Problem	3
1.3 Aim and Objectives of Study	4
1.4 Justification of Study	4
1.5 Scope of Study	5
1.6 Description of the Study Area	5
1.6.1 Drainage	6
1.6.2 Climate	6
1.6.3 Soil and Vegetation	6
1.6.4 The Geology of the Study Area	8

CHAPTER TWO: LITERATURE REVIEW

2.1	Review of Previous Studies	11
2.2	Theoretical Framework	14
2.2.1	Introduction to the Magnetic Method	14
2.2.2	Theory of Aeromagnetic Survey	16
2.2.2.1	Applications of Aeromagnetic Data	17
2.2.2.2	The Nature Of Magnetic Anomalies	19
2.2.3	Aeromagnetic Data Processing	19
2.2.3.1	Filtering of Aeromagnetic Map	20
2.2.3.2	Reduction to the Pole (RTP)	20
2.2.3.3	Regional- Residual Separation	21
2.2.3.3.1	Polynomial Fitting	22
2.2.3.4	Upward continuation of the potential Field	22
2.2.4	Depth Estimation	24
2.2.5	Aeromagnetic Data Interpretation	25
2.2.5.1	Qualitative Interpretation	25
2.2.5.2	Quantitative Interpretation	27
2.2.6	Theory of Remote Sensing	27
2.2.6.1	Principles of Electromagnetic Radiation	28

2.2.6.2	Characteristics of Remotely Sensed Data	30
2.2.6.3	Remote Sensing Instrumentation	31
2.2.7	Application of Landsat Satellite	33
2.2.8	Remote Sensing Data Analysis and Interpretation	34
2.2.8.1	Photographic/Image Interpretation and Photogrammetry	34
2.2.8.2	Digital Image Pre-processing	36
2.2.8.3	Image Enhancement and Feature Extraction	37
2.2.8.4	Image Classification	38
CHAPTER THREE: METHODOLOGY		
3.1	Aeromagnetic Data Source	40
3.2	Remote Sensing Data Source	40
3.2.1	Aeromagnetic Data Analysis	40
3.2.1.1	Regional-Residual Separation	41
3.2.1.2	Reduction to Pole	42
3.2.1.3	Continuation Filtering	42
3.2.1.4	Magnetic Depth Estimation	43
3.2.1.4.1	Spectral Analysis	43
3.2.1.4.2	3D Euler Deconvolution	47
3.2.1.5	Curie Point Depth Estimation	51
3.2.2	Remote Sensing Data Analysis and Interpretation	53
CHAPTER FOUR: RESULTS AND DISCUSSION		
4.1	Aeromagnetic Method	55

4.1.1	Total Magnetic Intensity (TMI) Map	55
4.1.2	Digital Filtering	60
4.1.3	Regional-Residual Separation	61
4.1.4	Upward Continuation Filter	68
4.1.5	Spectral Depth Estimation	71
4.1.6	Curie point Depth Estimation	73
4.1.7	3D Euler Deconvolution Depth Estimation	75
4.2	Remote Sensing	79
4.2.1	Digital Elevation Model	79
4.2.2	Colour Composites	80
4.2.3	Normalized Difference Vegetation Index (NDVI)	83
4.2.4	Lineament Analysis	86
4.2.5	Image Classification Analysis	90
4.2.6.	Generation of New Geologic Map	90
CHAPTER FIVE: CONCLUSION AND RECOMMENDATION		
5.1	Conclusion	92
5.2	Recommendation	93
5.3	Contribution to Knowledge	94
REFERENCES		95

LIST OF TABLES

1.0	Typical Magnetic Susceptibilities of Earth Materials. (Dobrin and Savit, 1988)	18
3.1	Structural Indices for Simple Magnetic Models Used For Depth estimations by 3D Euler Deconvolution (Reids, 1990; Thompson, 1982)	49
4.1	Basement depth estimates of the study area calculated from spectral analysis	70
4.2	Geothermal estimates of the study area calculated from spectral analysis	73
4.3	Appearance of features in the generated colour composite maps	82

LIST OF FIGURES

1.1	Topographic Map of the Study Area	7
1.2	Drainage Map of the Study Area	7
1.3	Geology map of Nigeria showing the younger granite ring complexes	9
1.4	Geology map of the study area.	9
2.1	The electromagnetic spectrum showing the spectral bands	29
2.2	Flow Diagrams for Supervised and unsupervised Image Classification	39
4.1	Aeromagnetic Field over the Study Area as a Colour Shaded contoured Map	52
4.2	Shaded Relief Map of Total Field	53
4.3	Shaded relief map of the aeromagnetic data of the study area.	53
4.4	Colour Image Map (Pixel Map) of the Aeromagnetic Data	55
4.5	Colour shaded total field map of the study area showing some of the regional faults area	55
4.6	3-D Map of the Total Magnetic Field of the Aeromagnetic Data	56
4.7	3-D Surface map of total magnetic field of the aeromagnetic data	56
4.8	Wireframe map of the total magnetic field of the aeromagnetic data	57
4.9	Low pass filter map of the aeromagnetic data of the study area.	59
4.10	High pass filter map of the aeromagnetic data of the study area	59
4.11	Band pass filter map of the aeromagnetic data of the study area	60
4.12	Non linear filter map of the aeromagnetic data of the study area	60
4.13	First Degree Residual Field over the Study Area as a	

	Colour Shaded Contour Map	62
4.14	Second Degree Residual Field over the Study Area as a Colour Shaded Contour Map	62
4.15	Third Degree Residual Field over the Study Area as a Colour Shaded Contour Map	63
4.16	Fourth Degree Residual Field over the Study Area as a Colour Shaded Contour Map	63
4.17	First to fourth Degree Regional Field over the Study Area as a contour Map	64
4.18	Upward Continued Aeromagnetic Field over the Study Area as a Colour Shaded contoured Map (H=1000m).	66
4.19	Upward Continued Aeromagnetic Field over the Study Area as a Colour Shaded contoured Map (H=2000m).	66
4.20	Upward Continued Aeromagnetic Field over the Study Area as a Colour Shaded contoured Map (H=3000m).	67
4.21	Upward Continued Aeromagnetic Field over the Study Area as a Colour Shaded contoured Map (H=4000m).	67
4.22	The cross section of processed Spectral blocks for Jos	69
4.23	The cross section of processed Spectral blocks for Kafanchan.	69
4.24	The cross section of processed Spectral blocks for Fadan	69
4.25	The cross section of processed Spectral blocks for Richa	69
4.26	3D Standard Euler deconvolution contour map of the study area showing cluster solutions for structural Index=0.0	76

4.27	3D Standard Euler deconvolution contour map of the study area showing cluster solutions for structural Index=1.0	76
4.28	3D Standard Euler deconvolution contour map of the study area showing cluster solutions for structural Index=2.0.	77
4.29	3D Standard Euler deconvolution contour map of the study area showing cluster solutions for structural Index=3.0.	77
4.30	Digital Elevation Model (DEM) Map	80
4.31	Contour Map of the study area	80
4.32	Colour Composite Map RGB 432	81
4.33	Colour Composite Map RGB 731	81
4.34	Colour Composite Map RGB 752	83
4.35	Normalized Difference Vegetation Index (NDVI) Map	83
4.36	Interpreted Lineament of the Study Area	86
4.37	Lineament Density Map	86
4.38	Lineament Rose Diagram	88
4.39	Unsupervised Classification Image	90
4.40	Comparison of the Old and New Maps.	90

ABSTRACT

Structural interpretation of Younger Granite complex of northern Nigeria using aeromagnetic and Landsat imagery was carried out to determine the depth to the magnetic basement, delineate the basement morphology and relief, delineate the structural features associated with the basin and to infer the influence of such structures on mineralization in the study area. Also, this study is aimed at determining the geothermal potentials of the area. The application of directional edge enhancement techniques to band 5 of the Landsat-TM data using convolution models in ILWIS 3.2 academic software were to further enhance these linear features. Results of the structural analyses revealed several lineaments at the northwestern, central and southwestern parts of the study area. Trend analysis of the lineaments revealed structural trends in the NW-SE, NE-SW, N-S and E-W directions with the NW-SE and NE-SW been the dominant trends in the area. These trends stand for the positions and directions of the paleo-tectonic fracture zones in the area. High lineament densities were also observed in areas where basement rocks outcrop or are close to the surface. The relationship between lineament densities and Younger granites occurrences in the study area is an indication of tectonic control probably associated with paleo-tectonic structures. This correlation shows that the emplacement of the Younger granite ring complexes may be associated with epeirogenic uplift. The marked relationship between the Younger granites and the lineaments are interpreted as the presence of controlled mineralization in the study area. In most parts of the study area, heat flows were found to be less than 60mWm^{-2} . This implies that the heat flows in the study area differ from region to region, which possibly indicates that the magma conduits were randomly distributed. The heat flow is significantly high in the South-Eastern area with the study area having an average heat flow of 56.06mWm^{-2} .

Keywords: *Magnetic basement depth, Euler deconvolution, Geothermal, Aeromagnetic, Spectral analysis, Curie depth, Younger Granite Nigeria.*

CHAPTER ONE

INTRODUCTION

1.1 BACKGROUND INFORMATION

The study area comprising Younger Granite ring complex of North Central Nigeria is bordered by latitudes 9°00'N and 10°00'N and Longitudes 8°00'E and 9°00'E. It has an estimated area of 6104 square kilometres. This study area falls within the Central North (Kaduna- Jos) region of Nigeria. The bedrock geology is predominantly Basement Complex consisting of Biotite Gneisses, Granites (Older and Younger) and Bathyliths. However, rocky granitic residuals form inselbergs of varying sizes and shapes, and constitute the main local relief here and there with Kufena, Kagoro hills and Dutsen Waikudaru Ring Complex standing out very predominantly. The valleys are shallow but wide, stretching several tens of kilometers into the headwater areas with gentle sloping valley sides. This area experiences a typical tropical continental climate with distinct seasonal regimes, oscillating between cool to hot dry and humid to wet (Tunar, 1972).

This present study is aimed at exploiting the merits inherent in magnetic and remote sensing method in the structural interpretation of the Younger Granite ring complex which possibly controls the mineralization of the area. The past few years have seen a transformation in the combination of aeromagnetic and landsat images for interpretation of structural and lithologic variations in the sedimentary section. Aeromagnetic method can be used in mapping of fracture and fault system of the basement rock which feasibly controls the mineralization of any area (Opara et al., 2014). By outlining the various basins and sub-basins geometries we could be able to map the regional hydrocarbon and mineral fetch areas. Trends in magnetic features often have related trend in the overlying sediments. Systematic offset of magnetic anomalies may indicate strike-slip faults; which have displaced basement rocks; and possibly affected the sediment section. In many sedimentary basins, magnetic anomalies arise from secondary mineralization along fault planes, which are often

disclosed on aeromagnetic maps as surface linear features. Most mineral deposits are linked to some form of deformation of the lithosphere, and most principles of ore formation and concentration embody tectonic or deformational theories (O'Leary et al., 1976; Ananaba and Ajakaiye., 1987). Linear features are clearly visible on aeromagnetic maps and often suggest the form and position of individual folds, faults, joints, veins, lithologic contacts, and other geologic features that may lead to the location of individual mineral deposits. They often reveal the general geometry of subsurface structures of an area thereby providing a regional structural pattern. Likewise, Magnetic basement is an assemblage of rocks that underlines sedimentary basins and may also outcrop in places. If the magnetic units in the basement occur at the basement surface, then depth determinations for these will map the basin floor morphology and its structure (Onyedim et al., 2006). The use of satellite imagery for regional mapping of geologic units and structures has long been demonstrated as a vital tool for regional geologic mapping. It has been widely used in the production of new geological maps and revision of existing ones.

Numerous geological and geochemical studies have been carried out within the Nigerian Younger Granite province; the researches were mainly carried out because of the economic importance of some of the ring complexes in the area. The earliest gravity surveys were used to define and provide information about the ring complexes (Ajakaiye, 1989). However, the studies have been futile in providing information on structural setting because of the sparse station density of the surveys; which additional data set would have provided. In view of the significance of the additional data set, the aeromagnetic data of the study area and beyond, acquired in 1974 by the Geological Survey of Nigeria (at supposed flight height of 152.4 m, along N-S flight lines that were spaced at 2 Km interval), have been interpreted. Much could not be construed, because the data only denotes anomalies greater than 4km (twice spatial sample interval, because of aliasing effect. The interpretation by Aina and Olarewaju., (1992), which mainly focused on the Younger Granites, was general and it

related the distinct magnetic character as the expression of ring complexes. The study also revealed lineaments that trend along NW-SE and NE-SW direction. Interestingly, high resolution aeromagnetic data of the study area, whose interpretation will reveal subtle anomalies, have been acquired by the Nigerian Geological Survey Agency (NGSA). However, the data have not been studied to fill the gap created by the limitations of the previous geophysical studies.

1.2 STATEMENT OF PROBLEM

The Younger Granites have been studied in most detail in Nigeria, mainly because in the early 1900s they were recognized as the source of rich alluvial cassiterite deposits that had long been known to exist on and around the Jos Plateau. Detailed field mapping of the ring complexes has demonstrated a consistent succession of magmatic activity from volcanism to plutonism associated with the emplacement of mainly granite melts at high levels in the crust. The most striking petrographic feature of the whole province is the overwhelmingly acid nature of the rocks and the similarity of the rock types found in all areas.

The study of the Younger Granite ring complexes is based on the prevalence of cassiterite, wolframite, scheelite and zinc mineralization, and have sustained an important alluvial tin mining industry. In order to contribute to the knowledge of the structural trends and patterns of the Mesozoic Younger Granite ring complex, we have decided to carry out an Aeromagnetic study of the Younger Granite, with a view to providing a more detailed structural features of the study area and after their relationship with mineralization.

1.3 AIM AND OBJECTIVES OF THE STUDY

This research work is aimed at delineating the structural features related to the Younger Granite ring complex and to deduce based on the interpretations, their relationship to mineralization.

The research is designed to achieve the following objectives:

- i. To interpret Geological features and structures of the study area.
- ii. To generate lineament map and lineament density map of the study area.
- iii. To determine the dominant structural features and their trends using Rose diagrams and lineament maps.
- iv. To carry out a detailed structural study of the area and determine structural features using 3D-Euler convolution.
- v. To determine the depth to basement using spectral analysis.
- vi. To generate enhanced map and composite images that can aid structural interpretations of the study area.
- vii. To determine the Curie Point Depth, geothermal gradient and heat flow in the study area.

1.4 JUSTIFICATION OF STUDY

The necessity for more comprehensive work on the Younger Granites cannot be overstressed. This need becomes vital because of their classical structures, petrographic type, and mid-plate anorogenic character. Of all the African ring complex provinces the Younger Granites of Nigeria have been most studied, and although providing fine examples of ring structures and petrogenetic evolution, these features can be as well seen in other provinces. They are however, economically more important than any of the other groups, excluding the carbonatite complex of Palabora (Bowden and Kinnaird, 1984).

The Younger Granite is yet to be fully mapped geologically; as such this study is to contribute to the knowledge of the geology of the area.

1.5 SCOPE OF STUDY

This study will be limited to the analysis and geologic interpretation of the aeromagnetic data and remote sensing data of the area which lies between Latitudes 9°00N

and 10°00'N and Longitudes 8°00'E and 9°00'E. The study area is enclosed within the four (4) aeromagnetic maps acquired from the Geological Survey of the Nigeria.

The study will also seek to generate information on the lithology, tectonics, geomorphology and drainage characteristics of the area from the integration of the geophysical and remote sensing data; to speculate on possible solid mineral potential within the area.

1.6 DESCRIPTION OF THE STUDY AREA

The study area is part of the Younger Granite complex, North central Nigeria which lies between Latitudes 9°00'N and 10°00'N and Longitudes 8°00'E and 9°00'E. The study area is enclosed within the four (4) aeromagnetic maps acquired from the Geological Survey of the Nigeria. The notable provinces within the study area includes Jos, Bukuru, Kwoi, Gwantu, Kagoro, Barkin-Ladi, Ganawuri, Jemaa and Andaha.

The topography of the study area comprises of chains of highlands of variable heights associated with areas of almost flat topography. The area has altitude which ranges from around 293m to a peak of about 1600m above sea level. Years of tin mining have also left the area strewn with deep gorges and lakes. Rocky granitic residuals form inselbergs of varying sizes and shapes, and constitute the main local relief here and there with Kufena, Kagoro hills and Dutsen Waikudaru Ring Complex standing out very predominantly.

The study area seems to be divided into three different reliefs, with Gwantu area having the lowest elevation above sea level, kagoro area the intermediate and Barkin-Ladi area having the highest elevation. The valleys are shallow but wide, stretching several tens of kilometres into the headwater areas with gentle sloping valley sides; imperceptibly grading into flat moist to marshy alleviated bottomlands or floodplains called "Fadamas" in Hausa (Tuner, 1972). Although stream valley incisions and dissections of the high plains are

evident in several areas, they are more due to anthropogenic influences and climatic factors than regional geologic instability.

1.6.1 DRAINAGE

The drainage pattern of the study area is dendritic. It is drained by network of streams that got their source mostly in the isolated hilly areas found around. The entire area is dissected by streams and rivers.

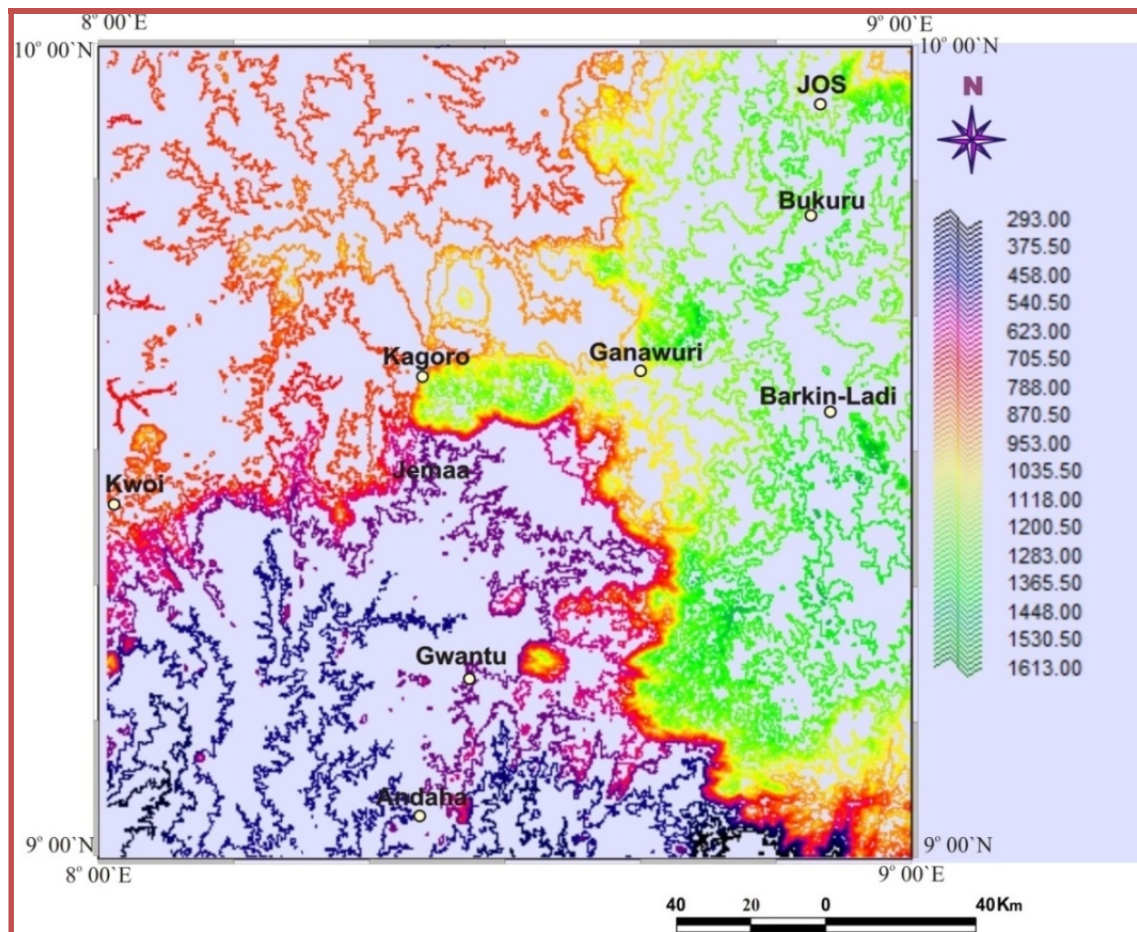


Figure 1.1: Topographic Map of the Study Area

1.6.2 CLIMATE

The study area experiences a typical tropical continental climate with distinct seasonal regimes, oscillating between cool to hot dry and humid to wet. These two seasons reflect the influences of tropical continental and equatorial maritime airmasses which sweep over the

entire country. However, the seasonality is pronounced with the cool to hot dry season being longer than the rainy season. Harmattan winds cause the coldest weather between December and February. The warmest temperatures usually occur in the dry season months of March and April. It is moderately hot with temperature between 24°C – 27°C.

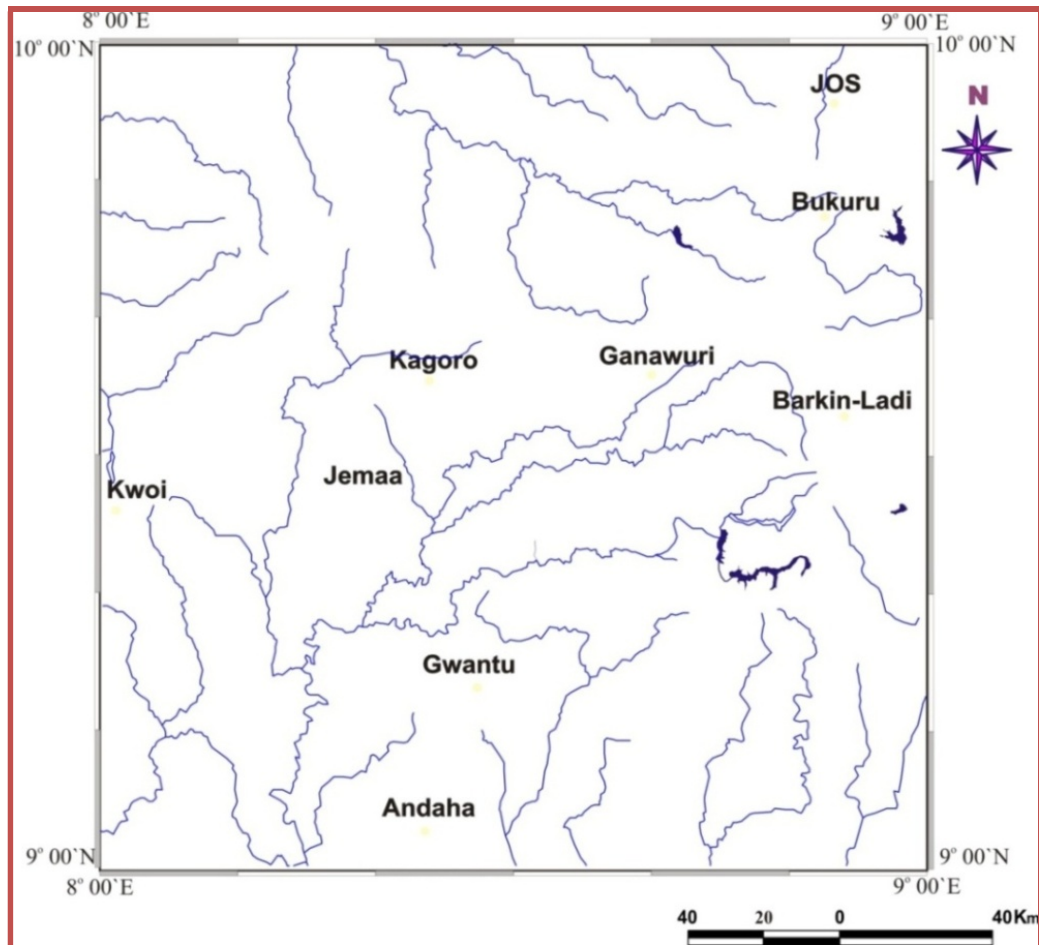


Figure 1.2: Drainage Map of the Study Area

1.6.3 SOIL AND VEGETATION

Generally the soils and vegetation are typical redbrown to redyellow tropical ferruginous soils and savannah grassland with scattered trees and woody shrubs. The soils in the upland areas are rich in red clay and sand but poor in organic matter. The trees grow long tap-roots and develop thick barks which enable them to survive the long dry season and resist bush fires. Examples of trees found here are the isoberlina, shear butter, locust bean

and oil bean tree. Soils in this Area are deeply corroded, generally sticky, impervious to water and of mediocre fertility. They are also known as laterite soils.

1.6.4 THE GEOLOGY OF THE STUDY AREA

The Younger Granite province consists of Precambrian to Lower Paleozoic Basement Complex rocks into which the Younger Granites suites are emplaced. Three quarters of the Younger Granites province are covered by Basement rocks and consist of ancient sediments which are made up of granulitic gneiss, dioritic rocks, migmatites, granite-gneiss, older granites and granodiorites (Oyawoye, 1972). Cone sheets and ring dykes are widely dispersed in the province. The ring dykes show outward dips both on the inner and outer contacts but some have steep or vertical contact. They were followed by acid volcanism and emplaced by ring faulting and block subsidence. Granites and rhyolites lie beneath major parts of the province. Intermediate and basic rocks occur. Emplacement of the Younger Granites is related with epeirogenic uplift (Turner, 1989). Their age is Jurassic. The Older Granites and accompanying metamorphism of the basement are Pan African age (Jacobson et al, 1958; van Breeman and Bowden, 1973). Numerous types and number of the Younger Granite complexes exhibit different degrees of erosion. The large complexes involved greater volumes of magma.

The Younger Granite complexes trend in an N – S belt with the ages of the complexes decreasing southwards. Rahaman et al., (1984) showed that key local magmatic activities were focused along ENE and WSW zones. The age pattern proposes that the parent magma were locally obtained from several concurrent high level magma chambers linked to a common deeper source. The emplacement of these ring complexes was structured by fracture systems in the basement.

The major segment of acid magmatism in Nigerian Younger Granite province begun during Triassic times and continued to migrate in a generally southerly direction until the close of the Jurassic (Bowden et al., 1971).

Bowden proposed three stages of development of the Nigerian ring complexes:

- i. Early stage of a large rhyolite volcano which prior to the end of its stage, accumulated large amount of magma in the synvolcanic reservoir about 5 km beneath the surface.
- ii. Caldera and ring dyke stage which occurred when the centre of the volcanic structure within a ring fault collapsed, magma arose along the fault and crystallized as granite porphyry which was extruded into the caldera rocks.
- iii. Intrusive stages which were the warming phase of igneous activity occurred when smaller granite intrusions were emplaced at increasing depth levels. The magma evolved and crystallized at lower temperatures and as lower assemblages. The rocks are composed of biotite granite.

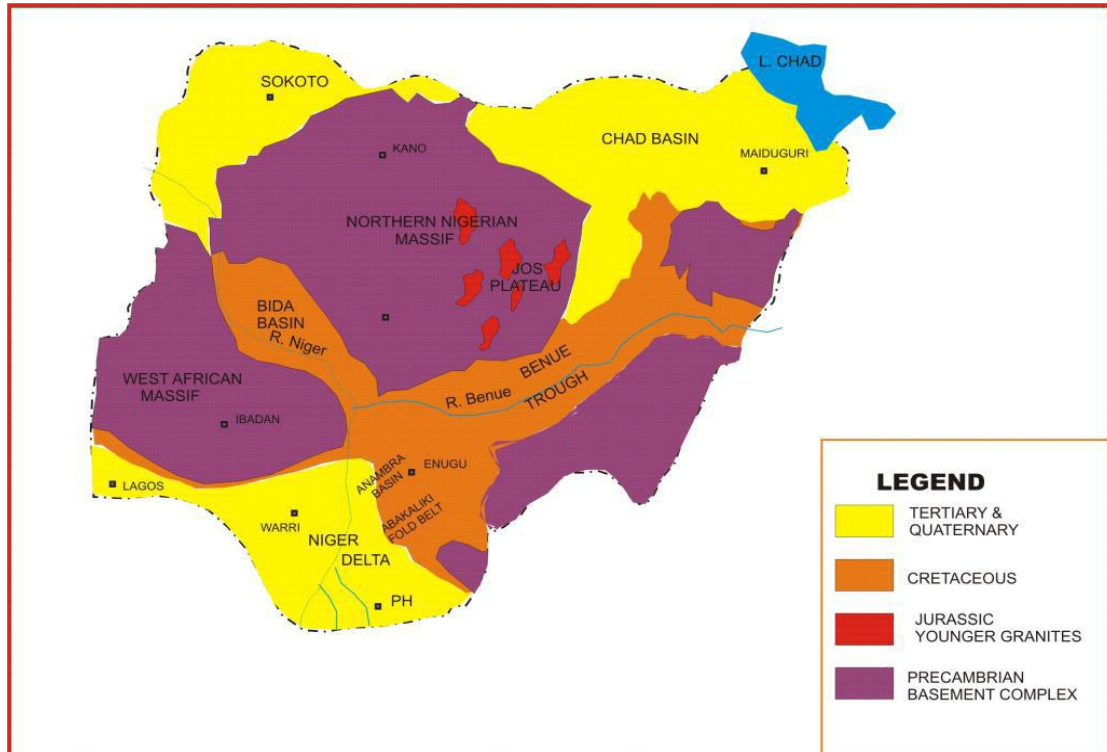


Figure 1.3: Geology map of Nigeria showing the younger granite ring complexes

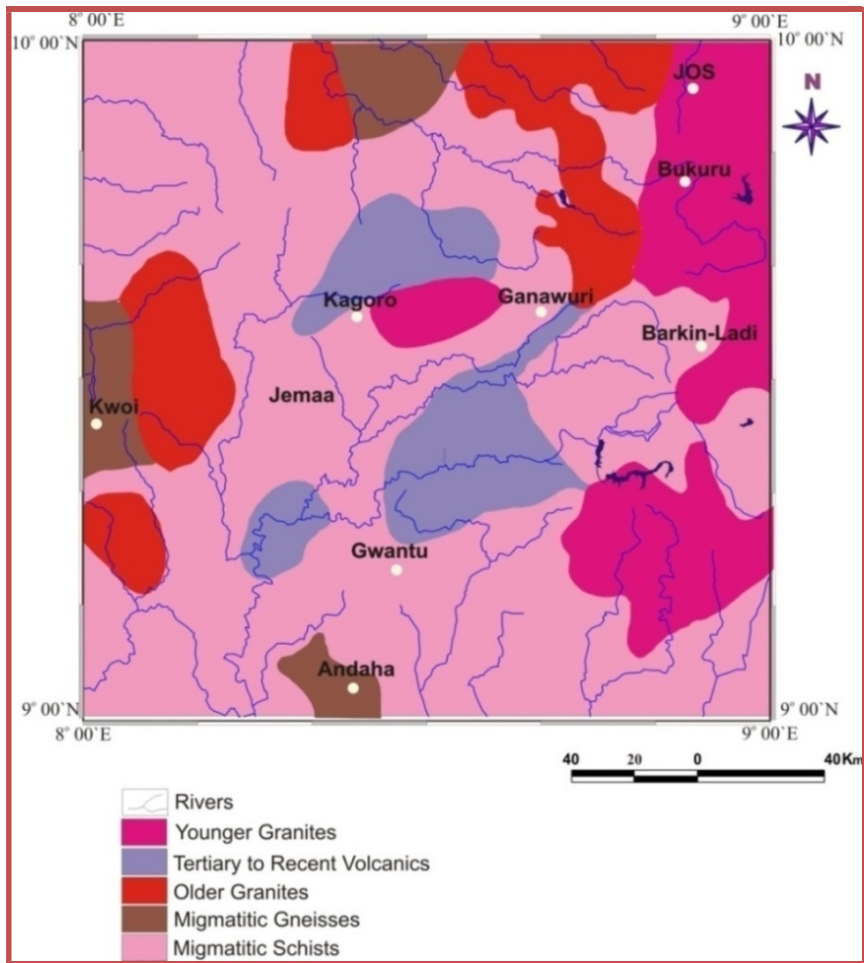


Figure 1.4: Geology map of the study area.

The Volcanic rocks in most of the complexes have either been destroyed by subsequent granite intrusions or weathered to the degree that their original pattern of distribution is conjectural. Where the lavas are preserved, they are kept within the major peripheral ring faults. The early groups are products of vent intrusion from group of vents aligned along ring-fractures. The fractures stretched to the surface and provided zones of weakness that facilitated the upward passage of the magma. These same ring-fractures often served as the loci of intrusion of the large ring-dykes. Pyroclastic rocks are abundant and there are thick interactions of tuffs and coarse agglomerates within the lava succession. Emplacement of ring-dykes within circular and polygonal features initiated many of the intrusive cycles. Emplacement of ring-dykes directly succeeded the volcanic cycle and many

of the initial ring-fractures, which control the dispersal of the volcanic eruptions, also served as the loci of the ring dykes (Nwokocha et al., 2016).

The ring dykes are generally sheer structures and contact dipping outwards at angles less than 80° are uncommon. Some of the ring dykes have lateral dimensions as much as two kilometres in widths. In the Younger Granite province there is a practically incessant order of intrusives formed from the narrow ring dykes to large irregular granite plutons. Many of the smaller granite intrusions represent the upper, flat-lying roof sections of the ring intrusions and, some of these are remarkably shallow in comparison with their lateral dimensions. Others are stock and bosses with steeply dipping contacts, which probably continued to a considerable depth.

CHAPTER TWO

LITERATURE REVIEW

2.1 REVIEW OF PREVIOUS STUDIES

The Younger Granite Province comprises of Precambrian to Lower Paleozoic basement rocks into which the Younger Granites suites are emplaced (MacLeod et al, 1965). The basement rocks cover about three quarters of the province and consist of ancient sediments (MacLeod et al, 1965; Oyawoye, 1964; Oyawoye, 1972).

Four major oceanic fracture zones cut the Atlantic coast to the northeast on approaching the coast of Guinea at the north and terminated at a relatively short distance inland (Burke, 1969; Grant, 1971; Le Pichon and Hayes, 1974). These fractures seems to have developed near pre-existing zones of weakness inherited from previous orogenic activities in the continents (Syke, 1978) and often show on maps as lineaments. Aeromagnetic anomalies and tectonic trends around and in the Benue Trough of Nigeria indicates that the Nigerian continental landmass have lineaments with definite magnetic signatures (Ajakaiye et al, 1987) which, are enhanced by the presence of anorogenic ring complexes.

In delineating the linear structures of the Younger Granite, Alkali and Gaiya (2011) working on the western part of the Younger Granites of the North central Nigeria analyzed the major and minor fracture lines on bidirectional rose diagrams organized into class intervals of 15° and recorded five classes for the major lineaments and four for the minor ones. The main structural units of their rose diagrams are oriented along the N – S, NE – SW, NNE – SSW, NW – SE and NNW – SSE directions. The NE - SW and NNE - SSW trending lineaments are interpreted as belonging to major fracture lines, which probably controlled the emplacement of the granite and the NE – SW trending joints. They therefore interpreted the NE - SW set as representing fractures associated with major movements attributable to

past tectonics activities and that the pegmatite zones and quartz veins are associated with the NNE – SSW linear structures.

Lawal et al (2012) used spectral analysis to interpret the aeromagnetic anomalies of the Younger Granite ring complex of Nigeria. They estimated average thickness of the sedimentary cover overlying the basement. From their result, two depth source models with the depth to deeper sources were 1.4km and the depth to shallow sources 0.17km. The isolated magnetic anomalies of geologic interest by the regional-residual separation technique they used revealed that there were three major magnetic regions in the area, these are regions of positive anomaly which could be due to the rock rich in ferromagnetic minerals, regions of intermediate which are found to be lying over the undifferentiated basement complex and region of negative anomalies which could be due to acidic basement complex rocks.

In the gravity study over Jos – Bukuru Younger Granite complex, North central Nigeria, Alkali and Yusuf (2010) obtained values of – 90 mGal at the centre of the complex. Lower values at the eastern side are separated from higher ones at the western side by a NW – SE diagonal line. The anomaly contour closures trend in the E – W, NE – SW, N – S and NNW – SSE directions. Using third order polynomial trend surface fitting, they observed that the contour levels of the regional anomaly field in a NNE – SSW direction, consists of increasing N – S values. Their map of the residual anomaly is characterized by both negative and positive values between -25 to +20 mGals. The negative values are probably located on the intrusive younger granite rocks while the positive values may explain areas underlain by volcanic rocks. They generated two and one half models of the residual anomaly along profiles which indicated depths up to 18.75 km for the plutonic rocks and 13.96 km for the volcanic rocks. These large depths are attributed to the presence of a large-scale fault

associated with the Romanche fracture zone in the basement around the Jos - Bukuru Younger Granite complex.

Alkali and Hassan (2014) generated a regional magnetic field intensity map from aeromagnetic data of the Kagoro Younger Granite complex. Their lowest magnetic contour values closure was observed to be centred over the central part of the Kagoro Granite rocks. This closure is structurally aligned along the NE – SW direction. Some of the closures in the study area are aligned along the NE – SW and E – W directions. Patterns of the closures of the magnetic maps are in conformity with those of the Nigeria basement and Younger Granite rocks. Isolations and magnitudes of the closures suggest that the various rock bodies occur separately and at different levels. With the residual anomaly accounted for, they estimated that the Kagoro Younger Granite complex was emplaced at depths between 9.5 and 15.2 km, and that the volcanic rocks and their associates were formed from depths between 4.7 and 13.0 km.

Raimi et al (2013) carried out an interpretation of high resolution aeromagnetic data to provide new information about the Nigerian Younger Granite province. Their interpretation revealed previously unknown folds and magnetic anomaly with a signature that is similar to those associated with ring complexes in the study area but without the surface manifestation that is associated with the complexes. Qualitatively interpreted as unexposed ring complex, they observed that the structure causing the anomaly is overlain by cross-over of major lineaments; implying presence of weak zone that probably allowed the volcanic eruption that initiated the emplacement of the source of the anomaly. The Euler deconvolution they carried out suggested a depth that ranges from outcrop to 1200 m and from outcrop to 1800 m for the unexposed ring complex and folds respectively.

In the study to estimate the depths extents of aeromagnetic anomalies over the Younger granite rocks and their associates in the western part of North Central Nigeria carried out by Alkali et al, (2012). The authors generated two and a half dimensional models of the subsurface structures which suggests deep seated fault along the profiles that attained maximum depths of 12.0 km each along sections Mag1 and Mag2; 13.0 km along Mag3 and 26.6 km along Mag4. With the steepness of the magnetic sources, they suggested possible relative displacement of the blocks of the rock bodies of these magnitudes. The fault correlate with Romanche fracture zone which, if extrapolated into Nigerian landmass will pass through the area diagonally in a NE-SW striking direction.

Opara et al (2014) in the interpretation of the structural and tectonic features of Ugep and Environs, Calabar Flank, Southeastern Nigeria concluded that the combined interpretation of airborne magnetic data and landsat ETM imagery added several significant structural elements that were previously unrecognized from the separate interpretations of the respective data-sets. The derived maps revealed several previously undetected linear structures. Some of these linear features corresponded to the strike and direction of some paleo-structures, faults, and tectonically related joints with dominant trend direction of NE-SW. Spectral analysis was used to estimate mean sedimentary thickness of the study area to be 2.289km. They concluded that the abundance of intrusives and the shallow basement depth is not conducive for hydrocarbon generation and accumulation.

2.2 THEORETICAL FRAMEWORK

2.2.1 Introduction To The Magnetic Method

The past years have seen a development in the application of aeromagnetic surveys in delineating the regional geology (lithology and structure) of buried basement terrain. The earth magnetic field, while acting on magnetic minerals in the crust of the earth induces a secondary field, which reflects the distribution of these minerals. The main field, which is the

inducing magnetic field, changes slowly from one place to another. Therefore, to understand the magnetic effects associated with Earth materials, one requires the knowledge of the principles of magnetism (Dobrin and Savit, 1988). Most mineral deposits are related to some type of deformation of the lithosphere, and most theories of ore formation and concentration embody tectonic or deformational concepts (O'Leary et al., 1976; Ananaba and Ajakaiye., 1987).

The magnetic method is useful whenever the object of investigation has a contrast in the magnetic susceptibility or remanence that can be detected by the magnetometer. The magnetic method is used for:

- i. Basin analysis
- ii. Location and definition of the coverage of a Sedimentary Basin
- iii. Depth estimation to the basement rock (Magnetic source)
- iv. Thickness of the sediment present which can be used to evaluate whether the sediment is sufficient to warrant exploration of petroleum.
- v. Local relief of the basement surface which may produce the structural relief in the overlying sediments.
- vi. Basement lineation
- vii. Provision of magnetic data for mapping the surface geology.

The qualitative interpretation of aeromagnetic survey data shows directly the geological information by looking at the map without any calculations. The very high gradient on an aeromagnetic map usually indicates the difference in magnetic susceptibility such as that between granite (acidic rock) andesite (intermediate rock) and basalt (basic rock); a condition called "intrabasement". In case of some variation of contour gradient on an aeromagnetic map, it usually indicates vertical movements (faults); a condition called

“suprabasement”. The shape of the causative body also could be considered, in case of circular contours and the magnetization is vertical, where the body may be a plug. In case of elongated closed contours, the source may be a dyke and the direction of elongation should indicate its strike. However, in the case of elongated zone of sheer gradient without well-defined closure, it is likely that this pattern results from subsurface faulting, which has displaced magnetized rocks (Dobrin, 1983).

2.2.2 Theory of Aeromagnetic Survey

Aeromagnetic survey is a well known type of geophysical survey carried out using a magnetometer aboard or towed behind an aircraft. They are widely used to aid in the production of geological maps and are also commonly used during mineral exploration. The principle is analogous to a magnetic survey carried out with a hand-held magnetometer, but permits much larger areas of the earth’s surface to be covered quickly for regional reconnaissance. The aeromagnetic geophysical method plays an eminent role when compared with other geophysical methods in its rapid rate of coverage and low cost per unit area explored. The aircraft typically flies in a grid-like pattern with height and line spacing determining the resolution of the data (and cost of the survey per unit area).

As the aircraft (typically a helicopter) flies, the magnetometer records tiny variations in the intensity of the ambient magnetic field due to the temporal effects of the constantly varying solar wind and spatial variations in the earth’s magnetic field, the latter being due both to the regional magnetic field, and the local effect of magnetic minerals in the earth’s crust. By subtracting the solar and regional effects, the resulting aeromagnetic map shows the spatial distribution and relative abundance of magnetic minerals in the upper levels of the crust. Different rock types differ in their content of magnetic minerals; hence, the magnetic map allows a visualization of the geological structure of the upper crust in the

subsurface, particularly the spatial geometry of bodies of rock and the presence of faults and folds.

2.2.2.1 Applications of Aeromagnetic Data

Aeromagnetic surveys provide generalized geologic information over a generalized area for ground investigation follow up. It is used mainly to detect minerals or rocks that have unusual magnetic properties which reveal them by causing anomalies in the intensity of the earth's magnetic field. Other applications of aeromagnetic data include: Geothermal applications, geological studies, mineral and oil exploration, nuclear fuels exploration, geotechnical and archaeological investigations, earthquake hazards and site evaluation, ground-water studies and general scientific uses.

Rock Magnetic Properties

The vector sum of induced and remnant components gives the total magnetization. The induced component of a rock is the product between the Earth's present-day magnetic field vector and the magnetic susceptibility. Magnetic susceptibility is a scalar measure of the quantity and type of magnetic minerals (commonly titanomagnetites) in the rock. The remnant component is based on the permanent alignment of magnetic domains within magnetic minerals and is measured using Paleo-magnetic methods (Butler, 1992).

In every case, the susceptibility (K) of rocks depends on the amount of magnetite (Fe_3O_4) contained in the rock unit. K is the significant variable in magnetic method playing the same role as density in gravity exploration. Magnetic susceptibility, as a property of rock is represented as a range even for a particular rock and a wide overlap exists between rock types. The magnetic susceptibility is measured either in nanotesla or gamma (γ) values. Igneous and crystalline metamorphic rocks ordinarily have high total magnetizations compared to other rock types, while sedimentary rocks and poorly consolidated sediments have much lower magnetizations (Reynolds *et al.*, 1990; Hudson *et al.*, 1999). Aeromagnetic

anomalies over volcanic rocks commonly produce high-amplitude positive or negative anomalies. Where a correspondence between volcanic edifices and anomaly shape can be demonstrated, positive and negative anomalies indicate normal and reversed-polarity remnant polarities of the rocks respectively. Theoretically, the magnetic methods are based on the measurement of the small variation in the distribution of the magnetized or polarized rocks. The magnetic susceptibilities of some basic rocks are shown in Table 1.0 below

Table 1.0: Typical Magnetic Susceptibilities of Earth Materials. (Dobrin and Savit, 1988).

Rock (Mineral)	Susceptibility (c.g.s.)
Magnetite	0.3 -0.8
Pyrrhotite	0.028
Ilmenite	0.044
Specularite	0.004
Iron Formation	0.056
Basalt	0.00295
Diabase	0.00259
Rhyolite	0.00112
Gabbro	0.00099
Granite	0.00047
Other Acid Intrusive	0.00035
Ely Greenstone	0.00009
Slates	0.00005
Sedimentary Rocks	0.00001 to 0.001

Hypothetically, the magnetic methods are based on the measurement of the small differences in the distribution of the magnetized or polarized rocks.

Depth to basement, faults in the basement surface and relief of the basement have direct significance to the depositional and structural history of a basin. Lots of examples

exist of positive basement block being directly associated to depositional isopachs and / or structure which reveal the underlying basement structure. In general, igneous rocks have greater concentration of magnetic minerals particularly magnetite than sedimentary rocks and can be identified and mapped in the sedimentary basin from the magnetic data. Igneous features such as intrusive plugs, dykes, sills, lava flows and volcanic centers can occur at any stage of a basin's evolution and therefore be preserved at any level in the sedimentary section. Such features are significant in understanding the history of a basin and assessing its petroleum or mineral prospectivity. Igneous intrusions can produce structural closure and here, magnetic anomalies can be indicators of hydrocarbon traps (Opara et al., 2014).

2.2.2.2 The Nature of Magnetic Anomalies

Mineral exploration were considered in discussing magnetic anomalies

Magnetic features related to mineralization

Isolate magnetic anomalies, generally are circular or oval in shape and several hundred metres across, with amplitude of tens to hundreds of nano-teslas and may give rise from accumulation of magnetite and / or pyrrhorthite which may be linked with economic grades of copper, lead, zinc , silver and gold. Such deposits which precipitate from mineral bearing solution are frequently located within or adjacent to major faults. Gunn & Dentith, (1997), reviewed the characteristics of such deposits which are much more numerous than most people realize and liable to occur at depth in many unexhumed sedimentary basins.

2.2.3 Aeromagnetic Data Processing

Data processing of the aeromagnetic data is primarily aimed at methodically separating the local anomalies from regional magnetic anomalies and for enhancement of these anomalies. Numerous analytical processes and methods are used for analysis of aeromagnetic data. They include: filtering and convolution of aeromagnetic data, reduction

to pole, regional- residual separation and depth estimation analysis. These methods are discussed in details for a better understanding.

2.2.3.1 Filtering of Aeromagnetic Map

Filtering is a way of separating signals of different wavelength to isolate and hence boosts any anomalous feature with a certain wavelength. The rule of thumb is that the wavelength of an anomaly divided by three or four is approximately equal to the depth at which the body producing the anomaly is buried. Thus filtering can be used to enhance anomalies produced by features in a given depth range. Traditional filtering can be either low pass (Regional) or high pass (Residual). Thus the technique is sometimes referred to as Regional-Residual Separation. Band pass filtering isolates wavelengths between user-defined upper and lower cut-off limits. In geophysical exploration, not every signal may be of interest thus; there is always a need for filtration processes. Near surface or shallow anomalous sources usually produce relatively short wavelength disturbance (Onyedim et al., 2006).

Practically, in the manual digitization of aeromagnetic map, certain short-wavelengths are removed to allow a pass of longer wavelength disturbances of lower wave numbers. This is known as a low-pass filter. The irregularities in aeromagnetic maps are removed by low pass filtering, which thus produces a smoother map than the original. Alternatively, the filter in the Fourier domain is designed to eliminate longer wavelengths and pass shorter ones. This is called a high pass filter. Wavelength filtering is a major consideration in selection of anomalies (Nwokocha et al., 2016). In studying a large-scale crustal structure, a low pass filter is employed as small local bodies are of less interest. Similarly, in the investigation of anomalies due to shallow crustal sources, high pass filtering is employed.

2.2.3.2 Reduction to the Pole (RTP)

Reduction to the Pole transformation is a tool that corrects for the offset between the locations of anomalies and their sources that is a consequence of the vector nature of the Earth's magnetic field. To apply the reduced-to-pole transformation correctly, one must assume that the total magnetizations of most rocks in the study area align parallel or anti-parallel to the Earth's main field. This approach makes it possible to determine from the observed total field the position and depth of the pole that has the magnetic effect equivalent to that of an external source with the inclined magnetization. This technique transforms induced magnetic responses to those that would arise where the sources are placed at the magnetic pole (vertical field) (Tuner, 1989).

Pole reduction is difficult at low magnetic latitudes, since N-S bodies have no detectable induced magnetic anomaly at zero geomagnetic inclination. Pole reduction is not a valid technique where there are appreciable remanence effects. Baranov (1957) introduced and improved the reduction to pole of magnetic data which served as an auxiliary method of qualitative analysis. This allows us to have a pseudo magnetic map where the magnetization vector of the rocks and the measured total field both are in vertical direction. The contribution of remnant magnetization is supposed to be irrelevant.

2.2.3.3 Regional- Residual Separation

Regional magnetic features are believed to be caused by the properties of materials deep within the earth or due to the dipole field of the earth. The methods employed in the isolation of the background field from survey data have been discussed extensively in various geophysical literatures. These methods involve either visual and or graphical procedures or analytical methods such as least squares fit.

The mapped potential field data are the sum of the effect of all sources causing a magnetic anomaly. The problem in applied geophysics is to eliminate or reduce to the

lowest, the effects of deep-seated, non-commercial sources with as little distortion of the resultant anomaly as possible. A geophysical anomaly is typically composed of a broad spectrum of frequencies, each frequency being characterized by specific amplitude. The anomalies of interest may be corrupted by multi-frequently “noise” consisting of regional trends, instrument drift, uninteresting geologic variation, etc. If the frequently content of both anomaly and noise is known, and there is no spectral overlap between them, then a filter of interest would be designed to eliminate the noise effects.

2.2.3.3.1 Polynomial Fitting

Polynomial fitting is a purely systematic method which involves matching of the regional field with a low order polynomial surface to produce the residual features as random errors. The system is based on statistical theory. The regional trend is represented by a straight line or generally by a smooth polynomial curve. The polynomial is fitted by the method of the least squares. But, it should be well noted that this method has the following inherent drawbacks:

- i. The higher the order of the polynomials, the better it fits the observations.
- ii. The ludicrous extreme when the order of the polynomial is less than the number of the observations, the curve then passes perfectly through all the data points but geologically has no meanings.

A curve fitted by least squares must pass through the mean of the magnetic values, so that the residual anomalies are divided equally between positive and negative values. Each residual anomaly is flanked by anomalies of opposite sign, which are due to the same anomalous mass that caused the central anomaly; and so they have no significance of their own. In practice, the polynomial is rarely extended beyond the second orders.

2.2.3.4 Upward continuation of the potential Field

Upward continuation is a filter operation, which smoothens the original data by attenuation of short wavelength anomalies relative to their long wavelength counterparts. In space, the upward continuation operation is a 2D convolution process given by the integral equation (Bhattacharyya, 1966).

$$\phi'(x, y) = \int_{-\infty}^{\infty} \int_{-\infty}^{\infty} f(\alpha, \beta) \phi(x - \alpha, y - \beta) d\alpha d\beta \quad (2.1)$$

$\phi'(x,y)$ is the input data, $\phi(x,y)$ is the output data and $f(\alpha,\beta)$ is the filtering function.

In order that a filtering function can be useful, it must be of finite extent, if $f(x,y)$ becomes zero for $|x|=|X|$ and $|y|=|Y|$ then equation (2.1) can be replaced by

$$\phi'(x, y) = \int_{-X}^X \int_{-Y}^Y f(\alpha, \beta) \phi(x - \alpha, y - \beta) d\alpha d\beta \quad (2.2)$$

Convolution in the space domain is equivalent to multiplication in the frequency domain. In order to arrive at the spectrum of the output, the spectrum input is multiplied by the spectrum of the filtering function. Denoting the Fourier transform of a function by corresponding capital letter, with a frequency argument and taking the Fourier transform Equation(2.2). Thus we have:

$$\phi'(f_x, f_y) = F(f_x, f_y) \phi(f_x, f_y) \quad (2.3)$$

where f_x and f_y are the angular frequencies along x and y axes respectively, From the results of the potential theory, the upward continuation of the potential function $\phi(x,y,0)$ in a source free region to a height(h) above the plane $Z=0$ is given by (Fuller,1967)

$$\phi'(x, y, h) = \int_{-\infty}^{\infty} \int_{-\infty}^{\infty} \frac{h\phi(\alpha, \beta, 0)d\alpha d\beta}{2\pi \sqrt{[(x-\alpha)^2 + (y-\beta)^2 + h^2]^3}} \quad (2.4)$$

Comparing equation (2.4) and

(2.1), and realizing that the convolution integral is commutation, allows recognition of equation (2.4) as a two dimensional convolution and hence a filtering operation. The potential function $\phi(x, y, 0)$ is operated upon by the filtering function $f_u(x, y, h)$ in order to arrive at $\phi(x, y, h)$, where:

$$f_u(x, y, h) = \frac{h}{2\pi \sqrt{(x^2 + y^2 + h^2)^3}} \quad (2.5)$$

The theoretical frequency response of a true upward continuation operator may be obtained by the Fourier transform of equation (2.5) or the solution of the integral

$$f_u(f_x, f_y, h) = \int_{-\infty}^{\infty} \int_{-\infty}^{\infty} \frac{he^{-2\pi i(f_x x + f_y y)}}{2\pi \sqrt{(x^2 + y^2 + h^2)^3}} dx dy \quad (2.6)$$

Solution of this equation by gamma functions (Fuller, 1967) yields

$$F_u(f_x, f_y, h) = e^{-2\pi h \sqrt{(f_x^2 + f_y^2)}} \quad (2.7)$$

Transformation from space domain to the frequency domain provides a fast and convenient way in which otherwise complicated numerical filtration operations on magnetic fields can be performed.

2.2.4 Depth Estimation

The depth to the top of the source is a useful tool for finding thickness of sedimentary succession and sometimes for locating major structures in basement rocks. Some anomalies arising from basement rocks may be due to lithologic changes rather than to structural features. In certain geologic situations, the depth to the bottom of magnetic sources is sought

where it can correspond to the Curie-temperature. Reliable depths help drilling plan for both magnetic and non-magnetic targets. If one can reliably estimate the thickness of non-mineralized cover rocks, accurate budgeting and planning of any exploitation program could be achieved.

The depth to the top surface can be estimated from the form of a magnetic profile, at right angles to the strike, and traversing an anomaly centre or its immediate neighborhood. The strike length can be fairly accurately estimated from the shape of the magnetic anomaly. The depth obtained from a magnetic anomaly is dependent on the selection of appropriate source geometry. Parasnis (1997), stated that the selection of horizontal characteristic parameters can be directly related to the depth of burial.

The use of contours, stretched histogram pseudo-colour compositions and first vertical derivative data were the traditional depth estimation techniques. But recently there are exciting suite of new-generation depth estimation tools and products. These tools include: Spectral analysis, Matched filter depth separation and slicing, Traditional and Extended Euler Deconvolution, Phillips method, Complex amplitude and instantaneous phase, Analytic signal, Magnetic coherence map, Vertical derivative, pass, continuation and directional filters, Powerful visualization and hard copy composition language and tools.

All the methods are based on the transform of the potential field anomalies into special functions that form gradient peaks and ridges over the sources. These maxima peak values are located directly above the magnetic contacts, depending on an assumed geometric model. All the methods can use the same function to locate the contacts and estimate the source depths.

2.2.5 Aeromagnetic Data Interpretation

Aeromagnetic datum is interpreted qualitatively and quantitatively as discussed below.

2.2.5.1 Qualitative Interpretation

Qualitative interpretation involves the description of the survey results and the explanation of the major features disclosed by a survey in terms of the types of possible geological formations and structures that give rise to the evident anomalies. The qualitative interpretation of a magnetic anomaly map begins with a visual inspection of the shapes and trends of the major anomalies. Typically, some geological information is available from outcrop evidence within the survey area (or nearby) and very often the role of the geophysical data is to extend this geological knowledge into areas where there is no outcrop information (i.e. extrapolation from the known to the unknown) or to extend mapped units into the depth dimension (i.e. to help add the third dimension to the mapped geology).

After delineation of the structural trends, a closer examination of the characteristic features of each individual anomaly is carried out. These features are:

- i. The relative locations and amplitudes of the positive and negative contour parts of the anomaly,
- ii. the elongation and aerial extent of the contours and
- iii. the sharpness of the anomaly as seen by the spacing of contours

Accordingly, the following items are taken into consideration during qualitative interpretation of the aeromagnetic map:

- i. In sedimentary regions, mainly where the basement depth exceeds 1.5 km, the magnetic contours are normally smooth and variations are little, reflecting the basement rocks rather than the near surface features (Telford *et al.*, 1998). The

magnetic relief observed over sedimentary basin areas is virtually always controlled more by the lithology of the basement than by its topography (Dobrin and Savit, 1988). Meanwhile, in regions where igneous and metamorphic rocks predominate, complex magnetic variations are usually exhibited.

- ii. Changes in the magnetization of basement rocks a kilometer or more deep may result in magnetic anomalies up to several thousand gammas (nT) in magnetic readings at the surface. The density of contour lines often provides a useful criterion for indicating structures. The closer the contours, i.e., the greater the gradients, the shallower, in general, is the source. Any abrupt change in the spacing over a considerable distance implies a discontinuity in depth, possibly a fault (Dobrin, 1983).
- iii. The magnetic anomalies of large areal extent reflect a deeper source than small-size anomalies.
- iv. Often, a well-defined boundary between zones with considerable different degrees of magnetic relief can denote the presence of a major basement fault (Dobrin and Savit, 1988).

2.2.5.2 Quantitative Interpretation

This involves making numerical estimates of the depth and dimensions of the sources of anomalies and this often takes the form of modeling of sources which could, in theory, replicate the anomalies recorded in the survey. In other words, conceptual models of the subsurface are created and their anomalies calculated in order to see whether the earth-model is consistent with what has been observed. The model parameters are then attuned in order to obtain a better conformity between observed and calculated anomalies (Ofoegbu and Onuoha, 1997).

2.2.6 Theory of Remote Sensing

Remote sensing is the acquisition of information about an object or phenomenon without making physical contact with the object and thus in disparity to on the site observation. It refers to the activities of recording, observing, and perceiving (sensing) objects or events in far-away (remote) places.

In modern usage, remote sensing in general refers to the use of aerial sensor technologies to detect and classify objects on Earth by means of propagated signals (e.g. electromagnetic radiation) (Rothery, 1987). It may be split into active remote sensing (when signal is first emitted from aircraft or satellites) or passive (e.g. sunlight) when information is merely recorded. The output of a remote sensing system is usually an image representing the scene being observed. A further step of image analysis and interpretation is required to extract useful information from the image. Depending on the scope, remote sensing may be broken down into:

- i. Satellite remote sensing; when satellite platforms are used,
- ii. photography and photo grammetry; when photographs are used to capture visible light,
- iii. thermal remote sensing; when the thermal infrared portion of the spectrum is used,
- iv. radar remote sensing; when microwave wavelengths are used, and
- v. LIDAR remote sensing; when laser pulses are transmitted toward the ground and the distance between the sensor and the ground is measured based on the return time of each pulse.

The applications of remote sensing includes archaeology, agriculture, cartography, civil engineering, meteorology and climatology, coastal studies, emergency response, forestry, geology, geographic information systems, hazards, land use and land cover, natural disasters, oceanography, water resources, and so on.

2.2.6.1 Principles of Electromagnetic Radiation

Remote sensing takes one of the two forms depending on how the energy is used and detected. Passive remote sensing systems record the reflected energy of electromagnetic radiation or the emitted energy from the earth, with devices such as cameras and thermal infrared detectors. Active remote sensing systems send out their own energy and record the reflected portion of that energy from the earth's surface, using instruments such as radar imaging systems.

Electromagnetic radiation is a form of energy with the properties of a wave, and its major source is the sun. Electromagnetic spectrum is solar energy traveling in the form of waves at the speed of light (denoted as c and equals to $3 \times 10^8 \text{ ms}^{-1}$). The waves propagate through time and space in a manner rather like water waves, but they also oscillate in all directions perpendicular to their direction of travel. Electromagnetic waves may be characterized by two principal measures: wavelength and frequency. The wavelength λ is the distance between successive crests of the waves. The frequency μ is the number of oscillations completed per second. Wavelength and frequency are related by the following equation:

$$C = \lambda \cdot \mu \quad 2.8$$

The electromagnetic spectrum, despite being seen as a continuum of wavelengths and frequencies, is divided into different portions by scientific convention (Fig. 2.1). Major divisions of the electromagnetic spectrum, ranging from short-wavelength, high-frequency waves to long-wavelength, low-frequency waves, include gamma rays, x-rays, ultraviolet (UV) radiation, visible light, infrared (infrared) radiation, microwave radiation, and radiowaves.

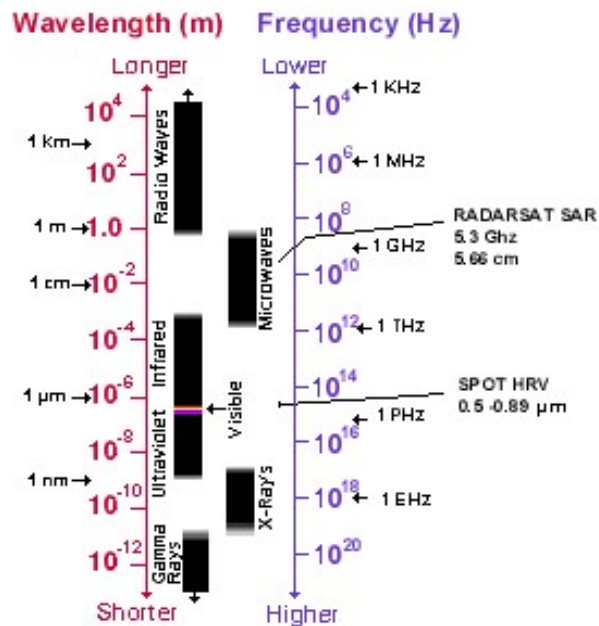


Figure 2.1: The electromagnetic spectrum showing the spectral bands

The visible spectrum, commonly known as the *rainbow of colors* we see as visible light (sunlight), is the portion of the electromagnetic spectrum with wavelengths between 400 and 700 billionths of a meter (0.4–0.7 μm). Although it is a narrow spectrum, the visible spectrum has a great utility in satellite remote sensing and for the identification of different objects by their visible colors in photography.

The infrared spectrum is the region of electromagnetic radiation that extends from the visible region to about 1 mm (in wavelength). Infrared waves can be further partitioned into the near-infrared, mid-infrared, and far-infrared spectrum, which include thermal radiation.

Microwave radiation has a wavelength ranging from approximately 1 mm to 30 mm. Microwaves are emitted from the earth, from objects such as cars and planes, and from the atmosphere. These microwaves can be detected to provide information, such as the temperature of the object that emitted the microwave. Because their wavelengths are so long, the energy available is quite small compared with visible and infrared wavelengths. (Jenson, 2005).

2.2.6.2 Characteristics of Remotely Sensed Data

Data collected by these remote sensing systems can be in either analog format (e.g., hardcopy aerial photography) or digital format (e.g., a matrix of “brightness values” corresponding to the average radiance measured within an image pixel). Digital remote sensing images may be input directly into a GIS for use; analog data also can be used in GIS through an analog-to-digital conversion or by scanning. More often, remote sensing data are first interpreted and analyzed through various methods of information extraction in order to provide needed data layers for GIS. The achievement of data collection from remotely sensed imagery needs an understanding of four basic resolution characteristics, namely, spatial, spectral, radiometric, and temporal resolution. These characteristics are discussed below.

Spatial resolution It refers to the number of pixels utilized in the construction of digital image. It is a measurement of the minimum distance between two objects that will allow them to be distinguished from one another in an image and is a function of sensor altitude, detector size, focal size, and system configuration. Spatial resolution for aerial photography is measured in resolvable line pairs per millimeter, while for other sensors; it refers to the dimensions (in meters) of the ground area that falls within the instantaneous field of view of a single detector within an array or pixel size.

Radiometric resolution: It portrays how well the differences in brightness in an image can be perceived. It refers to the sensitivity of a sensor to incoming radiance. Coarse radiometric resolution would record a scene using only a few brightness levels, that is, at very high contrast, whereas fine radiometric resolution would record the same scene using many brightness levels.

Temporal resolution: It is the amount of time it takes for a sensor to return to a previously imaged location. Therefore, temporal resolution has a significant inference in change

detection and environmental monitoring. Many environmental phenomena constantly change over time, such as vegetation, weather, forest fires, volcanoes, and so on.

2.2.6.3 Remote Sensing Instrumentation

The most common types of remote sensor are radiometers, multispectral scanners, spectrometers, and film camera. The first two convert radiation (photons) emanating from each surface target into electrical signals whose magnitudes are proportional to the spectra radiances in the intervals (bands) sensed. The surface is usually sampled successively, as by a mirror scanning from side to side while the sensor moves forward on its platform. Each pixel provides the collective radiation from the material within it to the record as a single discrete quantity so that the converted signal is a measure of the combined ground target variation from one successive pixel area to the next (Jenson, 2005).

The airborne imaging spectrometer developed by the Jet propulsion laboratory uses a slit to pass radiation from the ground onto a multi-linear array Charge Coupled Detector (CCD) to sense successive area along a moving track. The film camera differs from the sequential sensor types in that it allows the radiation from all surface targets sensed at the same instant to strike the film (recorder) simultaneously in their correct positions as determined by the optics of the system.

Remote sensing as a technology refers to the acquisition of data and derivative information about object, classes or materials located at some distance from the sensors by sampling radiation from selected region (Wave bands) of the electromagnetic (EM) spectrum for sensors mounted on moving platforms (e.g. aircraft and satellites) operating in or above the earth's atmosphere,. The principal sensing regions are in the visible, reflected near- infrared, thermal infrared, and microwave radar regions of the EM spectrum. The particular wavelength (or frequencies) detectable by visible infrared sensors depend in large measure on the extent to which the waveband radiation is absorbed, scattered, or otherwise

modified by the atmosphere (“Windows of transparency” concept). The radiation measured from space platform is usually secondary in that it is reflected or emitted energy generated from molecular interaction between incoming radiation (irradiant) and the earth material being sensed. Because most material absorb radiation over the sensed parts of the Enhanced Thematic Mapper spectrum, only fraction of the incoming radiation are returned to the sensor. Layer of a negative on development are yellow, magenta and cyan, being sensitive to blue, green, and red light respectively. However, when producing a “colour composite” from individual waveband images are needed to make a Multispectral colour composite (Campbell, 2007).

Colour composite photographs can be produced by passing white light successively through a primary colour filter. The red band activates red colour on the film if projected through a red filter. Light tones (clear in a transparency) representing red objects pass red-filtered high onto the film while screening out blue and green filters. The resulting composite is a natural colour photograph. When an infrared band transparency is projected through a red filter, and red and green bands through green and blue filters, respectively, vegetation, in particular, which is highly reflective (very bright) in the infrared, moderately reflective in the green and low in the red because of absorption of red light by chlorophyll, will appear red in the colour composite (little blue and almost no green contribution). Thus, in a false-colour composite, red is almost always a reliable indicator of vegetation (Campbell, 2007).

A set of Multispectral images is produced by breaking the image-forming radiation into discrete spectral intervals through the use of waveband filters (or other light dispersion or selection devices). If a surface material has high reflectance or remittance in some given interval, it will be recorded as a light (bright) tone on a position film-based image conversely, a dark tone represents a low reflectance or emittance. Because the same material normally has varying value of reflectance or emittance in different spectral regions,

it will produce some characteristic gray level (on film) in the image from each particular waveband. Different materials give rise to different gray levels in any set of waveband images, thus creating the varying tonal patterns that spatially define classes, objects or features. Multispectral images of the same scene are characterized by different tonal levels for the various classes from one band to the next (Campbell, 2007).

2.2.7 Application of Landsat Satellite

Landsat data has a wide range of applications which has been proved undoubtedly to be of benefit to humanity. These applications are listed below:

- i. **Geology:** It is used for recognition of rock types, mapping of major geology units, revising geology maps, mapping igneous intrusions, mapping land forms, search for surface guides to mineralization and mapping of lineaments.
- ii. **Environment:** Monitoring surface mining and reclamation, mapping and monitoring of water pollution (e.g. tracing oil spills and pollutants), determination of effects of natural disasters and monitoring environmental effects of man's activities (Lake Entrophication, defoliation etc, are some of the applications in environmental studies).
- iii. **Agriculture, Forestry And Range Resource:** Discrimination of vegetative types; crop types, timber types, range vegetation, determination of range readiness and biomass, determination of vegetation stress, determination of soil conditions and assessment of grass and forest fire damage.
- iv. **Land Use And Mapping:** it is used in the classification of land uses, cartographic mapping and map updating, separation of urban and rural categories (Monitoring urban growth), regional planning, mapping of transportation networks and mapping of land – water boundaries.
- v. **Water Resources:** Landsat data is also used in the determination of water boundaries and surface water area and volume, mapping of floods and flood plains, determination

of the real extent of snow and snow boundaries, determination of water depth and determination of irrigated fields.

2.2.8 Remote Sensing Data Analysis and Interpretation

Remotely sensed data can be used to extract thematic and metric information, making it ready for input into GIS. Thematic information provides descriptive data about Earth surface features. Themes can be as diversified as their areas of interest, such as soil, vegetation, water depth, and land cover. Metric information includes location, height, and their derivatives, such as area, volume, slope angle, and so on. Thematic information can be obtained through visual interpretation of remote sensing images (including photographs) or computer based digital image analysis. Metric information is extracted by using the principles of photogrammetry.

2.2.8.1 Photographic/Image Interpretation and Photogrammetry

Photographic interpretation can be defined as the process of examining aerial photographs/images for the purpose of identifying objects and judging their significance (Colwell, 1997). The activities of aerial photo/image interpreters may include: detection/identification, measurement, and problem solving.

In the process of detection and identification, the interpreter identifies objects, features, phenomena, and processes in the photograph and conveys his or her response by labeling. These labels are often expressed in qualitative terms, for example, *likely*, *possible*, *probable*, or *certain*. The interpreter also may need to make quantitative measurements. Techniques used by the interpreter typically are not as precise as those employed by photogrammetrists. At the stage of problem solving, the interpreter identifies objects from a study of associated objects or complexes of objects from an analysis of their component

objects, and this also may involve examining the effect of some process and suggesting a possible cause.

The elements used commonly in photographic/image interpretation are: tone/color, size, shape, texture, pattern, shadow, and association. Tone/color is the most important element in photographic/image interpretation.

- i. **Tone:** It is the specific quality of brightness, deepness, or hue of a tint, or shade of a color. It refers to each discernible variation from white to black and is a record of light reflection from the land surface onto the film. The more light received, the lighter is the image on the photograph.
- ii. **Color:** It is the property possessed by an object of producing different sensations on the eye as a result of the way it reflects or emits light. It refers to each distinguishable variation on an image produced by a multitude of combinations of hue, value, and chroma.
- iii. **Size:** It is the relative extent of something; something's overall dimensions or magnitude; how big something is. It provides another important clue in discrimination of objects and features. Both the relative and absolute sizes of objects are important. An interpreter also should judge the significance of objects and features by relating to their background.
- iv. **Shape:** It is the external form or characteristic of something. The shapes of objects/features can provide diagnostic clues in identification. It is worthy to note that human-made features often have straight edges, whereas natural features tend not to
- v. **Texture:** It is the frequency of change and arrangement in tones. The visual impression of smoothness or roughness of an area often can be a valuable clue in

image interpretation. For example, water bodies typically are finely textured, whereas grass is medium and bush is rough, although there are always exceptions.

- vi. **Pattern:** It is the spatial arrangement of objects. It is the regular arrangement of objects that can be diagnostic of features on the landscape. Human-made and natural patterns are often very different. Pattern also reveals a great deal of information about the lithology and structural patterns in an area.
- vii. **Shadow:** It relates to the size and shape of an object. Geologists like low-sun-angle photography because shadow patterns can help to identify objects. Steeples and smoke stacks can cast shadows that can facilitate interpretation.

2.2.8.2 Digital Image Pre-processing

In digital analysis of remotely sensed data, the basic elements of image interpretation, although developed initially based on aerial photographs, also should be applicable to digital images. However, most digital image analysis methods are based on tone or color, which is represented as a digital number (i.e., brightness value) in each pixel of the digital image. As multisensor and high spatial resolution data have become available, texture has been used in image classification, as well as contextual information, which describes the association of neighboring pixel values. Before main image analyses take place, preprocessing of digital images often is required. Image preprocessing may include detection and restoration of bad lines, geometric rectification or image registration, radiometric calibration and atmospheric correction, and topographic correction.

Geometric correction and atmospheric calibration are the most important steps in image preprocessing. *Geometric correction* corrects systemic and nonsystematic errors in the remote sensing system and during image acquisition (Lo and Yeung, 2002). It commonly involves

- i. *Digital rectification*, a process by which the geometry of an image is made planimetric, and
- ii. *Resampling*, a process of extrapolating data values to a new grid by using such algorithms as nearest neighbor, bilinear, and cubic convolution.

Accurate geometric rectification or image registration of remotely sensed data is a prerequisite, and many textbooks and articles have described them with details (e.g., Jensen, 2005).

2.2.8.3 Image Enhancement and Feature Extraction

Image-enhancement methods can be roughly grouped into three categories: contrast enhancement, spatial enhancement, and spectral transformation. They are applied to enhance visual interpretability of remotely sensed data as well as to facilitate subsequent thematic information extraction.

- i. ***Contrast enhancement:*** This involves changing the original values so that more of the available range of digital values is used, and the contrast between targets and their backgrounds is increased (Jensen, 2005).
- ii. ***Spatial enhancement:*** It applies various algorithms, such as spatial filtering, edge enhancement, and Fourier analysis, to enhance low- or high-frequency components, edges, and textures.
- iii. ***Spectral transformation:*** This refers to the manipulation of multiple bands of data to generate more useful information and involves such methods as band rationing and differencing, principal components analysis, vegetation indices, and so on.

Feature extraction is often an essential step for subsequent thematic information extraction. Many potential variables may be used in image classification, including spectral signatures, vegetation indices, transformed images, textural or contextual information,

multitemporal images, multisensor images, and ancillary data. Because of different capabilities in class separability, use of too many variables in a classification procedure may decrease classification accuracy (Price *et al.*, 2002). It is important to select only the variables that are most effective for separating thematic classes. Selection of a suitable feature extraction approach is especially necessary when hyperspectral data are used. This is so because the huge amount of data and the high correlations that exist among the bands of hyperspectral imagery and the large number of training samples required in image classification. Many feature-extraction approaches have been developed, including principal components analysis, minimum-noise fraction transform, discriminant analysis, decision-boundary feature extraction, nonparametric weighted-feature extraction, wavelet transform, and spectral mixture analysis (Neville *et al.*, 2003; Rashed *et al.*, 2001).

2.2.8.4 Image Classification

The objective of image classification is to assign all pixels in the image to particular classes or themes (e.g., water, forest, residential, commercial, etc.) and to generate a thematic “map”. Image classification uses spectral information represented by digital numbers in one or more spectral bands and attempts to classify each individual pixel based on the spectral information. The former refers to the categories of interest that the analyst is actually trying to identify from the imagery, and the latter refers to the groups of pixels that are uniform (or near alike) with respect to their brightness values in the different spectral channels of the data. Generally, there are two approaches to image classification: supervised and unsupervised classification.

- i. **Supervised classification:** Here, the analyst identifies in the imagery homogeneous representative samples of different cover types (i.e., information classes) of interest to be used as training areas. Each pixel in the imagery then would be compared spectrally with the training samples to determine to which information class they

should belong. Supervised classification employs such algorithms as minimum-distance-to-means, parallelepiped, and maximum likelihood classifiers (Lillesand *et al.*, 2008).

- ii. **Unsupervised classification:** here, spectral classes are first grouped based solely on digital numbers in the imagery, which then are matched by the analyst to information classes. The objective is to group multiband spectral response patterns into clusters that are statistically separable. Thus, a small range of digital numbers (DNs) can establish one cluster that is set apart from a specified range combination for another cluster (and so forth). The logic or steps involved in the two methods of classification can be grasped from these flow diagrams:

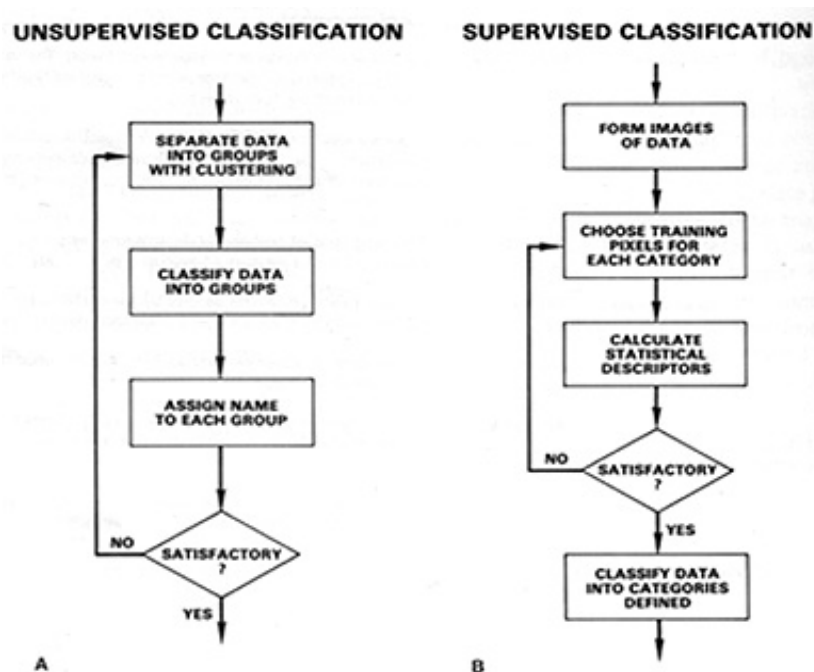


Figure 2.2: Flow Diagrams for (A) unsupervised and (B) supervised Image Classification

CHAPTER THREE

METHODOLOGY

3.1 Aeromagnetic Data Source

The aeromagnetic maps used for the study were obtained from the Geological Survey of Nigeria (NGSA 2011). The data were acquired and compiled by FAIREY SURVEYS LTD during an airborne geophysical survey in 2011. Unlike the data acquired in 1974 by the Geological Survey of Nigeria (at nominal flight height of 152.4 m, along N-S flight lines that were spaced at 2 Km interval), which will not yield much deductions, because the data only represent anomalies greater than 4km (twice spatial sample interval, because of aliasing effect) and the interpretation techniques used were ancient. This data is high resolution. The nominal flight height of 76m along N-S flight lines spaced at 500m interval using advanced equipments with far higher resolution was used. The geomagnetic gradient was removed from the data using the International Geomagnetic Reference Field (IGRF). In this study, the digitizing process follows the basic acquired data along flight lines drawn on the map and the obtained data are shown as coloured filled contour maps. The data was made in form of contoured maps on a scale of 1:100,000.

3.2 Remote Sensing Data Source

The seven-band Landsat 5 Thematic Mapper image acquired on the 17th of December, 2000, belongs to a scene with Path number 188 and Row number 56 was obtained from the earth Science Data Interface (ESDI) of the National Aeronautic and Space Agency (NASA). A Shuttle Radar Topographic Mission (SRTM) image of the same area was also obtained and a Shell 1:250,000 geologic map of the Study area was re-digitized.

3.2.1 Aeromagnetic Data Analysis

Interpretation of the aeromagnetic survey data aims to map the surface and subsurface regional structures (e.g., faults, contacts, bodies and mineralization).

Aeromagnetic data are mostly analyzed in these processes: Aeromagnetic data filtration (upward and/ or downward continuation, Reduction to pole, vertical derivatives, etc), Regional - Residual Separation, and Depth estimation analysis.

3.2.1.1 Regional-Residual Separation

The distinction between the regional and residual is somewhat arbitrary but the regional component can be thought of as the response of bodies large and/or deep compared with respect to the study area and, therefore, not readily interpretable within the bounds of the study area. To separate the regional field, a regional (or *low pass*) filter could be multiplied point-by point with the spectrum where low wave numbers are passed, high wave numbers rejected, with an approximately Gaussian *roll-off* between them to minimize *ringing* (also known as Gibb's phenomena) when the output is reverse-transformed to the space domain.

The complement of the low-pass regional filter is the *high pass* or *residual* filter. The residual grid may be obtained either by applying such a filter in the wave number domain, or by subtracting the regional field from the original data grid. In practical cases, the residual filter would usually be designed to roll-off again at wave numbers corresponding to noise so that noise could be eliminated simultaneously. The filter then becomes a *band-pass* filter, retaining only information from a range of wave numbers considered important for the study of the residual anomalies at hand.

For this study, the regional gradients of the aeromagnetic data were removed by polynomial fitting, this involved fitting a plane surface to the data by using multi-regression least squares analysis. The expression obtained for the regional field T(R) is given as:

$$T(R) = 76122.158 + 0.371x + 0.248y \quad (3.1)$$

where x and y are units of spacing. The regional field values are subtracted from the observed data to obtain the residual anomaly values. The technique is carried out on the

aeromagnetic data of the study area to produce the first to fourth residual and regional trend surfaces.

3.2.1.2 Reduction to Pole

The reduction to pole filtering process removes the effect of the earth's magnetic field by way of a gross shift of the observed magnetic readings. The procedure is nothing more than a correction factor applied across the study area to remove the non vertical magnetic component (the earth's magnetic field) and leave only the vertical component (causative body) in its correct spatial position. The RTP filtering was performed on the digitized aeromagnetic data of the study area via fast Fourier filtering using Oasis Montaj 6.4 program in order to remove the dipolar nature of the magnetic field.

3.2.1.3 Continuation Filtering

A potential field measured on a given observation plane at a constant height can be recalculated as though the observations were made on a different plane, either higher (upward continuation) or lower (downward continuation). The equation of the wave number domain filter to produce *upward* continuation is simply:

$$F(\omega) = e^{-h\omega} \quad (3.2)$$

where h is the continuation height. This function decays steadily with increasing wave number, attenuating the higher wave numbers more severely, thus producing a map in which the more regional features predominate.

The equation of the wave number domain filter to produce *downward* continuation is

$$F(\omega) = e^{h\omega} \quad (3.3)$$

This is a curve which is zero at zero wave number and increases exponentially at higher wave numbers, thus emphasizing the effect of shallow sources - and noise! Noise removal is thus an essential first step before downward continuation, and continuation depths should

not exceed real source depths. Some careful experimentation is usually necessary to obtain acceptable results (Reeves, 2005).

An upward continuation filtering of 1000m, 2000m, 3000m and 4000m were done on the aeromagnetic data to enhance the target anomalies.

3.2.1.4 Magnetic Depth Estimation

Often one of the most useful pieces of information to be obtained from aeromagnetic data is the *depth* of the magnetic source (or rock body). Since the source is usually located in the so-called 'magnetic basement' (i.e. the igneous and metamorphic rocks lying below the - assumed non-magnetic - sediments), this depth is also an estimate of the thickness of the overlying sediments. Sufficient depth estimates from a large number of magnetic sources allow the depth of the basement to be contoured and this is then a rough isopach map of the sediments.

For this reason, several methods have evolved in the early days of magnetic interpretation simply to estimate the depth of sources from their anomalies without reference to any specific source models

The methods of magnetic depth estimation were employed in this study, they include, Spectral Methods and 3D Euler Deconvolution Method.

3.2.1.4.1 Spectral Analysis

One of the main researches on magnetic anomaly maps is to estimate depth of the buried objects causing the anomaly. In the interpretation of magnetic anomalies by means of local power spectra, there are three main parameters to be considered. These are depth, thickness and magnetization of the disturbing bodies. It is necessary to define the power spectrum of a magnetic anomaly in relation to the average depth of the disturbing interface. The method of using spectral analysis in depth determination is based on the principle that a

magnetic field measured at the surface can be considered the integral of magnetic signatures from all depths. The power spectrum computes the thickness of the sedimentary basin and that of the crustal Moho depth (Spector and Grant, 1970). This same technique can be used to attempt identification of the characteristic depth of the magnetic basement, on a moving data window basis, merely by selecting the steepest and therefore deepest straight-line segment of the power spectrum, assuming that this part of the spectrum is sourced consistently by basement surface magnetic contrasts. A depth solution is calculated from the power spectrum derived from each grid sub-set, and is located at the centre of the window. Overlapping the windows creates a regular, comprehensive set of depth estimates.

The logarithm of the power of the signal at each wavelength can be plotted against wavelength, regardless of direction, to produce a power spectrum. A potential field grid may be considered to represent a series of components of different wavelength and direction. Most approaches used involve Fourier transformation of the digitized aeromagnetic data to compute the energy (or amplitude) spectrum. This is plotted on the Logarithmic scale against frequency. The plot shows the straight line segments which decrease in slope with increasing frequency. The slopes of the segments yield estimates of depths to magnetic sources. The application of spectral analysis to the interpretation of aeromagnetic anomalies is now sufficiently well established (Bhattacharyya, 1966; Spector and Grant, 1970; Mishra).

Given a residual magnetic anomaly map of dimension $L \times L$ digitized at equal intervals, the residual intervals, and total intensity anomaly values can be expressed in terms of double Fourier series expansion which is given by:

$$T(x, y) = \sum_{n=1}^N \sum_{m=1}^M P_m^n \cos\left(\frac{2\pi}{L}(nx + my)\right) + Q_m^n \sin\left[\left(\frac{2\pi}{L}\right)(nx + my)\right] \quad (3.4)$$

where: l is the dimension of the block, P_m^n, Q_m^n is the Fourier amplitude and N, M represent the number of grid points along the x and y directions respectively.

Equation (3.4) can be combined into a single partial wave thus:

$$P_m^n \cos\left[\left(\frac{2\pi}{L}\right)(nx + my)\right] + Q_m^n \sin\left[\left(\frac{2\pi}{L}\right)(nx + my)\right] = C_m^n \cos\left[\left(\frac{2\pi}{L}\right)(nx + my) - \delta_m^n\right] \quad (3.5)$$

$$\text{where } (P_m^n)^2 + (Q_m^n)^2 = (C_m^n)^2 \quad (3.6)$$

and δ_m^n is the appropriate phase angle.

Each (C_m^n) is the amplitude of the partial wave.

The frequency of this wave is given by: $F_m^n = \sqrt{n^2 + m^2}$ Similarly, using the complex form, the two dimensional Fourier transform pair may be written (Bhattacharryya, 1966; Bath, 1974)

$$G(U, V) = \int_{-\infty}^{\infty} \int_{-\infty}^{\infty} g(x, y) e^{-j(ux + vy)} dx dy \quad (3.7)$$

$$g(x, y) = \frac{1}{4\pi^2} \int_{-\infty}^{\infty} \int_{-\infty}^{\infty} G(U, V) e^{-j(ux + vy)} dx dy \quad (3.8)$$

where u and v are the angular frequencies in the x and y directions respectively.

G (u,v) when broken up into its real and imaginary parts is given by

$$G(u, v) = P(u, v) + jQ(u, v) \quad (3.9)$$

The energy density spectrum or simply the energy spectrum is

$$E(u, v) = |G(u, v)|^2 = P^2 + Q^2 \quad (3.10)$$

The Fourier transform of a section of a magnetic map digitized in a square grid therefore forms a rectangular matrix of coefficients which can be reduced to a set of average amplitude dependent only on the frequency (Hahn et al., 1976). These average amplitudes fully present a spectrum from which the depths to magnetic sources can be estimated. Residual total magnetic field intensity values are used to obtain the two dimensional Fourier

transforms from which the spectrum is to be extracted. From the residual values $\Delta T(x, y)$ the two dimensional Fourier transform is conducted.

Next the frequency intervals are subdivided into subintervals which lie within one unit of frequency range. The average spectrum of the entire partial wave falling within this frequency range is calculated and the resulting values together constitute the radial spectrum of the anomalous field. A plot of the logarithm of the energy values versus frequency consists of linear segments each of which group points in respect to anomalies caused by bodies occurring within a particular depth. If Z is the mean depth of a layer, the depth factor for this ensemble of anomalies is $\exp(-2ZK)$, where K is the magnetic moment per depth (Spector and Grant, 1970). Thus Logarithmic plot of the radial spectrum would give a straight line whose slope is $2Z$.

Spectral method involved some practical problems mostly inherent in the application of the discrete Fourier transform (DFT). These include the problems of aliasing, truncating effect or Gibb's phenomenon and the problems associated with the even and odd symmetries of the real and imaginary parts of the Fourier transform. The aliasing effect arises from the ambiguity in the frequency represented by the sampled data. Frequencies greater than the Nyquist frequencies, tend to impersonate the lower frequencies and this is known as the aliasing effect. To avoid or reduce the effect of aliasing, the frequencies greater than the Nyquist frequency must be removed through the use of an alias filter, which provides high attenuation above the Nyquist frequency. When a limited portion of the aeromagnetic anomaly is subjected to Fourier synthesis, it is difficult to reconstruct the sharp edges of the anomaly with a limited number of frequencies and this truncation leads to the introduction of spurious oscillations around the region of discontinuity. This is known as Gibb's phenomenon. An effective approach to reducing the problem of Gibb's

phenomenon is by the application of a cosine taper to the observed data (Bath,1974; Kanasewich,1975).

However, in this research, the solution to the problems associated with aliasing and truncation or Gibb's phenomenon, have been taken care of by the oasis montaj software. An alias filter has been incorporated into the computer program to reduce the aliasing effect and a cosine taper has been applied to the data to reduce the effects of truncation.

3.2.1.4.2 3D Euler Deconvolution

The Standard 3D Euler method is based on Euler's homogeneity equation, which relates the potential Field (magnetic or gravity) and its gradient components to the location of the sources, by the degree of homogeneity N , which can be interpreted as a structural index (Thompson, 1982). Euler deconvolution is a procedure applied to profile or gridded potential field data to solve Euler's homogenous equation for the locations and depths of sources for an assumed Euler structural index. The method makes use of a structural index in addition to producing depth estimates.

The objective of the 3D Euler deconvolution process is to produce a map showing the locations and the corresponding depth estimations of geologic sources of magnetic or gravimetric anomalies in a two-dimensional grid (Reid et al., 1990). In combination, the structural index and the depth estimates have the potential to identify and calculate depth estimates for a variety of geologic structures such as faults, magnetic contacts, dykes, sills, etc. The algorithm uses a least squares method to solve Euler's equation simultaneously for each grid position within a sub-grid (window). A square window of predefined dimensions (number of grid cells) is moved over the grid along each row. At each grid point a system of equations is solved, from which the four unknowns (x , y as location in the grid, z as depth estimation and the background value) and their uncertainties (standard deviation) are obtained for a given structural index. A solution is only recorded if the depth uncertainty of

the calculated depth estimate is less than a specified threshold and the location of the solution is within a limiting distance from the center of the data window (Whitehead and Musselman, 2008).

Thompson (1982) showed that for any homogenous, three-dimensional function $f(x; y; z)$ of degree n :

$$f(tx; ty; tz) = t^n f(x; y; z) \quad (3.11)$$

It can be shown that, the following equation, which is known as Euler's homogeneity relation can be satisfied:

$$x \frac{\delta f}{\delta x} + y \frac{\delta f}{\delta y} + z \frac{\delta f}{\delta z} = n f \quad (3.12)$$

In geophysics, the function $f(x,y,z)$ can have the general functional form:

$$f(x, y, z) = \frac{G}{r^N} \quad (3.13)$$

where $r^2 = (x - x_0)^2 + (y - y_0)^2 + (z - z_0)^2$, N is a real number (1, 2, 3...) and G is a constant (independent of x, y, z). Many simple point magnetic sources can be described by equation (3.13), where $(x_0; y_0; z_0)$ is the position of the source whose field F is measured. The parameter N is dependent on the source geometry, a measure of the fall-off rate of the field and may be interpreted as the structural index (SI). Clearly equation (3.13) is homogeneous and thus N is equivalent to $-n$ in Euler's equation (3.12).

Considering potential field data, Euler's equation can be written as:

$$(x - x_0) \frac{\delta T}{\delta x} + (y - y_0) \frac{\delta T}{\delta y} + (z - z_0) \frac{\delta T}{\delta z} = N(B - T) \quad (3.14)$$

Where B is the regional value of the total magnetic field and $(x_0; y_0; z_0)$ is the position of the magnetic source, which produces the total field T measured at $(x; y; z)$.

Thompson (1982) showed that simple magnetic and gravimetric models are consistent with Euler's homogeneity equation. Thus 3-D Euler Deconvolution provides an excellent tool for providing good depth estimations and locations of various magnetic sources in a given area, assuming that appropriate parameter selections are made (Reid et al., 1990).

The 3D Euler process is a fast method for obtaining depth and boundary solutions of magnetic sources for large areas in aeromagnetic surveys. Though it is a general advantage of the Euler Deconvolution method, that it is applicable to all geologic models and that it is insensitive to magnetic remanence and geomagnetic inclination and declination, an initial assumption of the source type has to be made (Reids et al., 1990; Thompson, 1982). Depending on the potential source type, a structural index is chosen. This structural index is also a measure of the distinctive fall-off rate of the geologic feature. Table 3.1 summarizes the structural indices (SI) for given geologic models. The number of infinite dimensions describes the extension of the geologic model in space.

Table 3.1: Structural Indices for Simple Magnetic Models Used For Depth Estimations by 3D Euler Deconvolution (Reids, 1990; Thompson, 1982).

Geologic Model	Number of Infinite Dimension	Magnetic Structural Index
Sphere	0	3
Pipe	1 (z)	2
Horizontal cylinder	1 (x-y)	2
Dyke	2 (z and x-y)	1
Sill	2 (x and y)	1
Contact	3 (x,y,z)	0

The significance of the location and depth estimates obtained by 3-D Euler Deconvolution is given by the specificity of the chosen parameters like the grid cell size, window size, structural index, chosen depth uncertainty tolerance, etc. The selection of the grid cell size should be based on the grid spacing and the wavelength of the anomalies to be analyzed, as the software Geosoft Oasis Montaj allows a square window size of up to 20 grid cell units. If the wavelengths of the anomalies are significantly longer or shorter than the window size, the 3D Euler method does not yield appropriate results. On the other hand, the limiting distance from the centre of the algorithm window, in which solutions are still recorded, should be chosen with respect to the wavelength of potential anomalies.

In general, 3D Euler Deconvolution yields results for each window position; therefore it is necessary to eliminate solutions with high uncertainties. A reliable tool for the limitation of results is the specification of a threshold value for depth and horizontal uncertainties. Geosoft Oasis Montaj presents the depth and location uncertainties as percentage of the depth below the recording sensor position. As a matter of principle, low SI values are associated with source bodies which give rise to low gradients, thus depth estimation solutions with low SI values have high uncertainties. The data quality determines the general level of uncertainty, so an examination of the recorded solutions will define the selection criteria.

The results of the Euler method are displayed in ordinary maps as point solutions combining the location (position of solution) and the depth (colour range). Given the choice of an appropriate structural index, 3D Euler Deconvolution will lead to a clustering of solutions, which can be interpreted. A vertical pipe structure will for example be shown as a cluster of solutions around a specific point, whereas an elongated dyke structure will be recognized as a linear trend of solutions. Another approach to limit the solutions obtained by

the Euler method is the Located Euler 3D method, which, unlike the Standard Euler method, tests and limits grid locations before calculating depth estimations by Euler deconvolution.

3.2.1.5 Curie Point Depth Estimation

Much attention has been given to the spatial variation in the temperature to know the thermal structure of the earth. In determining temperature variations, heat flow is the primary observable quantity. Since the obtained heat flow values may reflect local thermal anomalies and their measurements are distributed geographically unevenly, it is often insufficient to define regional thermal structures. Furthermore, determination of the Curie point depth based on spectrum analysis of magnetic anomaly data (e.g., Spector and Grant, 1970; Bhattacharyya and Leu, 1975) can be used to estimate regional thermal structures. This method is for a reconnaissance survey. The Curie point depth is the depth at which rocks in an area encounters curie temperature. This curie temperature is the temperature at which certain magnetic materials undergo sharp change in their magnetic properties (their permanent magnetism changes to induced magnetism). The obtained basal depth of a magnetic source is assumed to be the Curie point depth. The Curie point temperature is still controversial. It may depend upon composition and there are some problems on accuracy and resolution of the results. However, the Curie point depths should reflect the broad average temperature and they have been used to estimate the thermal structure in various regions (e.g., Bhattacharyya and Leu, 1975).

The methods for estimating the Curie depth have been classified into two categories: those that examine the shape of isolated magnetic anomalies (Bhattacharyya and Leu, 1975) and those that examine the patterns of the anomalies (Spector and Grant, 1970). However, both methods provide the relationship between the spectrum of the magnetic anomalies and the depth of a magnetic source by transforming the spatial data into frequency domain. In this study, the method adopted is the latter in which the top boundary Z_t and the Centroid of

magnetic sources Z_0 were calculated from the spectrum of magnetic anomalies and are used to estimate the basal depth Z_b of magnetic source.

Blakely (1995) while assuming that the layer extends infinitely far in all horizontal directions, Z_t is small compared with the horizontal scale of a magnetic source, and that magnetization $M(x, y)$ is a random function of x and y , introduced the radially averaged power-density spectra of the total-field anomaly ϕ_T :

$$\phi_T(|s|) = A_1 e^{-2|s|Z_t} (1 - e^{-|k|(Z_b - Z_t)})^2 \quad (3.15)$$

where A_1 is a constant and $|s|$ is the wave number. For wavelengths less than about twice the thickness of the layer, Eq. 3.15 approximately becomes:

$$\ln[\phi_T(|s|)^{1/2}] = \ln A_2 - |s|Z_t \quad (3.16)$$

where A_2 is a constant. We could estimate the top bound of a magnetic source by the slope of the power spectrum of the total-field anomaly.

On the other hand, Eq. 3.15 rewrites as:

$$\phi_T(|s|)^{1/2} = A_3 e^{-|s|Z_0} (e^{-|k|(Z_t - Z_0)} - e^{-|k|(Z_b - Z_0)}) \quad (3.17)$$

where A_1 is a constant. At long wavelengths, Eq. 3.17 is:

$$\phi_T(|s|)^{1/2} = A_3 e^{-|s|Z_0} (e^{-|k|(-d)} - e^{-|k|(d)}) \sim A_3 e^{-|s|Z_0} 2|s|d \quad (3.18)$$

where $2d$ is the thickness of the magnetic source. From Eq. 3.18,

$$\ln\{[\phi_T(|s|)^{1/2}]/|s|\} = \ln A_4 - |s|Z_0 \quad (3.19)$$

where A_4 is a constant. Estimate of the top bound and the centroid of the magnetic source could be done by fitting a straight line through the high-wavenumber and low-wave number parts of the radially averaged spectrum of Eqs. 3.16 and 3.19 respectively.

Then, the basal depth (Z_b) of the magnetic source was calculated from the equation:

$$Z_b = 2Z_0 - Z_t \quad (3.20)$$

The obtained basal depth (Z_b) of magnetic sources in the study area is assumed to be the Curie point depth (Bhattacharyya and Leu, 1975) and the graphs of the logarithms of the spectral energies for various blocks using the Oasis Montaj were obtained.

Estimation of Heat Flow and Thermal Gradient

In the absence of heat flow data in the study area, we use an empirical relation which is a one-dimensional heat conductive transport model is used to estimate heat flow and geothermal gradient. The model is based on Fourier's law. In one dimensional case under assumptions, the direction of temperature variation is vertical and the temperature gradient dT/dZ is assumed constant, Fourier's law then takes the form:

$$q = \lambda \{dT/dZ\} = 2.5Wm^{-1}C^{-1} \{dT/dZ\} \quad (3.21)$$

Where q is the heat flow and λ is the coefficient of thermal conductivity.

According to Tanaka, *et al*, (1999), the Curie temperature (θ_c) can then be defined as

$$\theta = [dT/dZ]Z_b \quad (3.22)$$

In addition to that, from Equation (3.21) and Equation (3.22) a relationship was determined between the Curie point depth (Z_b) and the heat flow (q) as follows.

$$q = \lambda [580^\circ C/Z_b] \quad (3.23)$$

It is evident that Curie point depth is inversely proportional to the heat flow, thus estimate of the heat flow (q) in the study area was made using equation (3.23). We also computed the thermal gradient from Equation (3.22) using a Curie point temperature of $580^\circ C$ and thermal conductivity of $2.5Wm^{-1}C^{-1}$ (Stacey and Banerjee, 1974).

However, using an average thermal conductivity, value of $2.5Wm^{-1}C^{-1}$ (Tanaka et al 1999), we then calculate the value for geothermal gradient in the study area using the empirical relation between, curie depth, Temperature and geothermal gradient (equation 3.22).

3.2.2 Remote Sensing Data Analysis and Interpretation

The Landsat 5 Thematic Mapper data obtained was subjected to various image enhancement and transformation routines. For the image transformation, band ratios were

generated using calculator module in IDRISI32. The ratios generated (3/4, 4/2, 3/1, 5/4) were employed to reduce the effects of shadowing as well as enhance the detection of certain features/ materials. For the image enhancement, 3 band RGB colour composites were created using the composite module of IDRISI32. This process was employed to enhance the spectral quality of the images. Generated composites include RGB 321, RGB 432, and RGB 541 as well as NDVI (Normalized Difference Vegetation Index).

The ratios generated were studied in detail and information extracted along with those obtained from Digital Elevation Model (DEM) was attributed to colour patterns observed from the Colour composites. The Resulting Data obtained was employed in the classification of the images.

For the purpose of this study, the maximum likelihood classification of IDRISI32 was utilized to perform supervised classification and it involved the following steps:

- i. Training sites were established on composites and digitized with polygons.
- ii. Particular spectral signatures were assigned to each training site using the MAKESIG module in IDRISI32 (which analyzes the pixels within each training site before assigning spectral signatures.
- iii. Classification of the entire image was then embarked on after assigning particular probability values for each signature using the MAXLIKE module in IDRISI32.

Information obtained from the classified images, colour composites as well as the DEM of the Study area were combined in generating a new geologic map for the area.

CHAPTER FOUR

RESULTS AND DISCUSSION

4.1 AEROMAGNETIC METHOD

4.2.1 Total Magnetic Intensity (TMI) Map

The total magnetic field intensity map presented as total field intensity map, image map, basement surface map and relief map (Fig.4.1- 4.8) are shown in this section. From these figures, magnetic anomalies of both short and long wavelengths were interpreted within the study area. These interpreted anomalies are represented by magnetic highs and lows respectively.

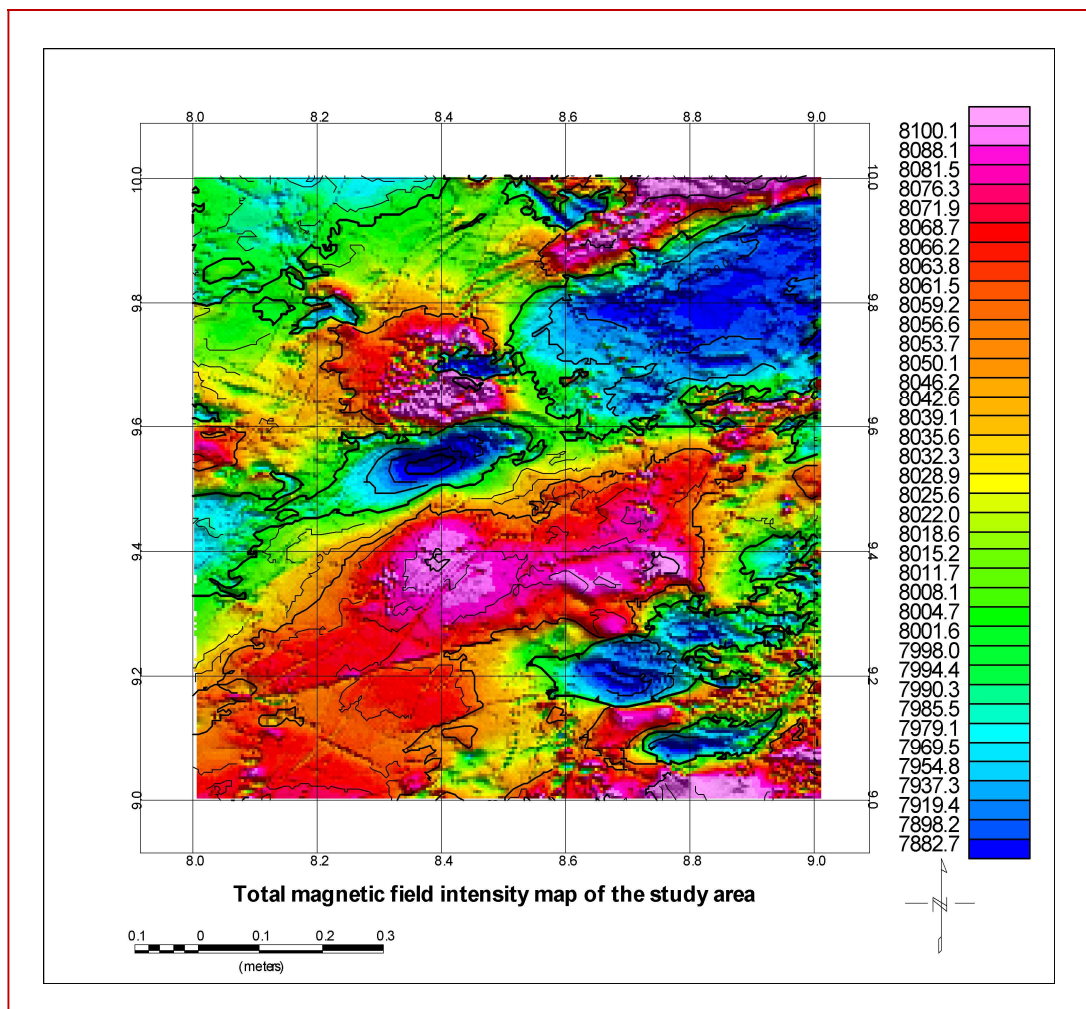


Fig. 4.1: Aeromagnetic Field over the Study Area as a Colour Shaded contoured Map

The total field of the aeromagnetic data revealed that the underlying basement within Bukuru, Kagoro and Jos are represented by magnetic intensities ranging from 7882 to 7937 gammas. This area has a broad magnetic anomaly with very low relief and low total magnetic intensity values surrounded by areas with high total magnetic intensity values and are therefore interpreted as resulting possibly from basement subsidence.

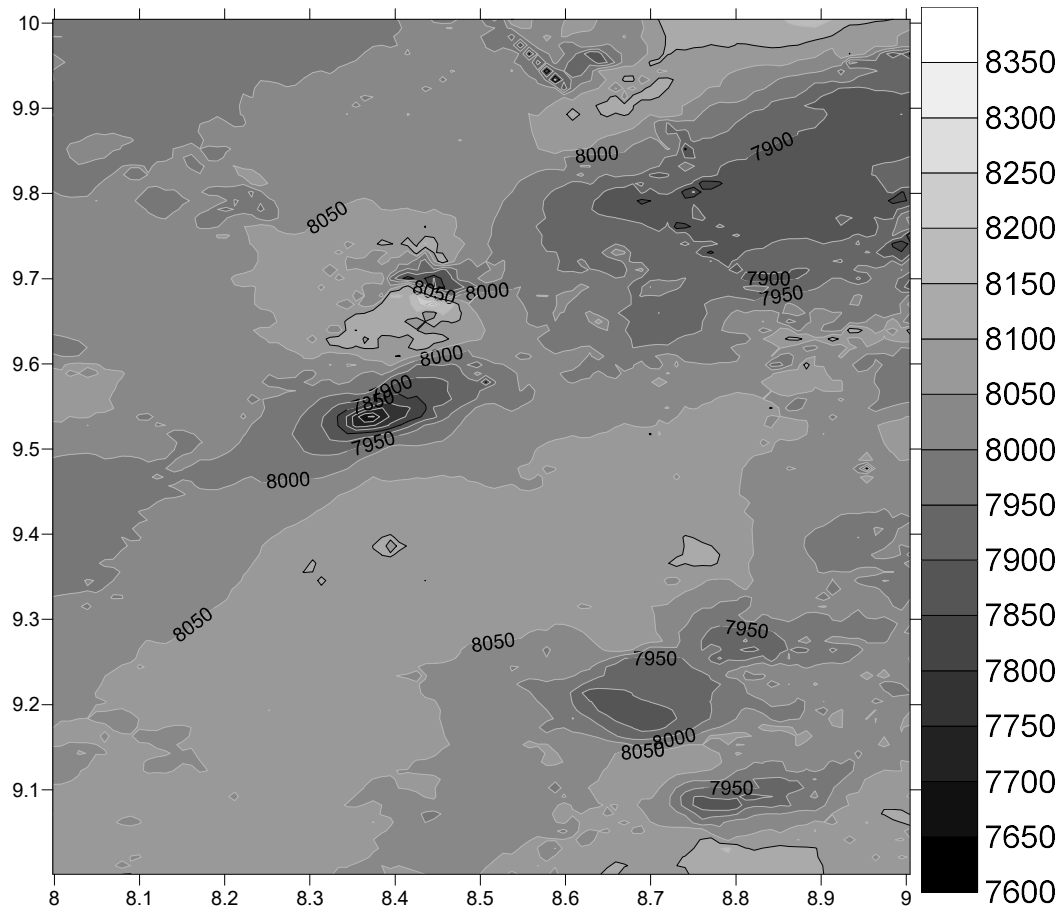


fig 4.2: Shaded Relief Map of Total Field

The high frequency anomalies are concentrated mainly within the central part of the study area with a conspicuous elongated NE-SW trend. Areas of high magnetic intensity values could be as a result of magmatic uplift or igneous intrusion towards the earth's surface. These major magnetic highs (closures) which cover most of the areas of Gwantu, Kafanchan, and Fadank are interpreted as linear magnetic features. The isolated high magnetic field represented by circular contours with magnetic intensity values of between

8050γ to 8150γ (see Figure.4.4) located in the eastern part of the study area is indicative of an intrusion. Intrusions are most often described on aeromagnetic maps as high magnetic anomalous region with elliptical or circular contours (Akanbi and Udensi, 2006). This intrusive body intruded into the surfaciale sedimentary overburden and is believed to contain aggregate mineral deposits.

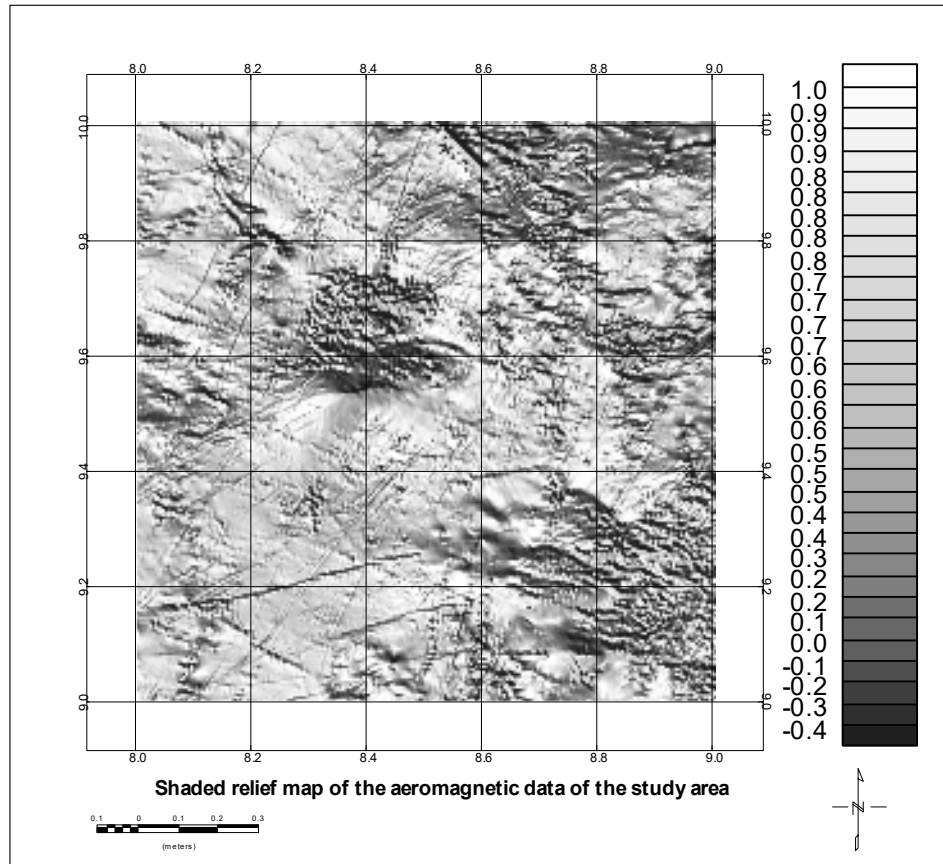


Fig 4.3: Shaded relief map of the aeromagnetic data of the study area.

Figure 4.3 shows the basement topography of the area as highs and lows. The basement relief of the study area does not show the correlation that the total intensity values are increasing with the altitude. Two prominent linear features of relatively low relief could be observed in the study area around Kafanchan and Miango.

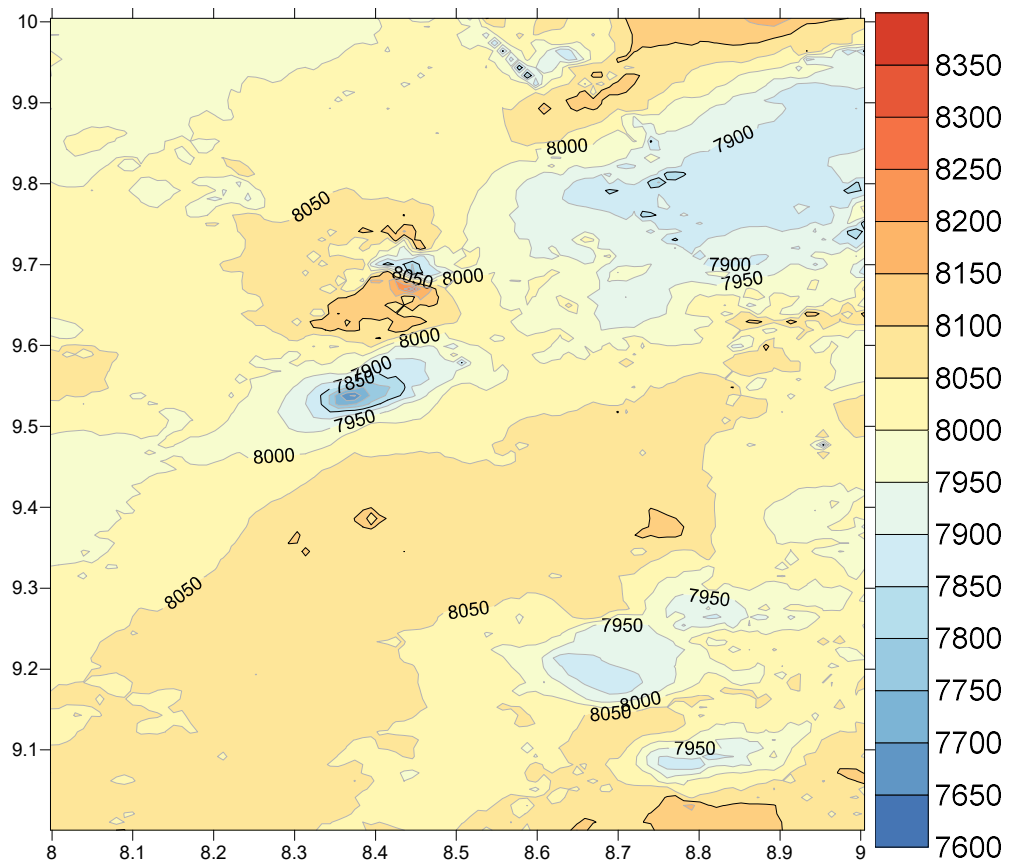


Fig 4.4: Colour Image Map (Pixel Map) of the Aeromagnetic Data

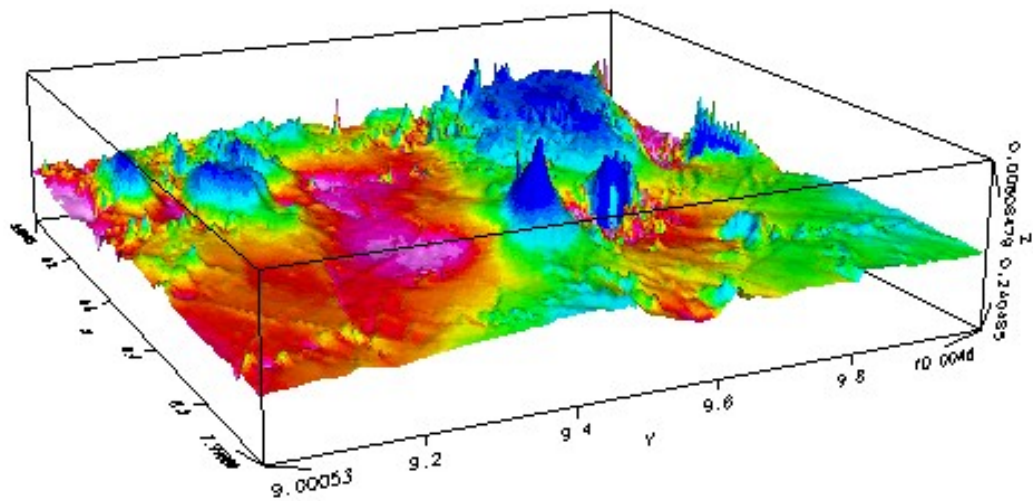


Fig.4.5: 3-D Map of the Total Magnetic Field of the Aeromagnetic Data

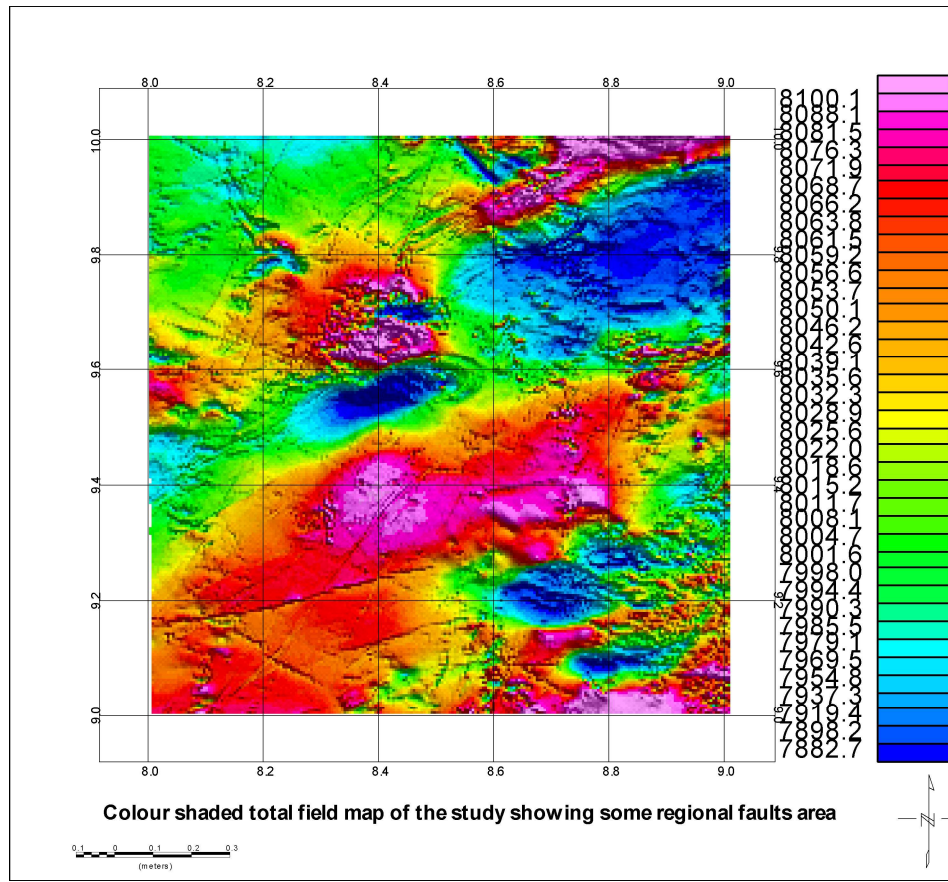


Fig.4.6: Colour shaded total field map of the study area showing some of the areas with regional faults area.

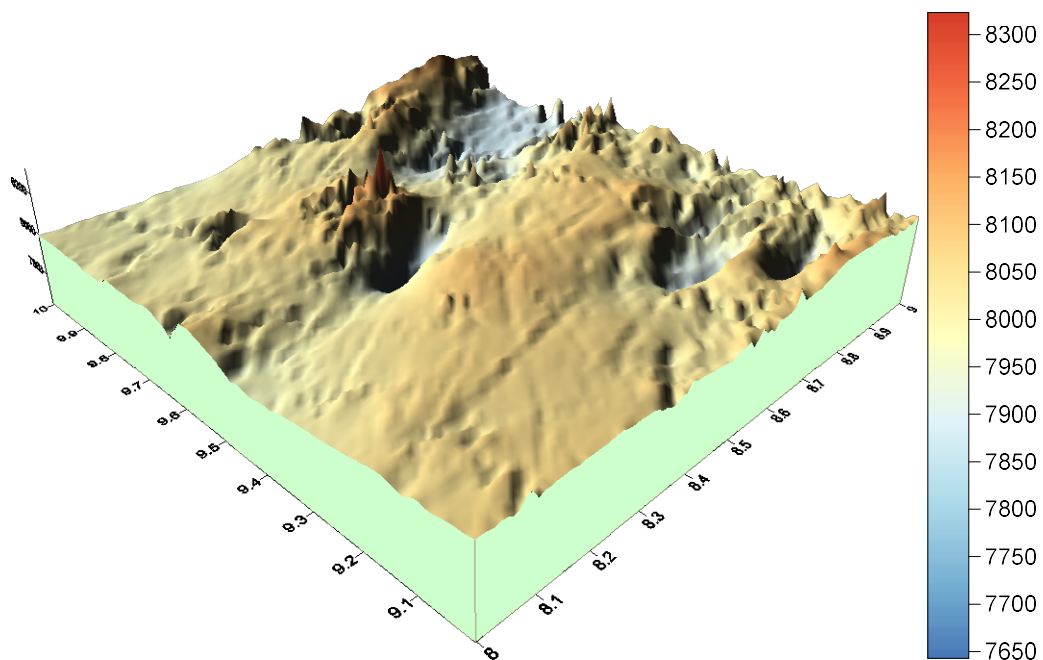


Fig.4.7: 3-D Surface map of total magnetic field of the aeromagnetic data

The 3-D representation of the topography of the magnetic basement surface of the study area is shown by figures 4.5 and 4.6. The map revealed two distinctive relief patterns: low and high relief. Areas with low relief are observed in the northeastern and central part of the study area around Bukuru, Jos and Kagoro, whereas the northwestern and southern fringes of the study area around kafanchan, Gwantu, and Andaha showed a relatively high relief.

On the southern fringe, from Fadank, an extensive linear anomaly trending in the E-W direction was observed. Along this linear anomaly, there exists a chain of circular magnetic closures believed to be granitic intrusions which is part of the volcanic ring complex.

The high relief areas are therefore believed to be more tectonically active than the low relief areas owing to the presence of chains of granitic intrusive bodies. Other magnetic closures interpreted to be intrusive magnetic bodies were observed around Andaha and Zonkwa areas.

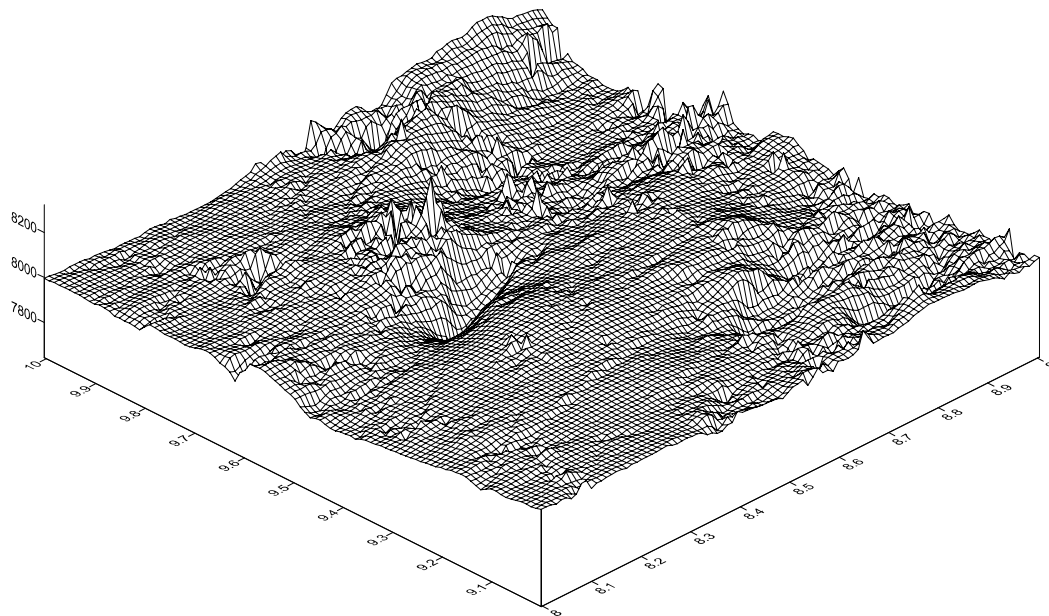


Fig.4.8: Wireframe map of the total magnetic field of the aeromagnetic data

4.1.2 Digital Filtering

Frequency filtering represents a major component of magnetic data processing. As a rule, digital filters are used for signal enhancement that is to remove unwanted noises and enhance desired signals. The nature of “noises” and “signals” varies from case to case. Therefore, the used filters are grouped into five categories, namely: regional (low-pass), residual (high-pass), Bsplin pass, non-linear and band-pass filters.

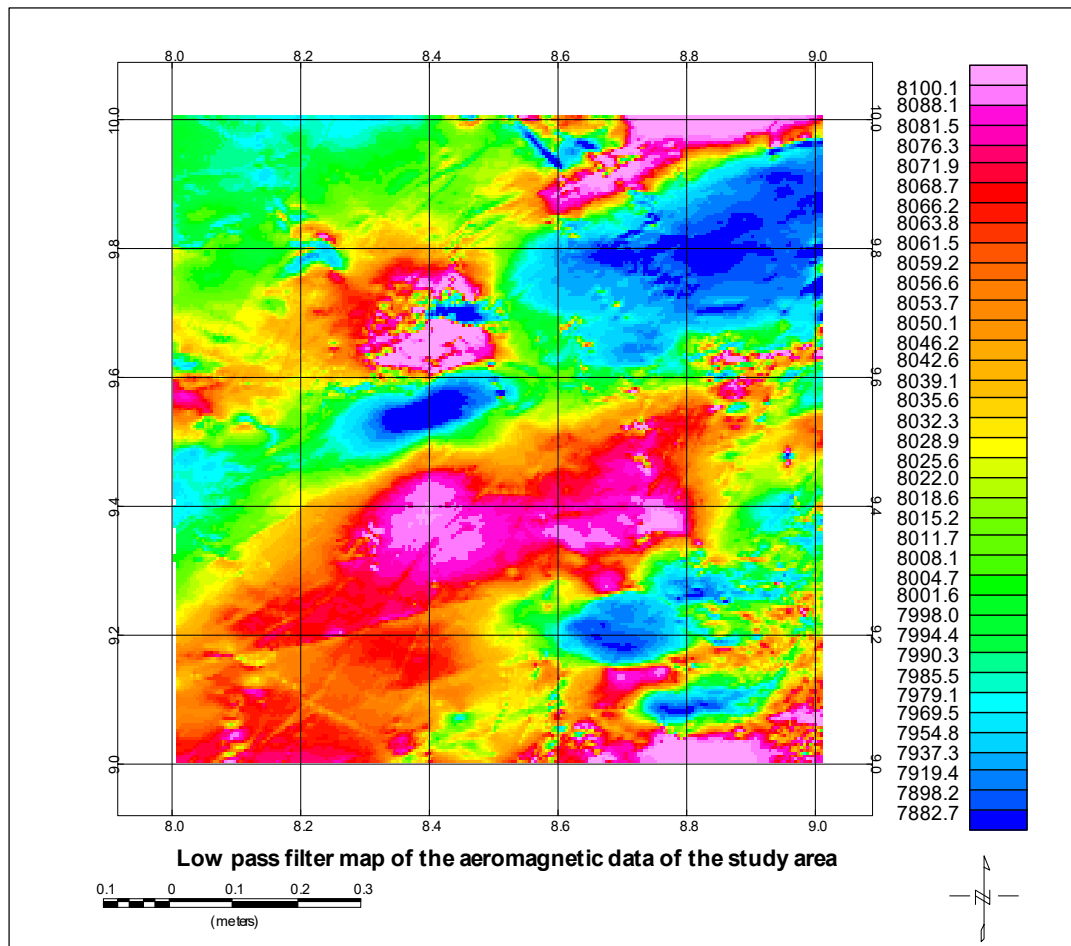


Fig.4.9: Low pass filter map of the aeromagnetic data of the study area.

The low-pass filter is defined as a filter which passes long wavelengths and rejects all wavelengths smaller than the cut-off wavelength. The low-pass filtering process is used to isolate the regional features from the local ones. The anomaly map with low-pass magnetic filter (Fig. 4.9) shows that, the well defined trends of anomalies in the aeromagnetic map are still persistent. This reflects the deep extension of the structures causing the anomalies.

A high-pass filter emphasizes short wavelengths and eliminates wavelengths larger than the cut off wavelength. The map clearly shows several clusters of positive and negative magnetic anomalies. These anomalies are found to be distributed with varying trends. The prominent NE–SW anomalies trends in the central part were retained, but with shorter wave lengths than the original one. This indicates that the prominent fault trends are extended in the subsurface up to the shallow depths.

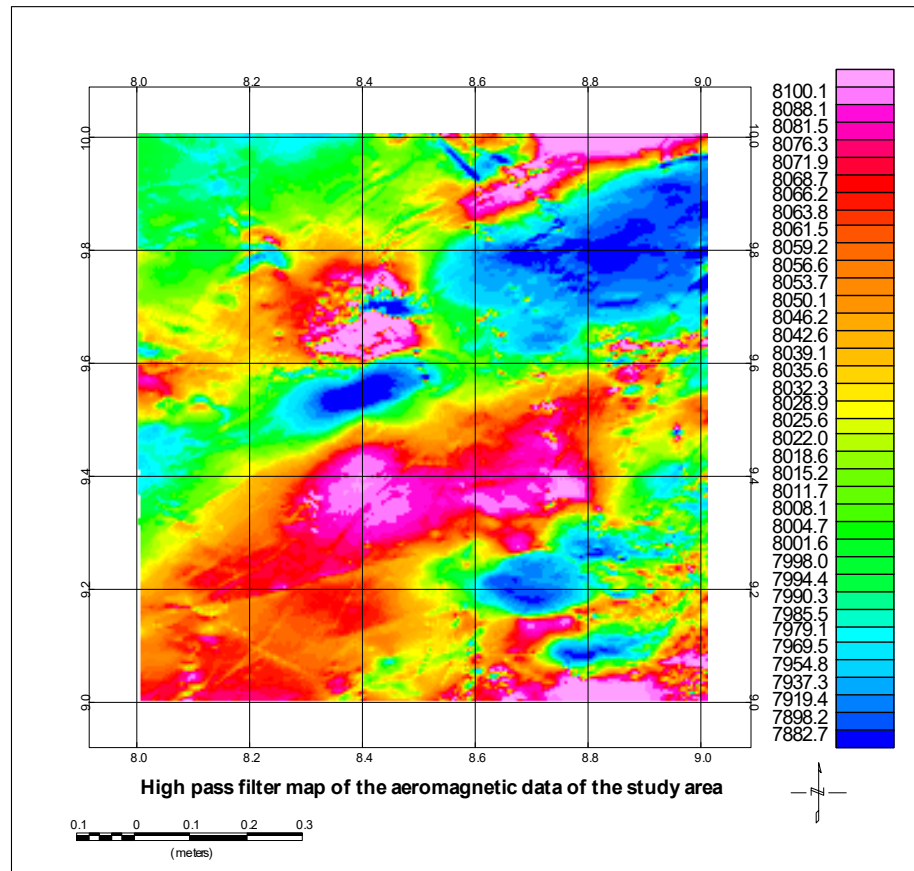


Fig.4.10: High pass filter map of the aeromagnetic data of the study area

The anomaly map with band-pass magnetic filter (Fig. 4.11) shows that there are still persistence of well-defined trends of anomalies on the aeromagnetic map. However, some regional anomalies that do not appear to be related to a subsurface structure are most probably a result of regional variations in the magnetization or magnetic susceptibility of the rocks at medieval depths.

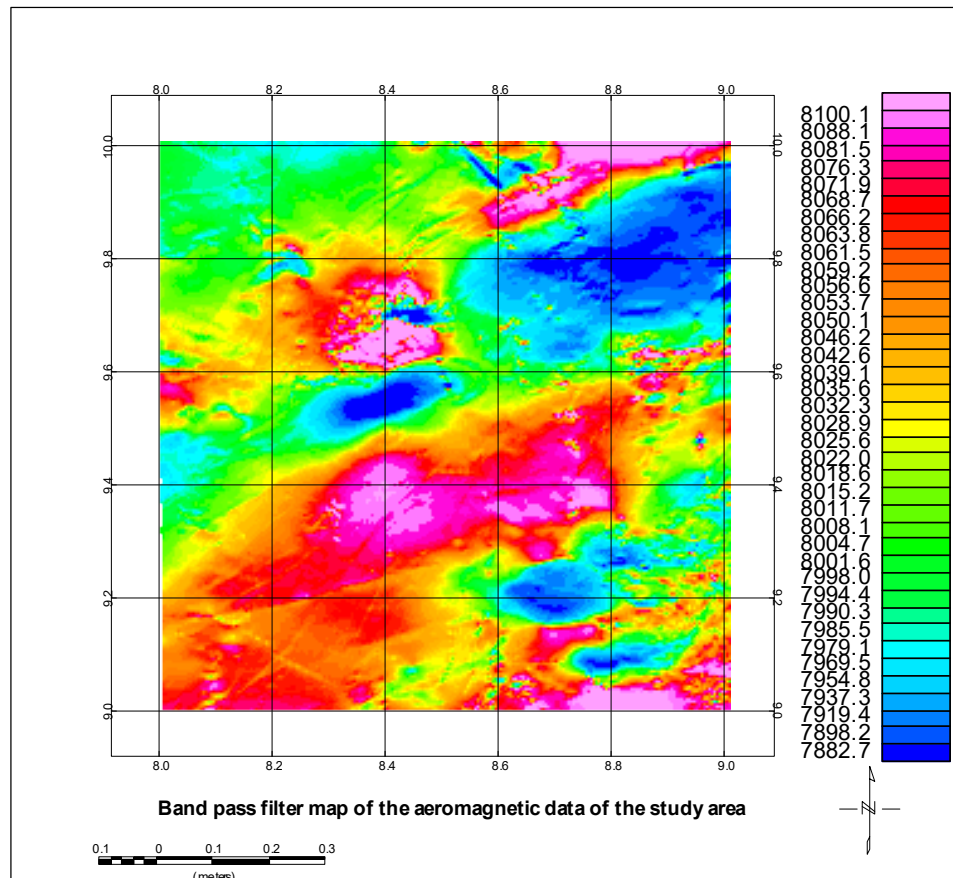


Fig.4.11: Band pass filter map of the aeromagnetic data of the study area

In the non linear filter map (Fig.4.12) the anomalies were found to be distributed with no change in the defined trend of the aeromagnetic map.

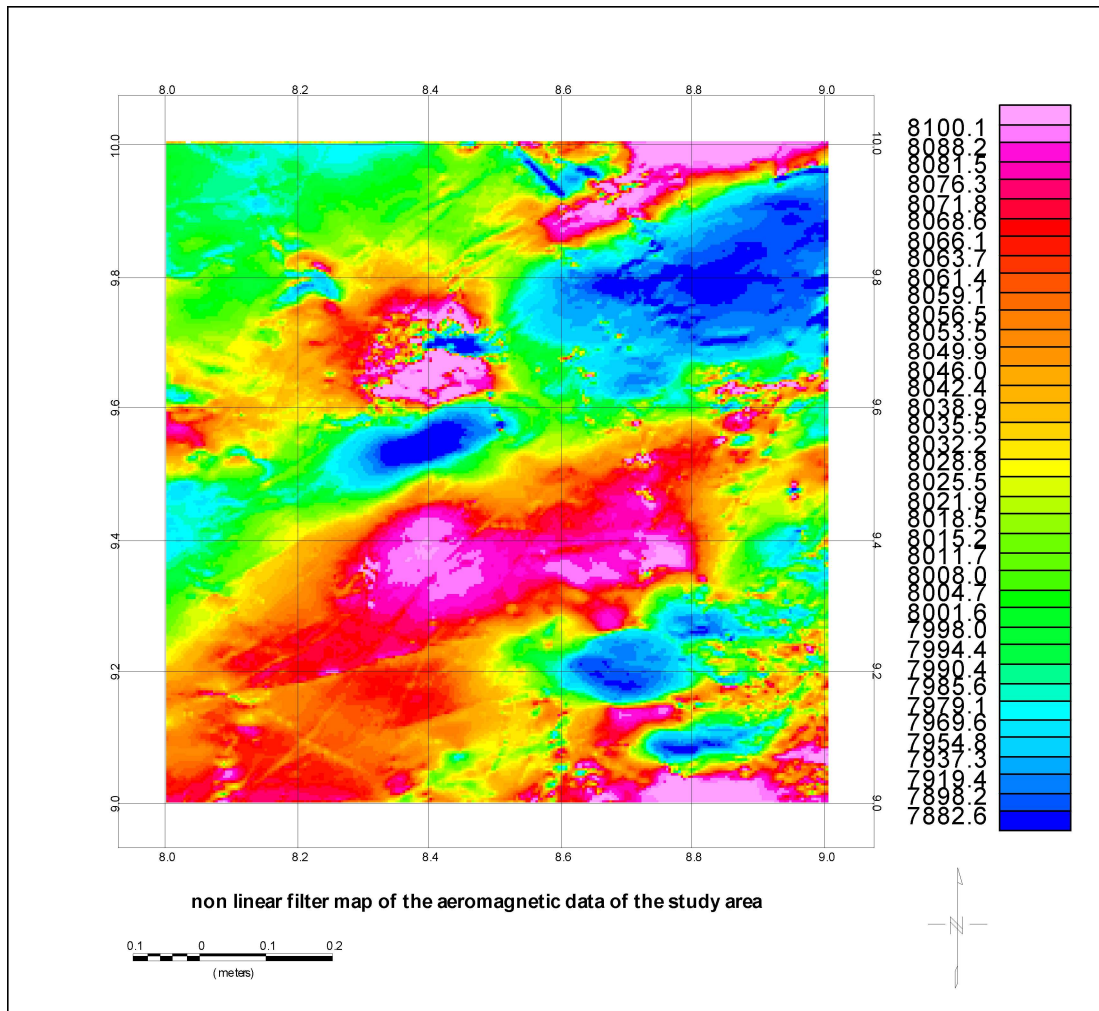


Fig.4.12: Non linear filter map of the aeromagnetic data of the study area

4.1.3 Regional-Residual Separation

The regional gradients of the aeromagnetic data were removed by fitting a plane surface to the data, using multi-regression least squares analysis. The expression obtained for the regional field $T(R)$ is given as:

$$T(R) = 76122.158 + 0.371x + 0.248y \quad (4.1)$$

where x and y are units of spacing. The regional field values are subtracted from the observed data to obtain the residual anomaly values. The technique is carried out on the

aeromagnetic data of the study area to produce the first to fourth residual and regional trend surfaces (figs. 4.13 – 4.16).

The regional magnetic field of the study area is shown in Figure 4.17 while figure 4.13 -4.16 shows the residual magnetic field of the aeromagnetic data. The very strong regional fields which mask the weak near surface residual fields were removed using regional-residual separation by fitting polynomials of first to fourth degree to the total magnetic field intensity data.

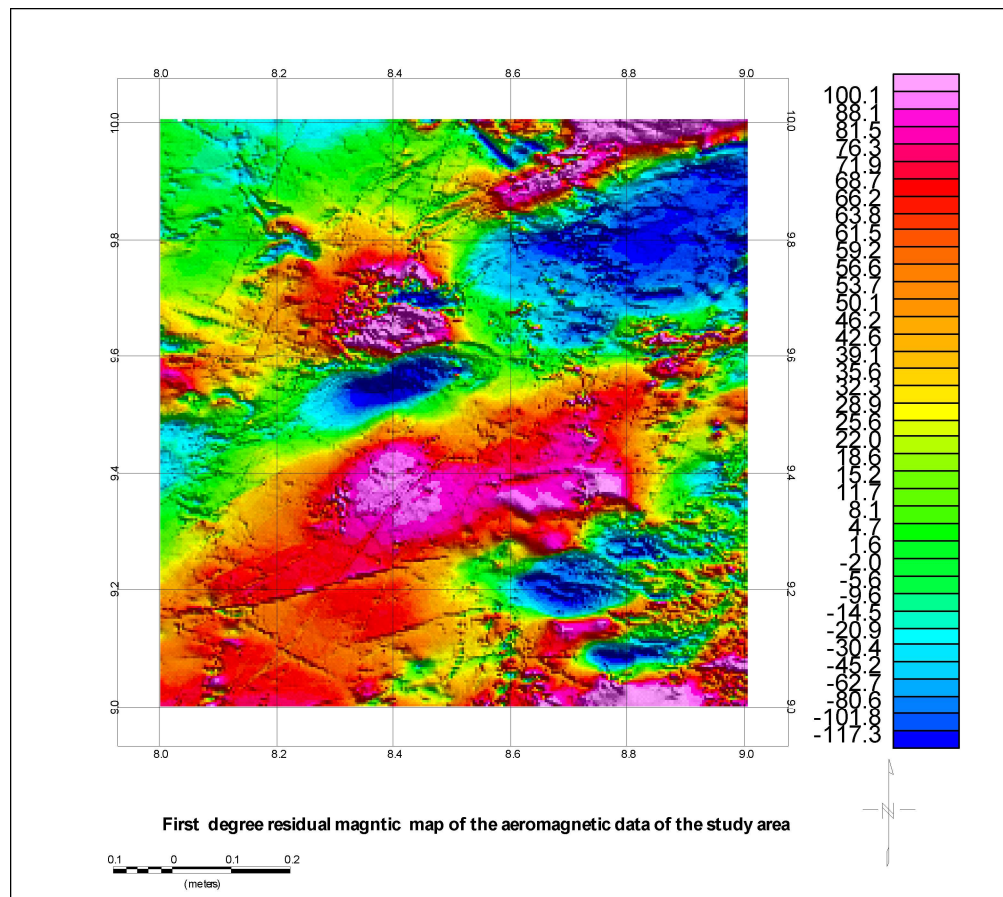


Fig. 4.13: First Degree Residual Field over the Study Area as a Colour Shaded Contour Map

The residual magnetic intensity map of the study area is shown in Figures 4.13 - 4.16 below, these ranges from -122gammas to 100gammas. The variation in the residual magnetic field in the area is indicative of various geological, magnetic and chemical compositions

anomalous bodies. The study area is revealed as composed of a central positive residual anomalous body flanked by areas of negative residual values. The areas with negative magnetic values are believed to be of low magnetization while the positive residual anomalous areas are indicative of high magnetization. This implies that there is an existence of shallow to near surface magnetized bodies in areas having positive residual values. This implies that the areas around Bukuru and Kagoro with negative residual values are underlain by deep seated magnetized bodies.

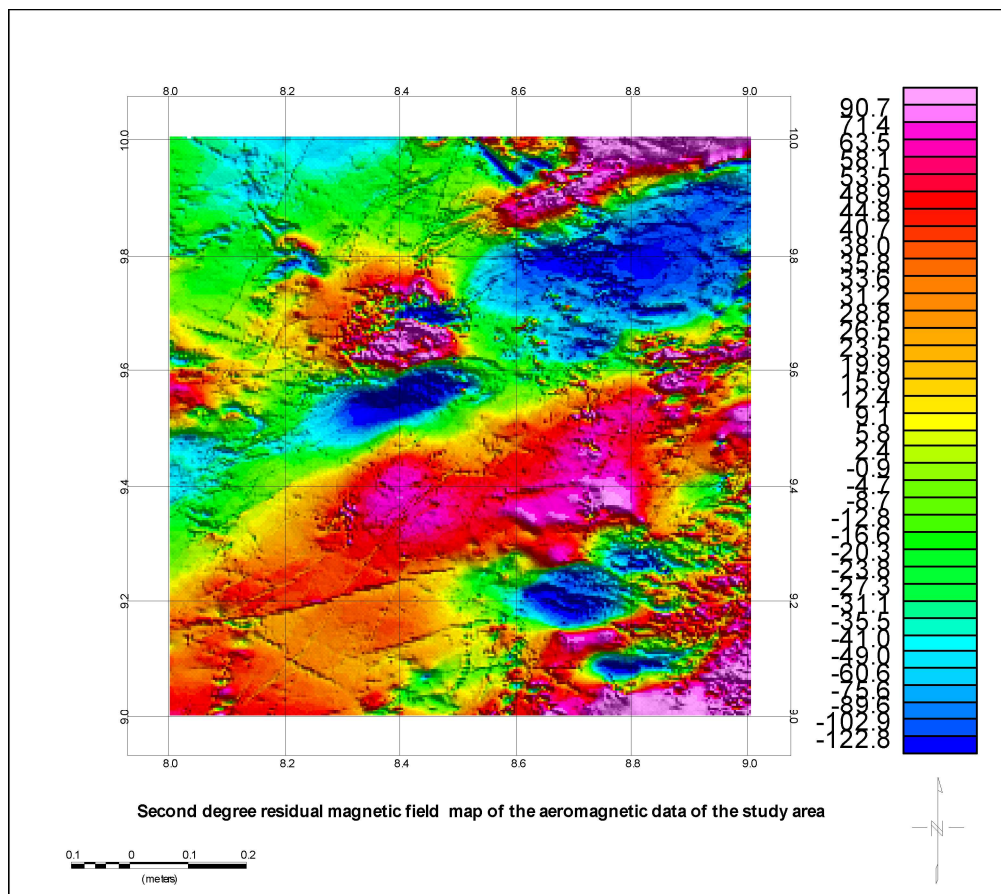


Fig. 4.14: Second Degree Residual Field over the Study Area as a Colour Shaded Contour Map

Another probable reason for the predominance of negative residual anomaly signatures in this area may be due magnetic basement subsidence resulting from the epeirogenic uplift of the central areas of the study area. Nevertheless, the existence of the elongated positive

anomaly in Gwantu area could be seen as a result of magmatic activity resulting in uplift which acted as conduits for primary mineralization of most of the near surface rocks thereby containing large amount of magnetic minerals. The positive residual magnetic anomalies in most part of the study area show that the Younger Granite ring complexes are probably exposed on the surface or may have been buried at relatively shallow depths.

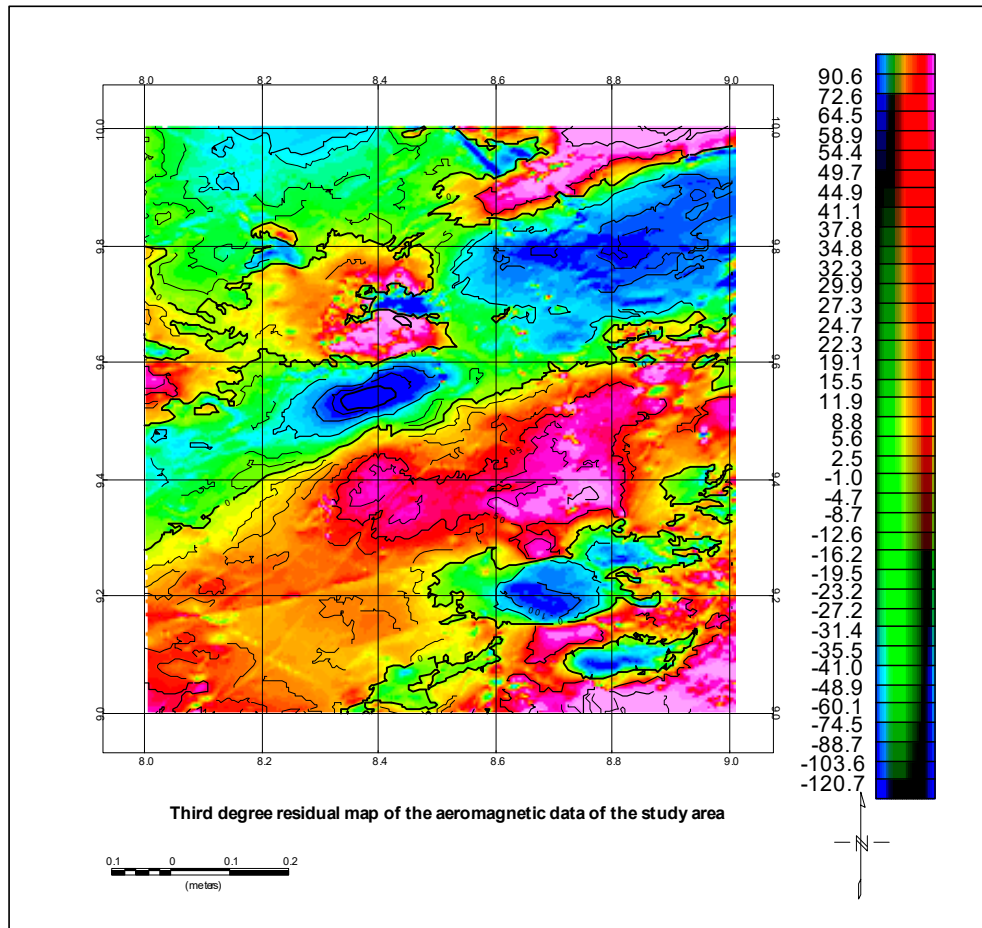


Fig. 4.15: Third Degree Residual Field over the Study Area as a Colour Shaded Contour Map

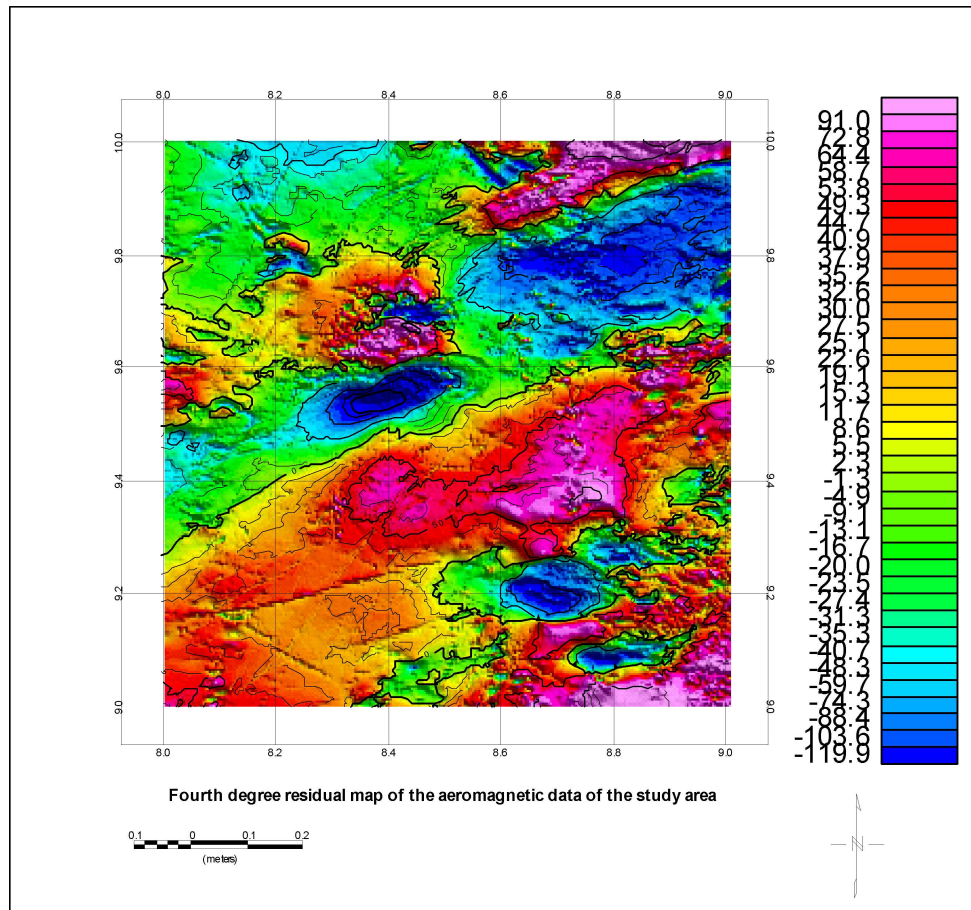


Fig. 4.16: Fourth Degree Residual Field over the Study Area as a Colour Shaded Contour Map

The magnetic structural trends interpreted from the total field intensity map revealed trend directions of NW-SE, N-S, E-W and NE-SW. The NW-SE trend is the dominant trend orientation in the study area and thus reflects the trend of the youngest tectonic episode, the Post pan-African orogenic activities in the study area which nearly obliterated the older E-W and NE-SW tectonic episodes.

These structural trends are correlatable with paleo-structures (including the Romanche and St. Paul's Fracture zone) in the study area which are believed to have affected major geologic events in the study area.

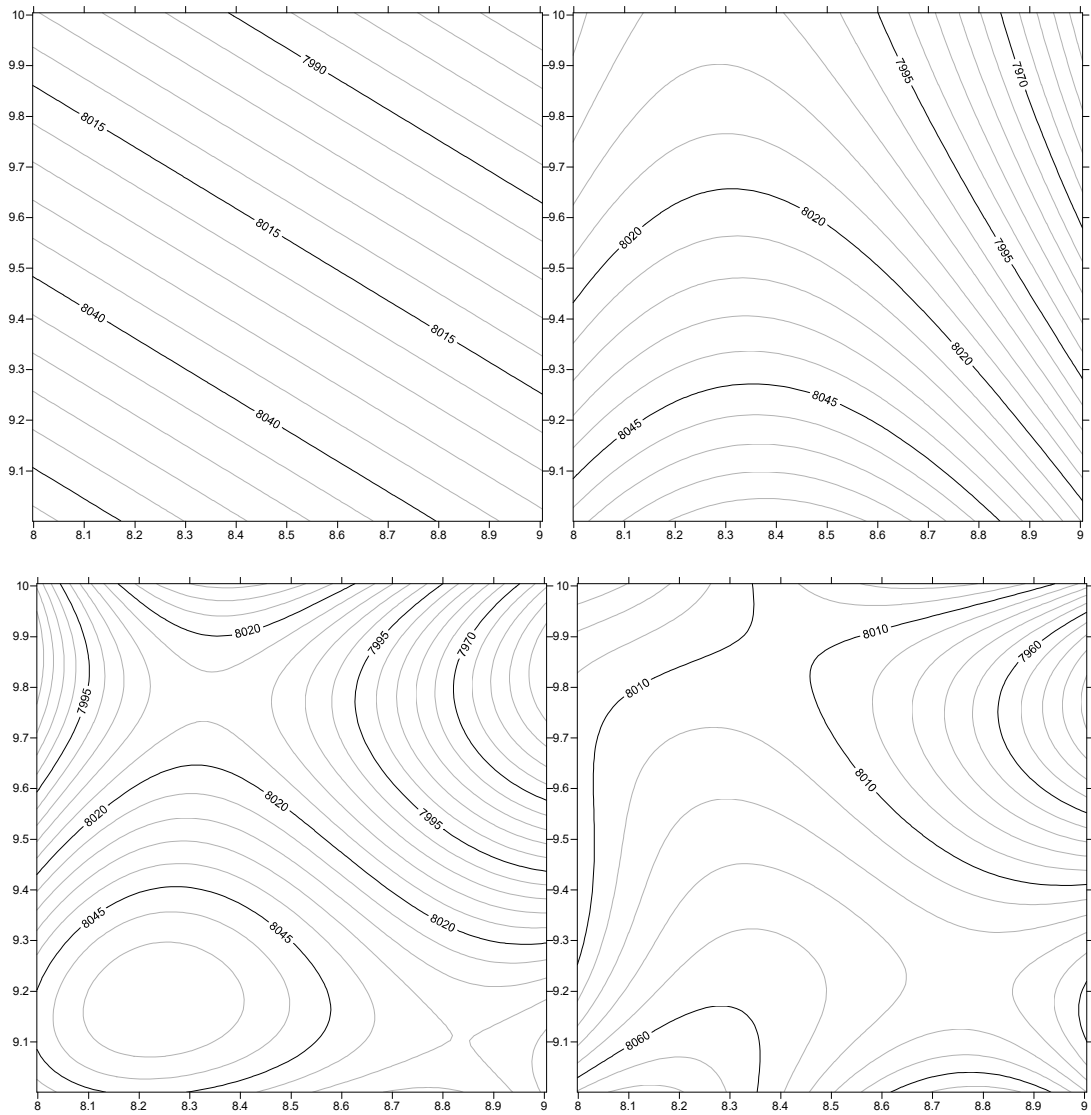


Figure 4.17: First to fourth Degree Regional Field over the Study Area as a contour Map

4.1.4 Upward Continuation Filter

Upward continuation tends to accentuate anomalies caused by deep sources at the expense of anomalies caused by shallow sources (Mekonnen, 2004). It is a mathematical technique that projects data taken at an elevation to a higher elevation. The effect is that short wavelength features are smoothed out because one is moving away from the anomaly.

Upward continuation attenuates anomalies with respect to wavelength the shorter the wavelength, the greater the attenuation. The upward continued ΔF (the total field magnetic anomaly) at higher level ($z = -h$) is given by,

$$\Delta F(x, y, -h) = \frac{h}{2\pi} \iint \frac{\Delta F(x, y, 0) dx dy}{\{[(x-x_0)^2 + (y-y_0)^2 + h^2]^{\frac{3}{2}}\}} \quad 4.2$$

The empirical formula (Henderson, 1960) given the field at an elevation h , above the plane of the observed field ($z = 0$) in terms of the average value $\Delta F(r_i)$ over a circle of radius r_i centred at the point $(x, y, 0)$ multiplied by the appropriate weighting coefficients. These coefficients enable calculation of the upward continued field to an accuracy of within 2%. Thus, the problem of calculating the field at higher level from the knowledge of the field at a lower level is a straight forward one of numerical integration of the surface data. In practice, the computations are made by replacing the surface integral with a weighted sum of values taken on a regular grid.

Analytic continuation to any altitude of above the flight-line reflects the geologic structures at such depths down which suppress the magnetic effects from shallow structures. The reason for producing these maps is to determine the trend and the nature of any observable deep seated anomalous body at deeper depths. The aeromagnetic data of the study area were upward continued at altitudes; 1km, 2km, 3km and 4km respectively above the flight-lines to produce figure 4.18 – 4.21 below.

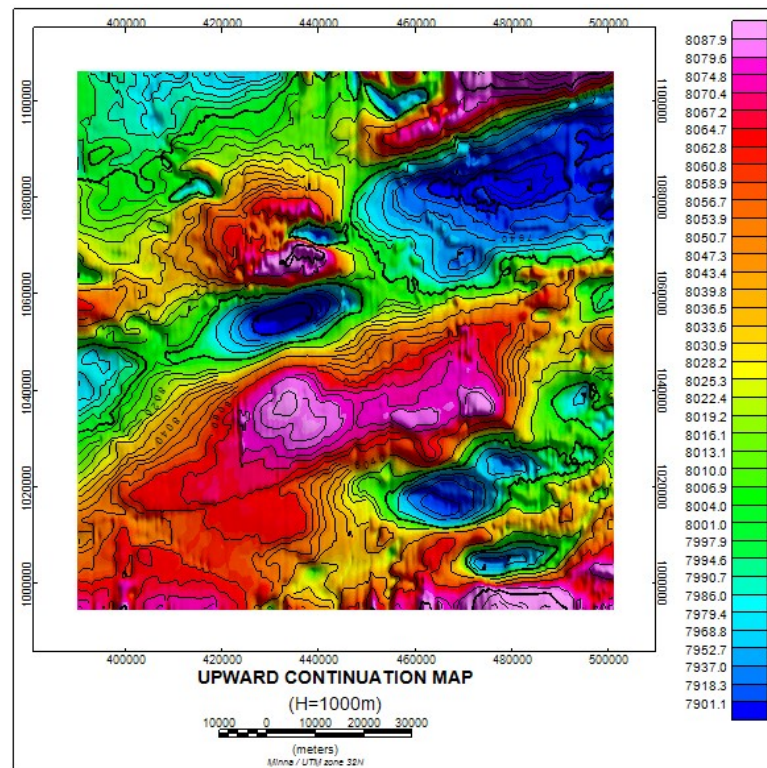


Fig. 4.18: Upward Continued Aeromagnetic Field over the Study Area as a Colour Shaded contoured Map (H=1000m).

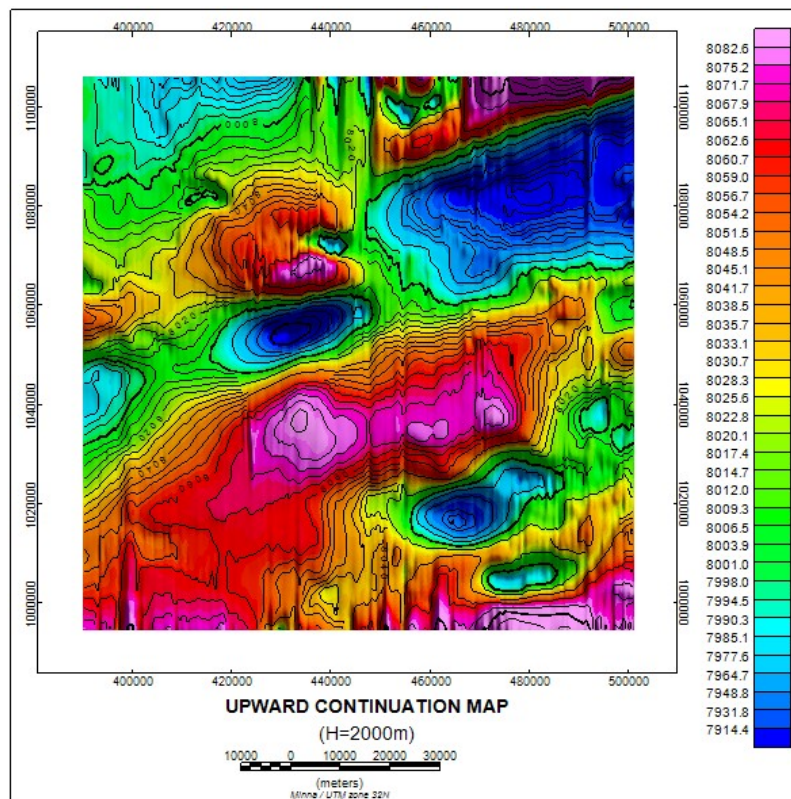


Fig. 4.19: Upward Continued Aeromagnetic Field over the Study Area as a Colour Shaded contoured Map (H=2000m).

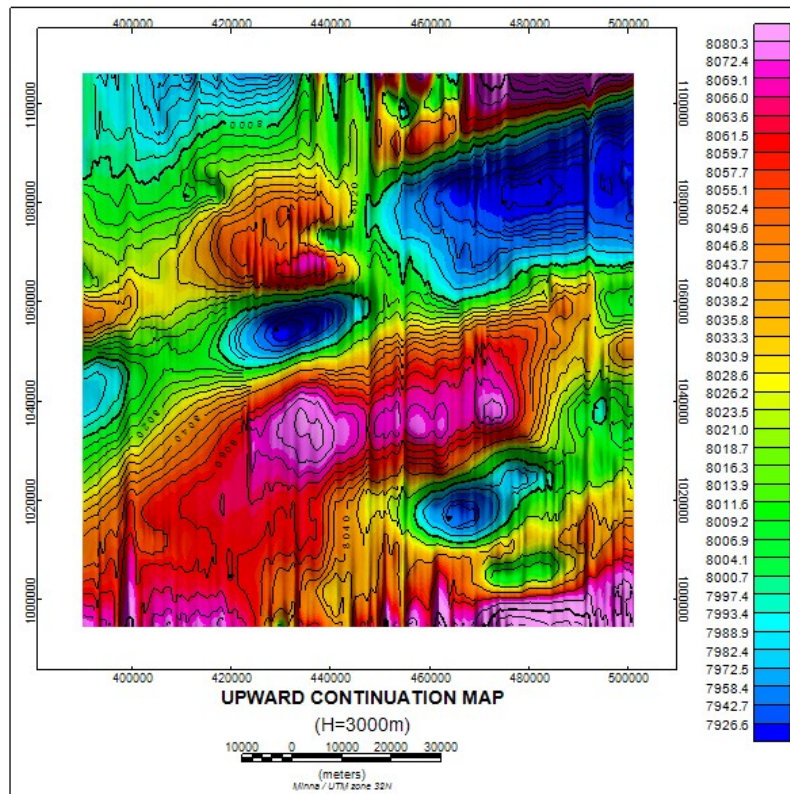


Fig. 4.20: Upward Continued Aeromagnetic Field over the Study Area as a Colour Shaded contoured Map (H=3000m).

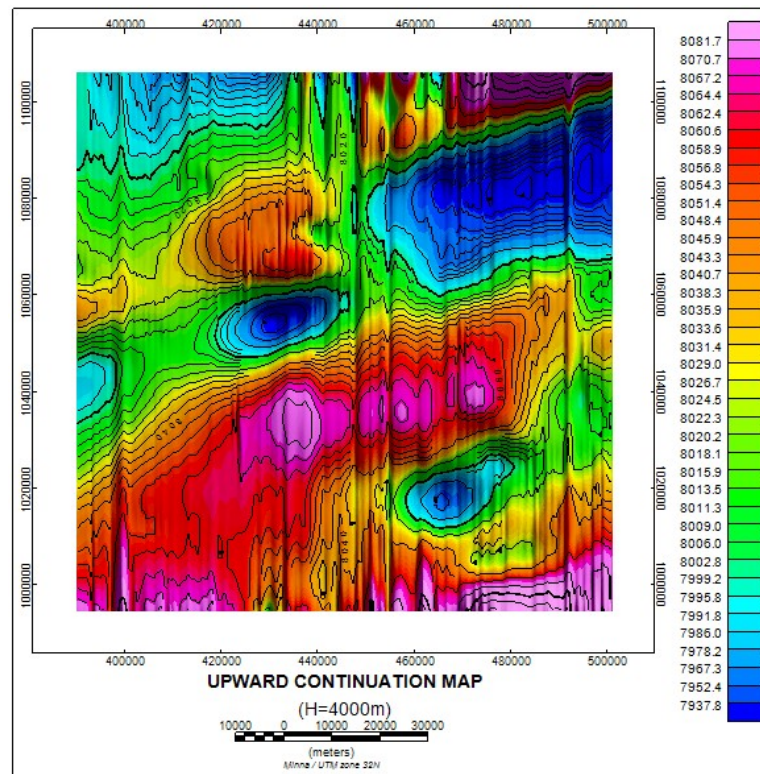


Fig. 4.21: Upward Continued Aeromagnetic Field over the Study Area as a Colour Shaded contoured Map (H=4000m).

At 1km to 4km above the flight elevation, most observed anomalies are NE-SW direction, a circular contour around Kagoro, the erosional escarpment and elongated NE-SW lineament around Bukuru. The basic fact is that the observed lineaments at such altitude are about 4km deep seated in the Earth crust.

4.1.5 Spectral Depth Estimation

A power spectrum module in the Oasis Montaj 7.2HJ software was used to carry out the spectral inversion of the aeromagnetic data. To determine the depths of the anomalous magnetic sources, the study area was divided into 16 overlapping grids. The locations of these grids and the computed spectral depths are presented in Table 4.1 below with X_1 , X_2 giving the limiting longitudes and Y_1 , Y_2 indicating the limiting latitudes for each of the blocks. Each of these spectral blocks covers a square area of about 13.85km x 13.85km of the data sheet. The representative plot of the power spectrum (spectral plot) for Jos sheet (BLOCK A) is represented as graphs of logarithms of spectral energies against frequency and is shown in figure 4.22 below. Each of these plots revealed a two layer depth model as represented by two clear segments. Thus, the logarithmic plot of a radial spectrum would give a straight line whose slope is $2z$. From the gradients of the segments the average depths to the causative layers were determined as D_1 , D_2 (Table 4.1)

The first layer depth (D_1), represents the depth to the shallow magnetic sources while the depth to the magnetic basement (sedimentary thickness) is represented by the second line segment of the power spectrum plots. The depth to the first layer (D_1) in the study area varies from 0.0568 km to 0.9885 km with an average depth of 0.5118 km while second layer depth (D_2) varies from 0.3569 km to 3.2600 km with the average depth of 1.7723 km. This result therefore indicates that the average basement depth of the study area as deduced

from power spectrum inversion is about 1.7723 km. The shallow magnetic sources are believed to be the resultant of basement rocks that were tectonically uplifted into the sedimentary overburden while the deeper basement depths may be attributed to lateral inversions in basement susceptibilities and intra basement structural deformations like faults and fractures (Ofoegbu and Onuoha, 1991; Kangoko et al., 1997).

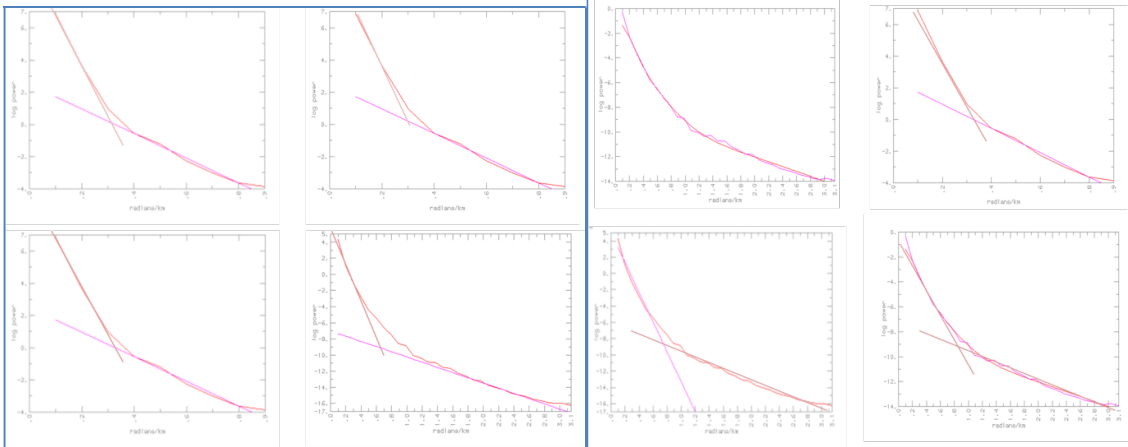


Fig. 4.22: The cross section of processed Spectral blocks for Zonkwa.

Fig. 4.23: The cross section of process Spectral blocks for Jos.

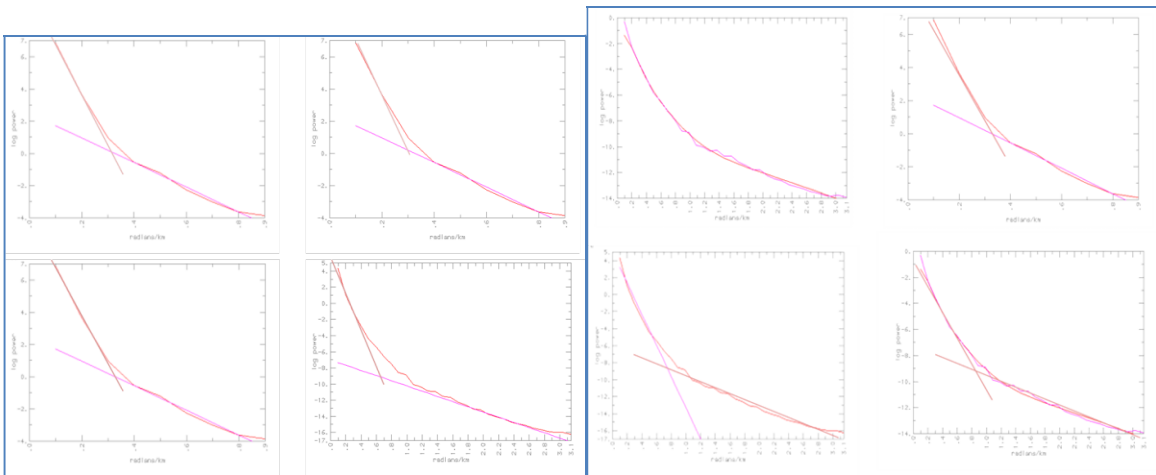


Fig. 4.24: The cross section of processed Spectral blocks for Andaha .

Fig. 4.25: The cross section of processe Spectral blocks for Richa.

It can be deduced that the D_2 values obtained from the spectral plots represents the average depths to the basement complex in the blocks considered. The depths to the shallower magnetic sources and that of the magnetic basement depths were noticed to

increase from the western part of the study area to the eastern parts where they decrease appreciably as shown in the magnetic contour map. This means that the basement outcrops may be seen around Makasuwa where the basement depth is low with sediment thicknesses being more in Kuru, Bukuru and Jos areas.

Table 4.1: Basement depth estimates of the study area calculated from spectral analysis

Location	Spectral Block	Longitude		Latitude		Spectral Depths(km)	
		X ₁	X ₂	Y ₁	Y ₂	D ₁	D ₂
Zonkwa	A	8.00	8.25	9.75	10.0	0.4500	2.0034
	B	8.25	8.50	9.75	10.0	0.9825	1.9985
	C	8.50	8.75	9.75	10.0	0.7650	1.8958
	D	8.75	9.0	9.75	10.0	0.5690	1.7589
Jos	E	8.00	8.25	9.50	9.75	0.3500	1.4590
	F	8.25	8.50	9.50	9.75	0.9885	1.5600
	G	8.50	8.75	9.50	9.75	0.7850	1.5690
	H	8.75	9.0	9.50	9.75	0.9568	1.3560
Andaha	I	8.00	8.25	9.25	9.50	0.2780	2.5460
	J	8.25	8.50	9.25	9.50	0.1750	3.0670
	K	8.50	8.75	9.25	9.50	0.2820	2.9000
	L	8.75	9.0	9.25	9.50	0.4560	0.8950
Richa	M	8.00	8.25	9.00	9.25	0.1860	3.2600
	N	8.25	8.50	9.00	9.25	0.4589	1.0568
	O	8.50	8.75	9.00	9.25	0.0568	0.3569
	P	8.75	9.0	9.00	9.25	0.4500	0.6750

4.1.6 Curie point Depth Estimation

From the graphs of the Logarithm of spectral energies versus frequencies plotted for each block (spectral window of 58 X 58 used for plots of Eq. 3.16 and 135 X135 used for plots of Eq.3.19) shows there were spectral peaks which were easily noticeable and the significance of this is the indication of the fact that Curie point depths are detectable as it defines the source bottoms.

The table below shows that the depth to the Centroid (Z_o) ranges from 12.12 km to 15.29 km. On the other hand, the depth to the top boundary (Z_t) of magnetic sources ranges from 0.3569 km to 3.26 km (below sea level). The equivalent curie depth ranges from 23.8831km to 27.5242Km. It is observed that the curie depth in the South-Eastern part of the study is shallower (23.8831-24.0050km) compared to the other part of the study area. The shallow Curie depth observed could be as a result of the intruded Older Granite unit spotted in that region.

Results of Curie point depth in conjunction with heat flow values revealed a distinct inverse relationship. From table 4.2, it is evident that, heat flow increases with decrease in Curie point depth, and vice-versa.

In most part of the study area, heat flows were found to be less than 60 mWm^{-2} . This implies that the heat flows in the study area are not uniform, which possibly indicate that the magma conduits were randomly distributed. The average heat flow obtained in the study area is 56.06 mWm^{-2} , this value may be considered as typical of the continental crust. The heat flow is significantly high in the South-Eastern area which corresponds with the area of shallow curie depth. Such heat flow values are suggestive of anomalous geothermal conditions and are recommended for detailed geothermal exploration.

The knowledge of the depth to Curie and its heat flow are of interest and can be related to the thermal history of an area. This study illustrates that surface magnetic data can be used to produce Curie depth estimates even for region with paucity of heat flow and geothermal gradient data.

Table 4.2: Geothermal estimates of the study area calculated from spectral analysis

Spectral Block	Longitude (°)		Latitude (°)		Spectral Depths (km)		CPD (km)	Geothermal Gradient (°Ckm⁻¹)	Heat Flow (mWm⁻²)
	X₁	X₂	Y₁	Y₂	Z_t	Z_o	Z_b	dT/dZ	q
A	8.00	8.25	9.75	10.0	2.0034	13.811	25.6186	22.64	56.60
B	8.25	8.50	9.75	10.0	1.9985	14.000	26.0015	22.31	52.28
C	8.50	8.75	9.75	10.0	1.8958	14.710	27.5242	21.07	52.68
D	8.75	9.0	9.75	10.0	1.7589	13.980	26.2011	22.14	55.35
E	8.00	8.25	9.50	9.75	1.4590	13.410	25.3610	22.87	57.18
F	8.25	8.50	9.50	9.75	1.5600	13.510	25.4600	22.78	56.95
G	8.50	8.75	9.50	9.75	1.5690	13.720	25.8710	22.42	56.05
H	8.75	9.0	9.50	9.75	1.3560	13.310	25.2640	22.96	57.40
I	8.00	8.25	9.25	9.50	2.5460	14.710	26.8740	21.58	53.95
J	8.25	8.50	9.25	9.50	3.0670	15.120	27.1730	21.34	53.36
K	8.50	8.75	9.25	9.50	2.9000	15.150	27.4000	21.17	52.92
L	8.75	9.0	9.25	9.50	0.8950	12.950	25.0050	23.23	57.99
M	8.00	8.25	9.00	9.25	3.2600	15.290	27.3200	21.23	53.07
N	8.25	8.50	9.00	9.25	1.0568	12.620	24.1832	23.98	59.96
O	8.50	8.75	9.00	9.25	0.3569	12.120	23.8831	24.28	60.71
P	8.75	9.0	9.00	9.25	0.6750	12.340	24.0050	24.16	60.40

4.1.7 3D Euler Deconvolution Depth Estimation

The 3D Euler Deconvolution depth estimate solutions are given as coloured point solutions. The 3D Euler Deconvolution leaves the interpretation of the significance of a calculated solution to the interpreter (Thompson, 1982), an additional assessment of the solution is crucial in order to obtain valid solutions. The 3D Standard Euler solutions for four geological models are presented. Figures 4.26 - 4.29 shows the computed depth estimates for a structural index of 0.0, 1.0, 2.0 and 3.0, respectively. As the presence of igneous intrusions and faults owing to the tectonic history of the area (Ofoegbu and Onuoha 1991)

are discussed as potential sources for the magnetic anomaly observed in the study area, a structural index of 0.0 and 1.0 were selected as criteria for valid solutions, where these structural indices applies for the simple model of a magnetic field caused by contact and dyke or sill structure respectively. The best results yielded a window size of 7 corresponding to 14 km, a maximum distance of the source from the centre of the window of 20 km and a maximum depth tolerance of dz : 15%. The suggested solutions calculated by the 3D Euler method, which also accounts for the flying height, give the depth in the ground to the top of the anomaly causing source body.

The Standard Euler solution for contacts shown in figure 4.26 revealed a depth range of 250m – 2500m with isolated cluster of solutions around Bukuru, Jos, Jemaa and Fadan areas. This indicated that magnetic contacts are not a dominant geological feature of the study area.

The depth estimation solutions calculated for a structural index of 1.0 which applies to a geologic model of dyke and sill structures as sources is presented in figure 4.27. This has dense clustering of solutions in the range of 250m to 2500m. It is therefore revealed that sills/dykes are dominant geological features in the study area as the cluster of solutions are in most part of the map. However, there is a complete absence of this geological structure around the south-western area of the map. With the presence of the deep seated structures which cut across the basement, the existence of fractures around Randa has been established. Randa river could then be suggested as emanating along a deep fracture trace (fault trace) that must have cut through the Randa area.

For structural index 2(horizontal cylinders/pipes), the estimated depth ranges from 250 to 3000m as shown in Figure 4.28. Several clusters of solutions were observed all over the map of the study area with Bukuru and Jos however having no noticeable cluster of

solution. Horizontal cylinders/pipes are therefore observed to be dominant structural/geological feature in the study area.

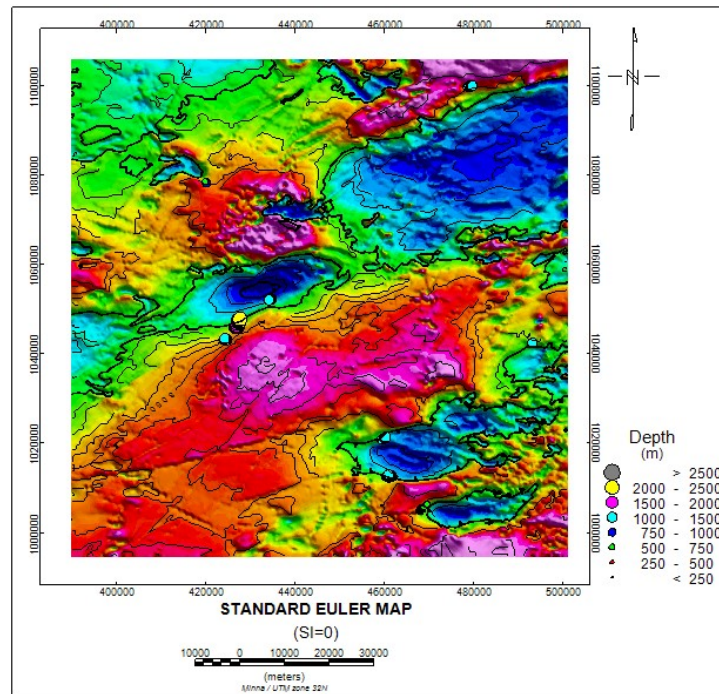


Figure 4.26: 3D Standard Euler deconvolution contour map of the study area showing cluster solutions for structural Index=0.0.

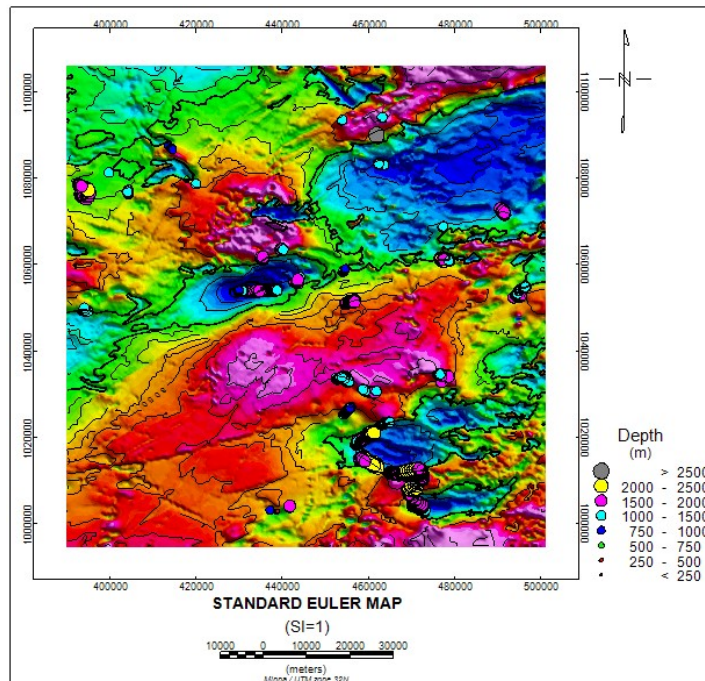


Figure 4.27: 3D Standard Euler deconvolution contour map of the study area showing cluster solutions for structural Index=1.0.

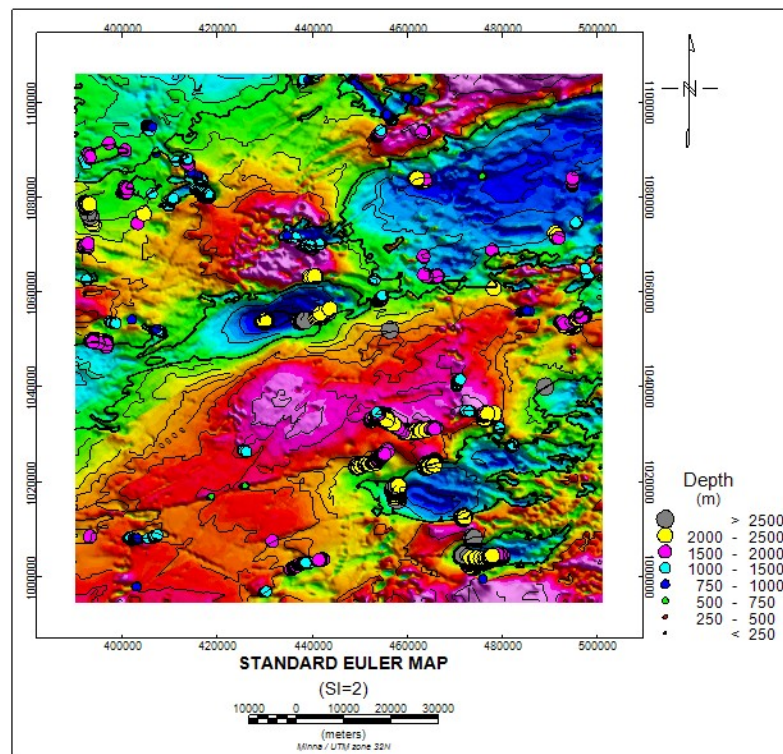


Figure 4.28: 3D Standard Euler deconvolution contour map of the study area showing cluster solutions for structural Index=2.0.

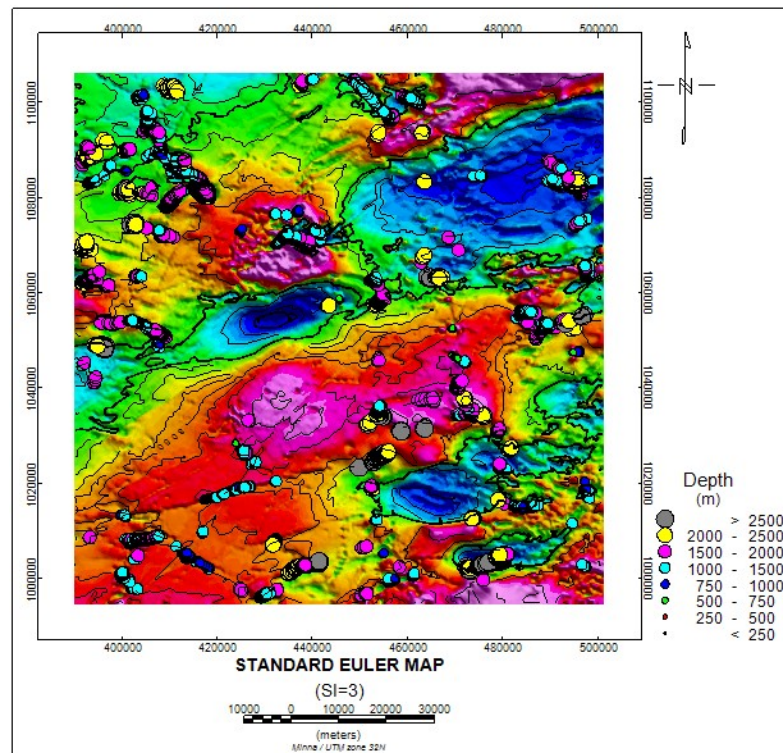


Figure 4.29: 3D Standard Euler deconvolution contour map of the study area showing cluster solutions for structural Index=3.0.

Spheres (figure 4.29) revealed a concentration of clusters of solution at the North-western and southern parts. There is also a concentration of the cluster of solutions representing spheres around Bukuru and Kafanchan area. The depth of the interpreted cluster of solutions varies between 250m- 2500m. In consideration of the fact, that a structural index that is too low gives depths that are too shallow and one that is too high gives estimates that are too deep (Reid et al., 1990), the structural indices of 2.0 and 3.0 are considered too high and cannot be explicitly correlated with known source bodies in the study area, hence the corresponding solutions were disregarded. However, a Euler depth range of 250m - 2500m (0.250km – 2.5km) for magnetic source bodies in the study which are very apt as this depth range agrees with result of spectral analysis.

Generally, the Euler deconvolution suggests a depth to the magnetic source of between 250m to a little above 2500m which is in agreement with earlier studies (Opara et al., 2015). Comparing these depth estimates with the information inferred from the spectral analysis result, there is a positive correlation between the results from both depth estimation methods.

4.2. REMOTE SENSING

4.2.1 Digital Elevation Model

The DEM of the Study area is shown in figure 4.28. The highest peaks represented by the red color are seen at Jos through Barkin-ladi area following a topographically high feature. The northeastern and southeastern area of the map characterized by the red color is interpreted as Younger granitic intrusion which corresponds to the Younger granite on the geologic map of the area. It is obvious that the northeastern, southeastern and northcentral responded to tectonic events. These areas form greatly the Younger granite ring complex. The slope of the ring dyke is identified where the red and yellow colours are closely packed together; representing a sudden change in topography from 1614 to 924meters. The slope is

characterized by streams, gullies and rivers. In the North central area of the map, the highest topographical relief represented by the red colour correlates to the Younger granite on the geological map; this is interpreted as an elliptic Younger granite ring complex which covers part of the Kagoro area. The slope of the ring complex is identified where the yellow and green colours are closely packed; representing sudden change in topography from 924 to 578 meters. The contour map confirms this as area of red contour. The slope is characterized by streams and gullies.

It will be correct to interpret that the topographically high areas are characterized by Younger granites and the low areas are characterized by older granites and migmatitic gneiss and schists. Almost everywhere these rhyolitic rocks (Younger granites) directly overlie the metamorphic basement, which means that the Younger granites were emplaced in uplifted areas that were undergoing erosion. This explains the emplacement of the Younger granite ring complexes been associated with epeirogenic uplift. The ring complexes are mainly associated with surface exposure that raised between the range of 1182 and 1614m above mean sea level. On the contour map, this area corresponds to the green coloured contours. There is Kagoro complex and parts of Jos, Bukuru, Barkin-Ladi and Ganawuri complexes outcropping in the study area. Their evolution and those in the province follow the same pattern. They began with volcanic phase that was associated with eruption of large volume of rhyolites via ring fractures, and then followed by formation of ring dykes of granite-porphyry upon subsidence of the rocks interior to the ring fracture.

4.2.2 Colour Composites

The composites were generated for the purpose of enhancing spectral signatures of the image for the study area thus, enhancing the observation of the different patterns which can be attributed to the different stratigraphic units existing in the study area thus, aiding the interpretation of their features.

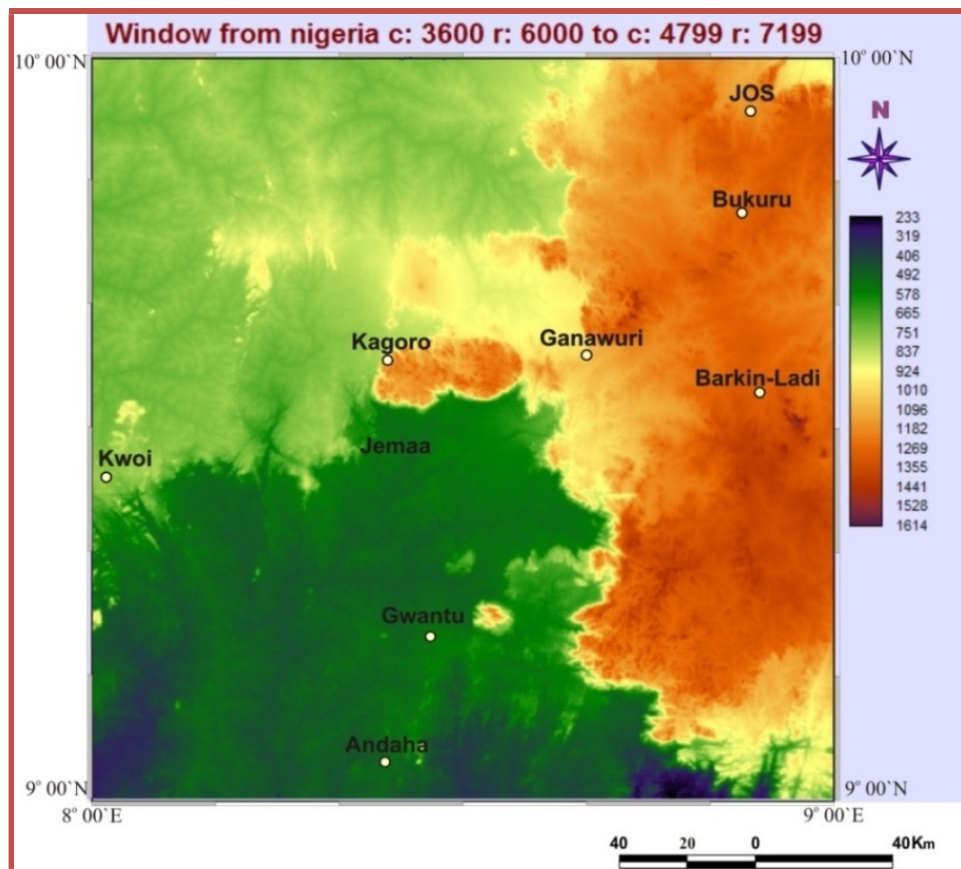


Figure 4.30. Digital Elevation Model (DEM) Map

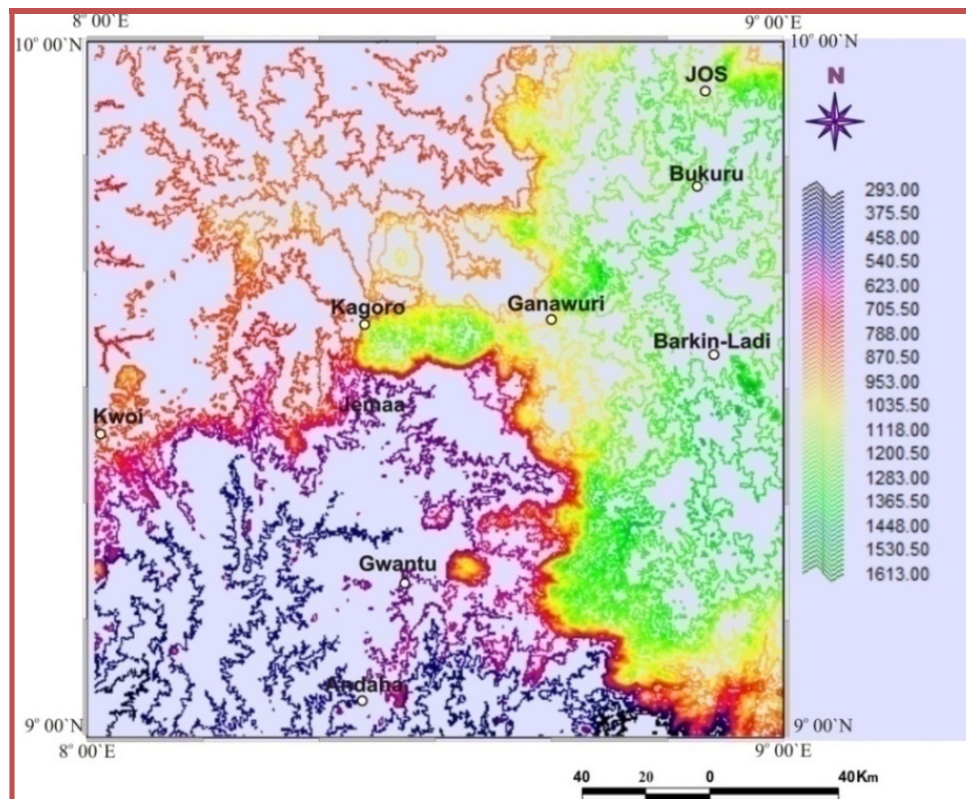


Figure 4.31 : Contour Map of the study area.

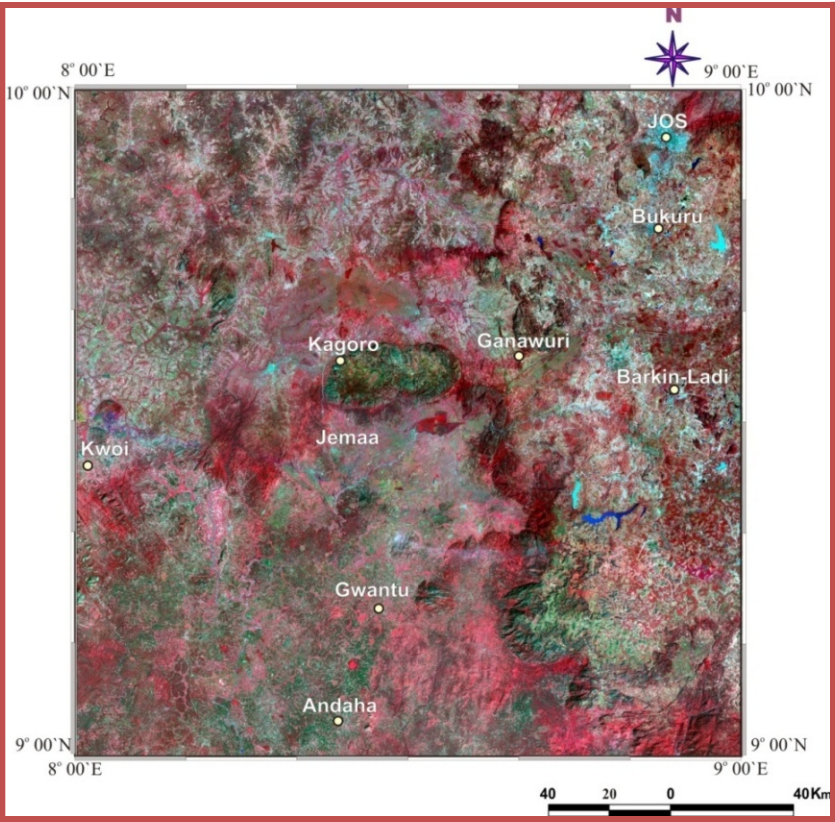


Figure 4.32. Colour Composite Map RGB 432

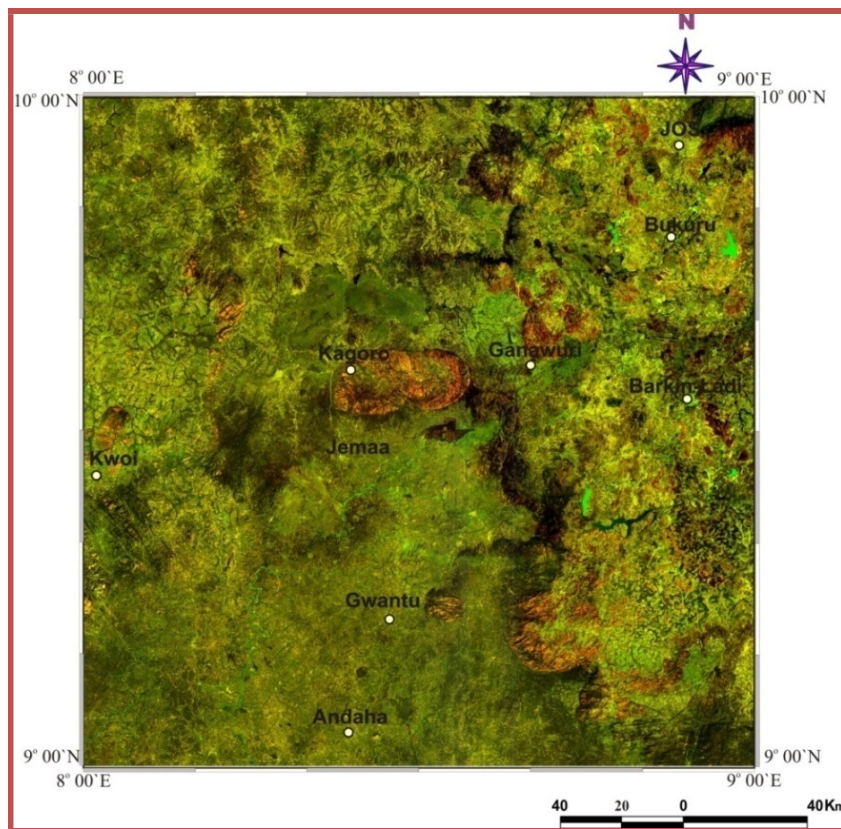


Figure 4.33: Colour Composite Map RGB 731

Table 4.3: Appearance of features in the generated colour composite maps

FEATURES	TRUE COLOUR	FALSE COLOUR	SWIR (GEOCOVER)
	Red: Band 7	Red: Band 4	Red: Band 7
	Green: Band 3	Green: Band 3	Green: Band 5
	Blue: Band 1	Blue: Band 2	Blue: Band 2
Trees	Olive Green	Red	Shades of green
Bushes			
Crops	Medium to light Green	Pink to red	Shades of green
Wetland vegetation	Dark green to black	Dark red	Shades of green
Urban areas	White to light blue	Blue to gray	Lavender
Water	Shades of blue & green	Shades of blue	Black to dark blue

Bare soil	White to light gray	Blue to gray	Magenta, lavender, pale pink.
-----------	---------------------	--------------	----------------------------------

4.2.3 **Normalized Difference Vegetation Index (NDVI)**

Ratio images are often useful for discriminating subtle differences in spectral variations, in a scene that is masked by brightness variations. Different band ratios are possible given the number of spectral bands of the satellite image. The utility of any given spectral ratio, depends upon the particular reflectance characteristics of the features involved and the application at hand. The Normalized Difference Vegetation Index (NDVI) is an index of plant “greenness” or photosynthetic activity. It is one of the most commonly used vegetation indices. Vegetation indices are based on the observation that different surfaces reflect different types of light differently. Photosynthetically active vegetation, in particular, absorbs most of the red light that hits it while reflecting much of the near infrared light.

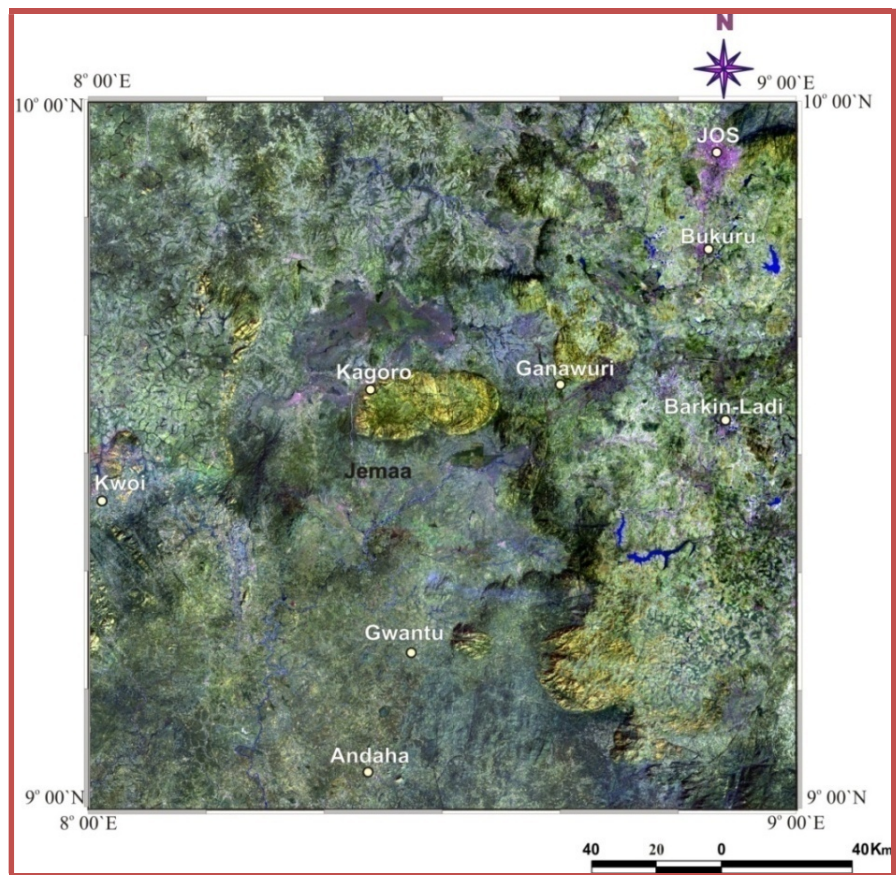


Figure. 4.34: Colour Composite Map RGB 752

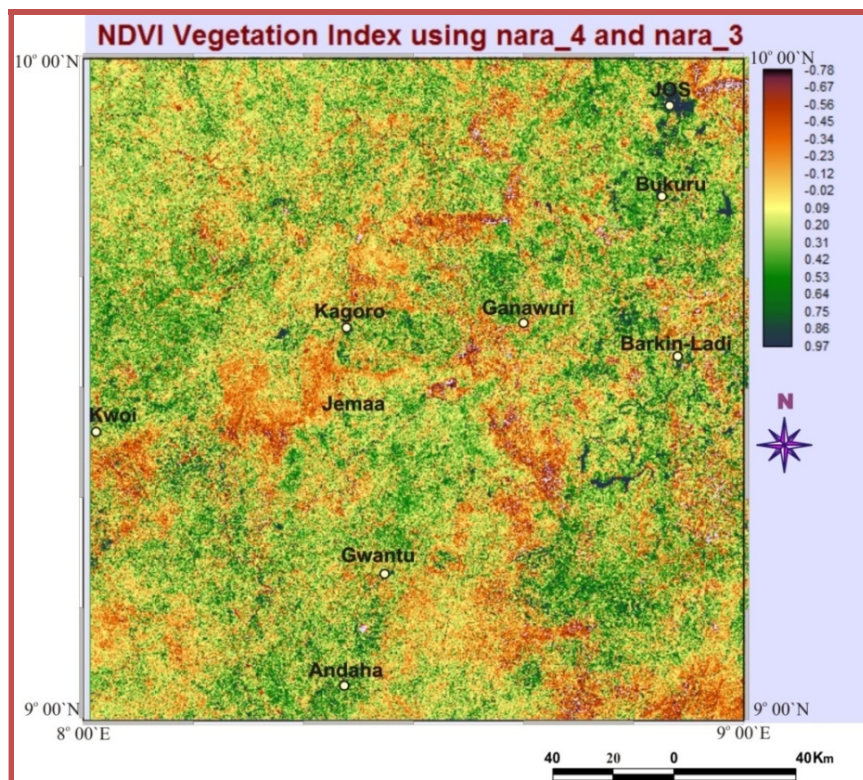


Figure 4.35: Normalized Difference Vegetation Index (NDVI) Map

Vegetation that is dead or stressed reflects more red light and less near infrared light. Likewise, non-vegetated surfaces have a much more even reflectance across the light spectrum. By taking the ratio of red and near infrared bands from a remotely-sensed image, an index of vegetation “greenness” can be defined.. NDVI is calculated on a per-pixel basis as the normalized difference between the red and near infrared bands from an image:

$$\text{NDVI} = \frac{\text{Ninfrared} - \text{RED}}{\text{Ninfrared} + \text{RED}} \quad 4.3$$

Where Ninfrared is the near infrared band value for a cell, RED is the red band value for the cell and NDVI can be calculated for any image that has a red and a near infrared band.

The output of NDVI (figure 4.35) is a measure of vegetation richness of an area. Values of NDVI can range from -1.0 to +1.0, but values less than zero typically do not have any ecological meaning, so the range of the index is truncated to 0.0 to +1.0. Higher values signify a larger difference between the red and near infrared radiation recorded by the sensor - a condition associated with highly photosynthetically-active vegetation. Low NDVI values means there is little difference between the red and Ninfrared signals. This happens when there is little photosynthetic activity, or when there is just very little Ninfrared light reflectance (i.e., water reflects very little Ninfrared light).

The NDIV map of the study area was generated to delineate zones of vegetation and bare rocks. Dark red areas (-0.34 to -0.78) corresponds to bare rock zones, light red areas (-0.12 to -0.34) corresponds to soil with little vegetation, yellow (0.20 to -0.12) to sparsely vegetated areas and green (0.97 to 0.20) to thick vegetation.

From the NDVI (Fig. 4.35) of the study area, it was discovered that areas with dominance of exposed rock are the western part of Jemaa, northeast part of Jos and North of Kagoro. Kagoro, southeast of Jemaa and the north-eastern part of the study area are sparsely vegetated. Bukuru, Andaha and Jos areas are densely vegetated. Interpretation is based on

the colour and pattern of features. This image will help in adequate planning of traverses for fieldwork.

4.2.4 Lineament Analysis

Lineaments are linear features in a landscape that expresses the underlying geological structure. Typically a lineament will comprise a fault aligned valley, a series of fault or fold-aligned hills, a straight coastline or indeed a combination of these features. Fracture zones, shear zones and igneous intrusions such as dykes can also give rise to lineaments.

Linear features shown on remote sensing imagery of increasingly smaller scale (greater extent) reflect increasingly more fundamental studies; their study often provide insights not only to the location of the mineral deposits, but also to metallogenic theories as well (O' Leary *et al*, 1976).

In addition, several studies have emphasized the importance of lineament interpretations and digital analysis in localizing the major mineral deposits and reveals that there is a strong correlation between mineral deposits and lineaments (Ananaba, 1991; O' Leary *et al*, 1976). Since one of the objectives of this study is to identify structures expressed as lineaments and classify them according to their spatial and directional attributes, it was necessary to process the Landsat Thematic Mapper data in a manner that would both enhance trends and facilitate the computation of locations and depths. In extracting lineaments from the Landsat data, only linear features equal to or greater than 1km in length were considered. The longer lineaments have the greatest potential of being more fully developed and of penetrating greater depths.

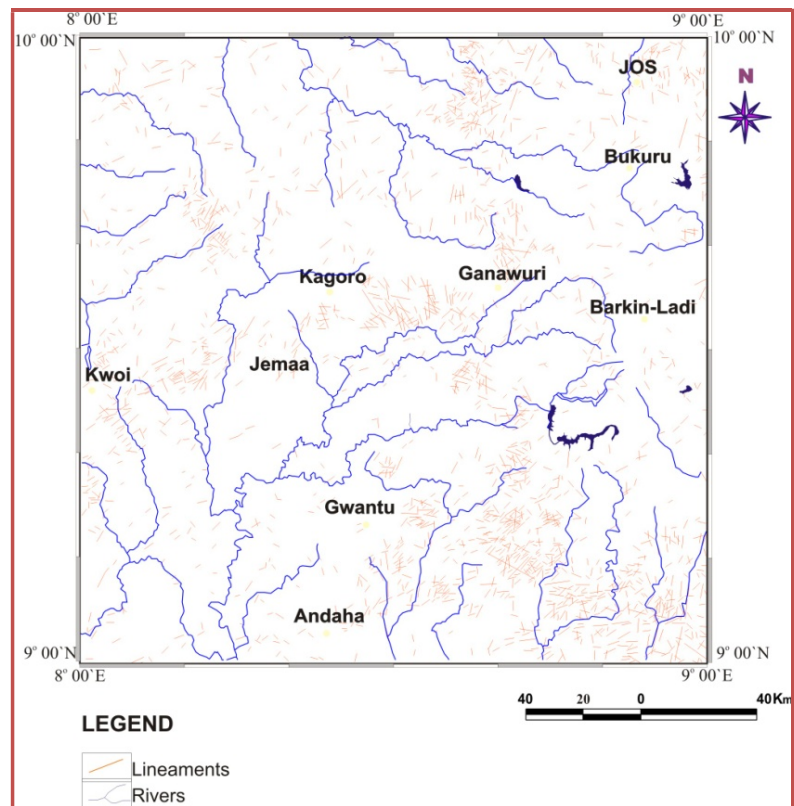


Figure 4.36.: Interpreted Lineament of the Study Area

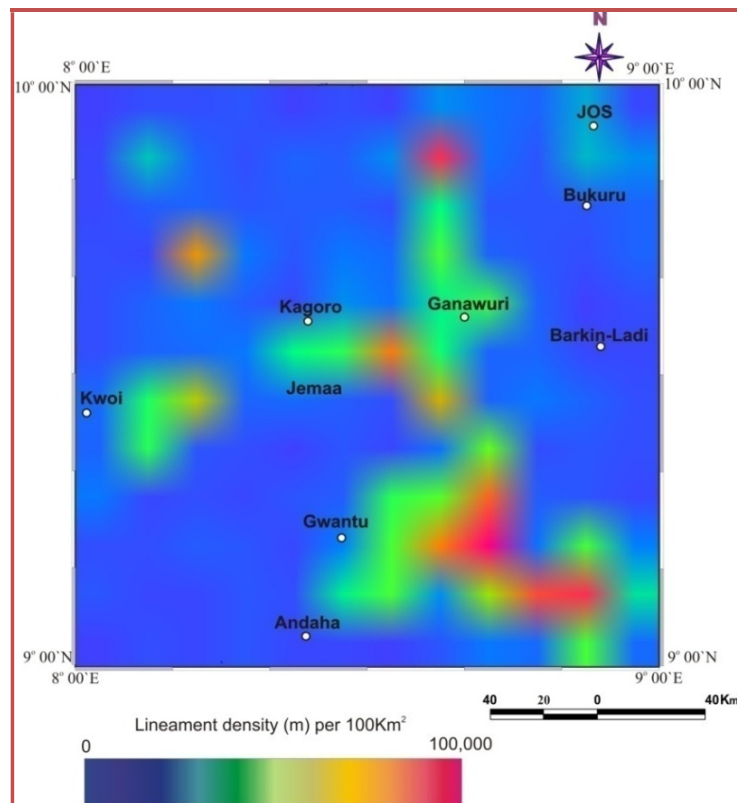


Figure 4.37 : Lineament Density Map

The lineaments extracted from landsat imagery revealed four groups of linear features in the NE-SW, NW-SE, N-S and E-W with the dominant region been the NE-SW direction. Umeji (1988), recognized the Pan African orogeny as characterized by NNW-SSE to NNE-SSW trending structures with varied amount of intrusive while the lower Cretaceous are of Nigeria are characterized by NE-SW oriented shear zones and fractures controlled by volcanism.

The interpreted lineaments of the study area are presented as a lineament map and lineament density map respectively (figs 4.36 & 4.37). The study area revealed that several lineament traces were observed where basement outcrops are closer to the surface. The lineament trends corresponded to the positions and directions of the paleo-tectonic fracture zones of the study area which includes St Pauls's and Romanche Fracture Zones. The NDVI reveals vegetation around 1km east of Kagoro, which could be of hydrographic origin. Lineaments having longer lateral extension revealed trends in the NE-SW, which indicates the direction of the last regional tectonic phase. The lineament density were observed to be very high around Ganawuri, Jos and within 10km of Gwantu and Andaha. The high lineament densities in these areas suggest that the areas are strongly deformed mainly as a result of basement uplift. There is marked correlation of the features/locations of areas of high lineament densities with the known locations of the Younger Granites ring complexes. A marked relationship between lineaments and mineralization was also established in the study area.

The lineament density map (Fig. 4.37) shows the spatial distribution of the density of lineaments in the study area. High lineament densities were also observed in areas where the basement rocks outcrop or are close to the surface. The relationship between lineament densities and Younger granites occurrences in the study area is an indication of tectonic control probably associated with paleo-tectonic stresses. This correlation is an indication

that the emplacement of the Younger granite ring complexes may be associated with epeirogenic uplift (Obaje, 2009). The epeirogenic uplift is believed to result from the intrusion of large masses of basic magmatic materials into the lower part of the continental crust in the area (Obaje, 2009).

Lineament quantification and statistical analysis were carried out with particular reference to the orientation frequency of the lineaments. This was done in order to construct a rose diagram with established structural trends (Figure 4.38). Rose diagrams were plotted from visually extracted lineaments with the lengths of the rosette blades proportional to the square of the relative frequencies of the lineaments. The rose diagram revealed lineaments with trend directions of NE – SW, NW – SE, N – S and E – W with the dominant structural trend being in the NE – SW which corresponds to the major lineament trend of the study area. The E-W, NW-SE, and N-S, reflect the old and deeper tectonic trends. However, the NE-SW trend reflects the younger tectonic events, because the younger events are more pronounced and tends to obliterate the older events.

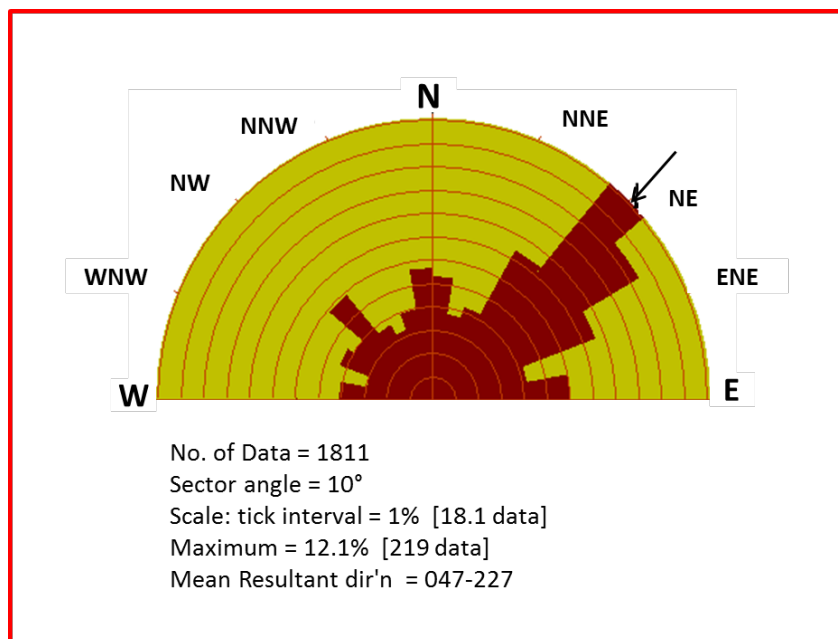


Figure 4.38: Lineament Rose Diagram

4.2.5 Image Classification Analysis

The image generated from the unsupervised classification to a large extent gives a fair knowledge of the various geologic units in the study area. In unsupervised classification, the classification is tied around tonal differences of the pattern seen. In the study area, four tonal features were observed. This classification becomes necessary when ground trotting was not done to ascertain the geology of the area. Looking at the image (Fig. 4.39), red and purple colours are observed in bare rock areas like northeast part of Jos and south-eastern part of the map. Other areas where this mixture of blue and green are observed include Jemaa, Gwantu, Kwoi and Bukuru. The red and purple areas indicate bare rock regions while the green and blue coloured areas indicate vegetation regions.

4.2.6. Generation of New Geologic Map

Extracted information from image classification, generated composites and DEM were employed in the generation of the new GIS-based map. This involves tracing of boundaries of the various patterns that are believed to represent geologic units; from the images especially the colour composites, the DEM and unclassified image. The tracing was done using the DIGITIZE module of IDRIS32.

Comparison of the two maps show that striking resemblance exists between various pattern identified on the updated map and the pre-existing map. But careful observation of the updated map reveals that the Andoha area which is characterized in the old map as Tertiary to Recent Volcanics is observed to be Migmatitic Schists in the New Map. Also part of the Barkin-Ladi area which is characterized as Tertiary to Recent Volcanics in the old map is seen to be Younger Granites in the new map. The top left of the map which has outcrops of Older Granites in the old map is seen to be plain of Migmatitic schists in the new map. It can be seen that the boundary patterns of the updated map and the pre-existing map differ considerably. The boundaries in the updated map generated from a combination

of information, derived from satellite remotely sensed data seems to be more representative of the relationship between the various formations.

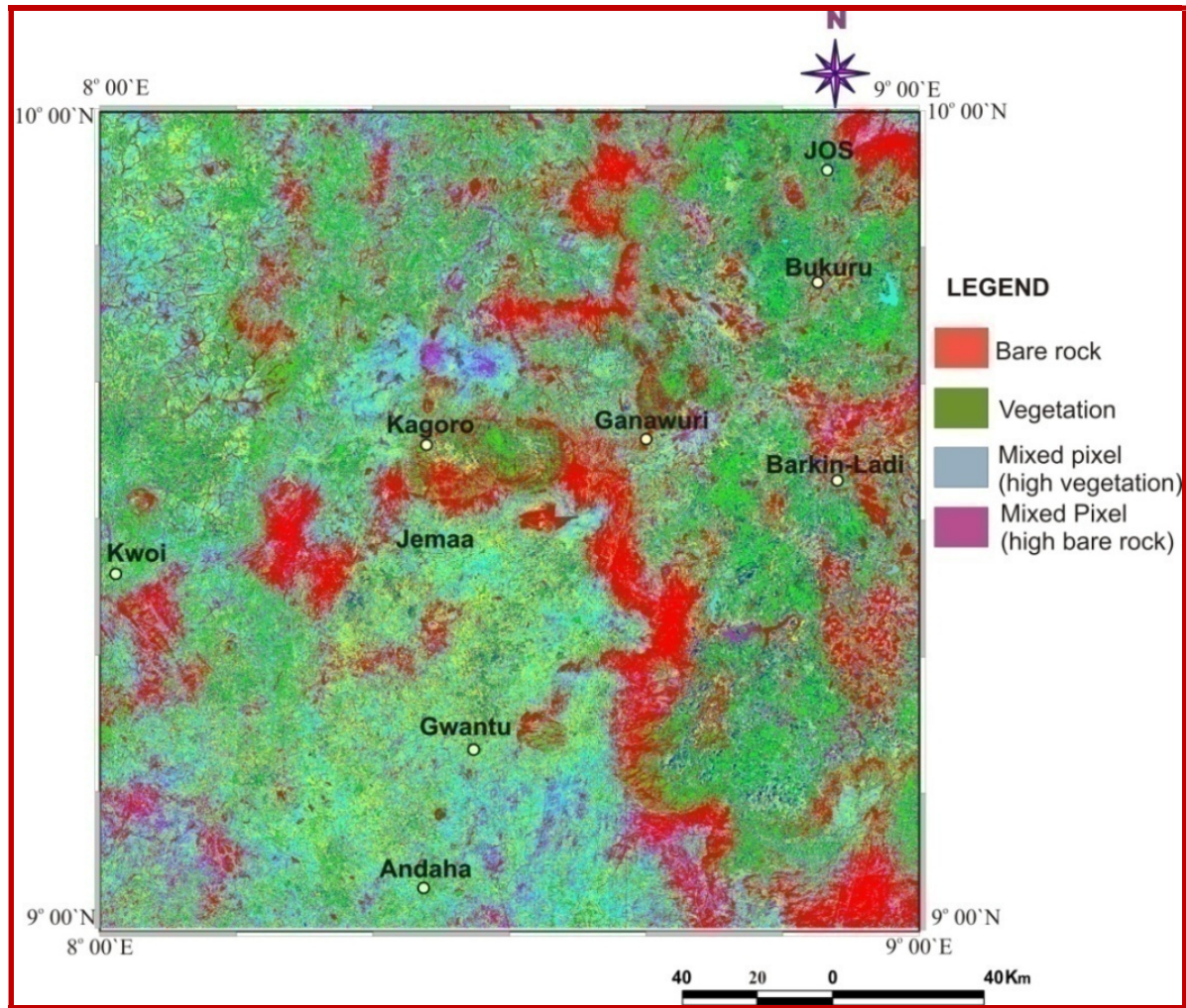
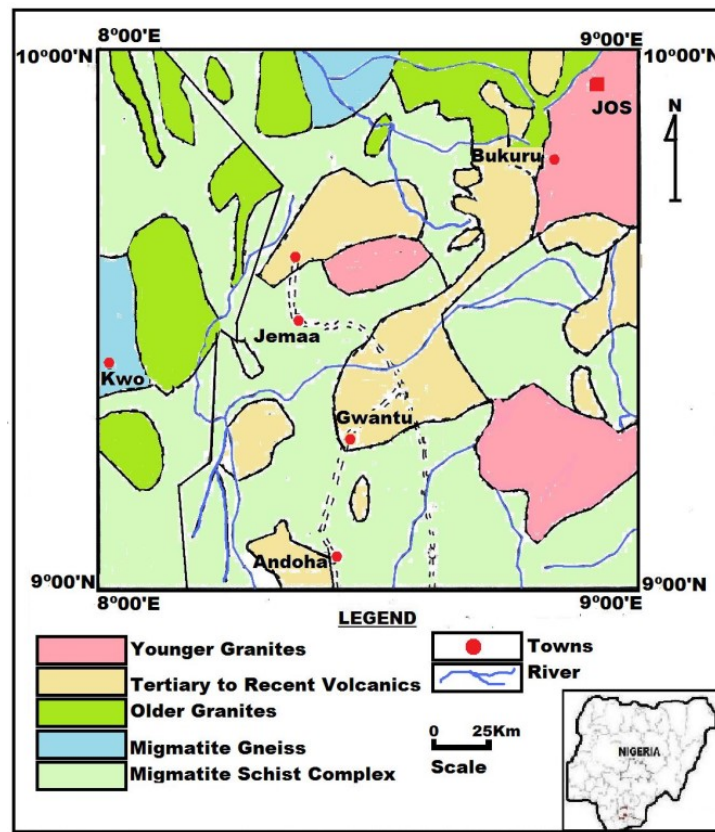


Figure 4.39. Unsupervised Classification Image

(a) OLD MAP



(b) NEW MAP

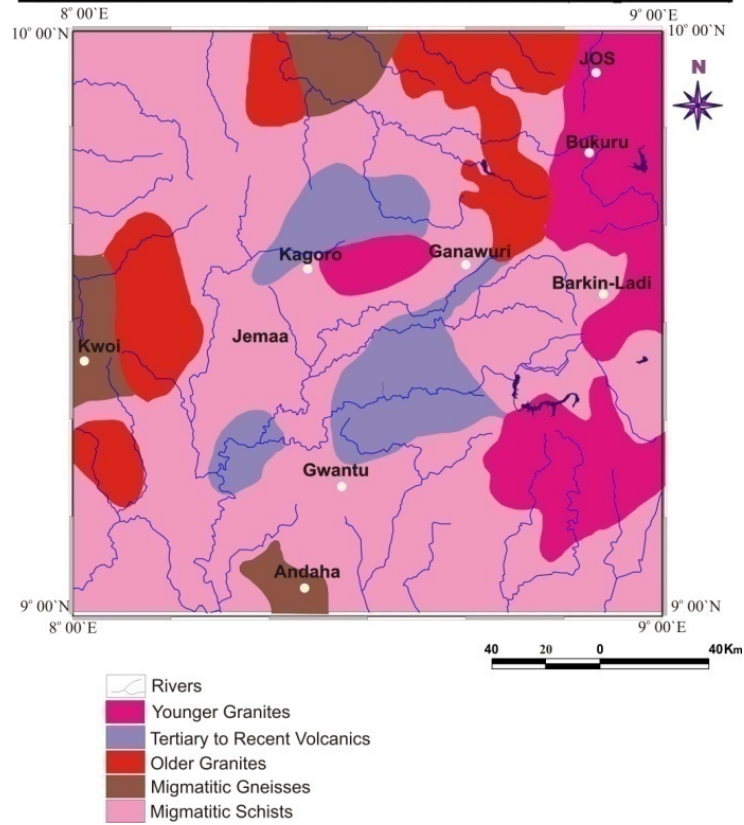


Figure 4.40 : Comparison of the Old and New Maps.

CHAPTER FIVE

CONCLUSION AND RECOMMENDATION

5.1 CONCLUSION

Qualitative interpretation of the lineament trends of the study area revealed that N-S, NE-SW and NW-SE are well developed principal structural trends both on the crystalline basement complex as well as the cretaceous and younger sediments. This finding is in agreement with previous work suggesting that Nigeria has a complex network of fractures and lineaments with dominant trend directions of NE-SW, NW-SE, and N-S directions. (Ananaba, et al 1987;). The structural trends were found to be controlled by structures in the underlying Precambrian rocks of the Basement complex. The depth to basement or deeper magnetic sources d_2 varies between 0.3569km and 3.2600km with the average depth of 1.7723 km. The variation or inhomogeneity in the basement composition is due to the structural and topographic relief of the basement surface, lateral variation in the susceptibilities and intra-basement features; faults and fractures. The d_2 values therefore represent the average sedimentary thickness in the study area. Generally, the Euler deconvolution suggests a depth to the magnetic source of between 0.2500 km to a little above 2.500 km. Comparing the two depth estimates the sedimentary thickness in the area therefore ranges from 0.250km to 2.5km. This result is in agreement with results of earlier studies (Obaje, 2009).

The Curie point depth in conjunction with heat flow values revealed a distinct inverse relationship. The result showed that heat flow increases with decrease in Curie point depth, and vice-versa. The curie depth ranges from 23.8831km to 27.5242Km. In most part of the study area, heat flows were found to be less than 60 mWm⁻². The average heat flow obtained

in the study area is 56.06mWm^{-2} , a value which may be considered as typical of the continental crust.

The calculated geothermal gradient in the study area varies between 91.6 and $882.8^{\circ}\text{Ckm}^{-1}$ with an average of $284.1^{\circ}\text{Ckm}^{-1}$. The heat flow is significantly high in the South-Eastern area which corresponds with the area of shallow curie depth. Such heat flow values are suggestive of anomalous geothermal conditions and are recommended for detailed geothermal exploration.

The trend surface analysis of the tectonic and structural features of the area in relation to the interpreted lineaments revealed trend directions of NE – SW, NW – SE, N–S and E – W directions with the dominant structural trend being in the NE – SW direction. The E-W, NW-SE, and N-S directions reflect the old and deeper tectonic episodes while the NE-SW trend reflects the younger tectonic events. This is because the younger events are more pronounced and seem to have obliterated the older events. Similarly, high lineament frequencies were observed in areas where basement rocks outcrop or are closer to the surface (i.e. area with thin overburden) whereas low lineament frequencies are characteristics of areas with deeply buried basement rocks. The correlation of high lineament density areas with the locations of the Younger Granites is an indication that primary mineralization in the area may be tectonically controlled (Nwokocha et al.,2016). Primary ore bodies in Nigeria are probably oriented following lineament trends (Ananaba, 1991). Similarly, many of the lineaments coincided with drainage lines indicating that the drainage in the study area may be structurally controlled (Samaila and Solomon, 2011). However, the absence of visible fractures and lineaments in parts of the study area may not be indicative of complete absence of linear structures.

5.2 RECOMMENDATION

Based on the success of this research, it is of utmost important to recommend the following:

- i. LANDSAT / Satellite imagery and gravity survey should be employed to investigate the regional geology of the area.
- ii. Areas of higher magnetic intensities may face some health hazards from the heavy element concentrations on the water table. Thus proper water analysis should run to produce portable water.
- iii. Also because of the high magnetic values and relatively small thickness around Kafanchan, Gwantu and Randa, more detailed mineral investigation should be carried on such areas.
- iv. Finally, the high heat flow observed especially in the South-Eastern area which corresponds with the area of shallow curie depth suggests of anomalous geothermal conditions and is recommended for detailed geothermal exploration.

5.3 CONTRIBUTION TO KNOWLEDGE

The following are considered as contribution to knowledge in this research

- i. Presence of high lineament density in the areas coinciding with the locations of the Younger Granite complexes has been established, which shows that the primary mineralization in the area is tectonically controlled.
- ii. The New Map has been derived from satellite remotely sensed data which reveals that the Andoha and Barkin-Ladi area which were characterized in the old map as Tertiary to Recent Volcanics are actually Migmatic Schists and Younger Granites respectively. The top left of the old map which has outcrops of Older Granites in found to be plain of Migmatic schists in the new map.

REFERENCES

- Aina, A. and Olarewaju, V.O., (1992). Geological Interpretation of Aeromagnetic Data in Some Part of Northcentral Nigeria. *Journal of African Earth Sciences*, **14**, 103-109.
- Ajakaiye, D.E., (1989). A Gravity Survey over the Nigerian Younger Granite Province. In: C. A. Kogbe, Ed., *Geology of Nigeria*, 2nd Edition, Elizabethan Publ. Co., Lagos, 227-244.
- Akanbi, E.S., Ugodulunwa, F.X.O. and Gyang, B.N., (2012). Mapping Potential Cassiterite Deposits of Naraguta Area, North Central, Nigeria using Geophysics and Geographic Information System (GIS). *Journal of Natural Sciences Research*. Vol.2, (8),
- Alkali, S. C. and Yusuf, S. N., (2010). Gravity study over Jos – Bukuru younger granite complex, North Central Nigeria. *Scholars Research Library, Archives of Physics Research*, 1(4), pp. 178 – 191.
- Alkali S. C. and Gaiya S. (2011). Delineation of Linear Structures From Digitized Aeromagnetic Data of the Western Part of the Younger Granite Complex of North Central Nigeria. *New York Science Journal*. Pp 97 – 111.
- Alkali S. C. and Hassan M. (2014). Magnetic Study of Kagoro and Environs, North Central Nigeria. *Journal of Applied Geology and Geophysics*. Pp 35-43.
- Ananaba, S.E. and Ajakaiye, D.E., (1987). Evidence of tectonic control of mineralization of Nigeria from lineament density analysis: A Landsat study; *Int. Jour. Rem. Sensing*; vol.1, (10), pp. 1445-1453.
- Ananaba, S.E., (1991). Dam sites and crustal mega-lineaments in Nigeria. *ITC Journal* Vol. 1, pp. 26-29
- Bath, M. (1974). *Spectral Analysis in Geophysics*, Elsevier Scientific Publishing company Amsterdam
- Bhattacharyya, B. K. (1965). Two-dimensional harmonic analysis as a tool for magnetic interpretation, *Geophysics* Vol. 30: pp. 829-857

- Bhattacharyya, B. K. (1966). Continuous Spectrum of the total magnetic Field Anomaly due Rectangular Prismatic body. *Geophysics* 31, pp. 97-121.
- Bhattacharyya, B.K. and L.K. Leu., 1975. Spectral analysis of gravity and magnetic anomalies due two dimensional structures, *Geophysics*, Vol. 40, pp. 993-1031.
- Blakely, R.J., (1995). *Potential theory in gravity and magnetic applications*: Cambridge Univ. Press.
- Bowden, P., Breemen, V. O., Hutchinson, J., and Turner, D. C., (1971). Palaeozoic and mesozoic age trends for some ring complexes in Niger and Nigeria. *Nature* 259, pp. 297 – 299.
- Bowden, P, and Kinnaird, J.A., (1984). Geology and mineralization of the Nigerian anorogenic ring complexes. *Geologisches Jahrb (Hannover)* B56, pp.3–65
- Burke, K. (1969). Seismic Areas of the Guinea Coast where Atlantic Fracture Zones Reach Africa. *Nature*. 222 pp 655-657.
- Bulter, R.F. (1992). *Paleomagnetism*. University of Arizona.
- Campbell, J. B. (2007). *Introduction to Remote Sensing*, 4th ed. New York: Guilford Press.
- Colwell, R. N. (1997). History and place of photographic interpretation. In *Manual of Photographic Interpretation*, 2nd ed., edited by W. R. Philipson. Bethesda, MD: American Association of Photogrammetry and Remote Sensing.
- Dobrin, M. B. (1983). *Introduction of Geophysical Prospecting*. McGraw-Hill Book Co.; Tokyo, Japan.
- Dobrin, M. and Savit, C. (1988). *Introduction to Geophysical Prospecting*, McGraw Hill, 4th edn.
- Geological Survey of Nigeria (NGSA). (2011).
- Grant, N. K. (1971). South Atlantic, Benue Trough and Gulf of Guinea Cretaceous Triple Junction. *Geol. Soc. Amer., Bull* 82, pp 2295 – 2298.

- Gunn, P. J., and Dentith, M. C. (1997). Magnetic Responses Associated with Mineral Deposits. AGSO J. Geol. Geophys. Vol. 17. pp. 145-155
- Hahn, A., Kind, E. G. and Mishra, D. C. (1976). Depth estimation of Magnetic sources by means of Fourier amplitude spectra, Geophysical. Prospecting, 24, 287-308.
- Hudson, M. R., Mikolas, M., Geissman, J. W., and Allen, B. (1999). Paleomagnetic and rock magnetic properties of Santa Fe group sediments in the 98th Street core hole and correlative surface exposures, Albuquerque Basin, New Mexico: New Mexico Geological Society, 50th Field Conference, Guidebook, pp. 355-362.
- Jensen, J. R. (2005). Introductory Digital Image Processing: A Remote Sensing Perspective, 3rd ed. Upper Saddle River, NJ: Prentice-Hall.
- Jacobson, R. R. E., MacLeod, W. N. And Black, R. (1958). Ring Complexes in the Younger Granite Province of Northern Nigeria. Geological Society of London, Mem. 1, pp.72.
- Kangoko, R., Ojo, S.B. and Umego, M.N., (1997). Estimation of Basement depths in the Middle Cross River basin by Spectral analysis of the Aeromagnetic field. Nig. Journ. of Phys. Vol. 9, pp.30-36.
- Lawal, T. O., Lukman A.S. Nwankwo L.I. and Abiodun S.M., (2012). Interpretation of Aeromagnetic Data Over the Younger Granite Complex of Northern Nigeria. International Journal of Advancement in Physics. Vol 4, No 1.
- Le Pichon, X and Hayes, D. E. (1974): Marginal Offset Fractures Zones and the Early Opening of the South Atlantic. Journal of Geophysical Research, 76, pp. 6283 – 6293.
- Lillesand, M. T., Kiefer, R. W., & Chipman, J. W. (2008). Remote sensing and image interpretation (6th ed.). Hoboken, NJ: Wiley.
- Lo, C.P., Albert K.W. Yeung. (2002). Concepts and Techniques of Geographic Information Systems. New Jersey: Prentice-Hall, Inc. pp. 212-216.
- MacLeod, W, N., Turner, D. C. and Wright, E. P., (1965): The Geology of the Jos Plateau. Vol. 1; General Geology. Geological Survey of Nigeria. Bull. No. 32, pp. 118.

- Mekonnen, T. K. (2004). Interpretation and Geodatabase of Dukes using Aeromagnetic data of Zimbabwe and Mozambique. M. Sc. Thesis, International Institute for Geoinformation science and Earth Observation, Enschede, the Netherlands.
- Neville, R. A., Levesque, J., and Staene, K. (2003). Spectral unmixing of hyperspectral imagery for mineral exploration: Comparison of results from SFSI and AVinfraredIS. *Canadian Journal of Remote Sensing* 29, pp. 99–110.
- Nwokocha, K. C., Opara A. I., Onyekuru, S. O., Okereke, C. N., Emberga, T. T., Ugwuegbu, E. I., Ijeomah, K. C., (2016). Linear Features interpreted Over Parts of the Younger Granite Complex, North Central Nigeria Using HRAM and LANDSAT –ETM Data. *Arabian journal of earth sciences*. Vol. 3, pp. 35-56.
- O’Leary, D.W., Friedman, J.D., and Phn, H.A. (1976). Lineament, Linear, Lineation: Some proposed new standard for old terms. *Geol. Soc.Amer. Bull.*, Vol. 87 pp. 1463-1469.
- Onyedim, G. C., Awoyemi, M. O., Ariyibi, E. A. and Arubayi, J. B. (2006). Aeromagnetic imaging of the basement morphology in part of the Middle Benue Trough, Nigeria, *Journal of Mining And Geology*, vol.42 (2), pp.157-163.
- Opara, A. I. Onyewuchi, R.A. Selemono, A. O. Onyekuru, S. O. & Ubechu, B. O., (2014). Structural and tectonic features of Ugep and environs, Calabar flank, Southeastern Nigeria; evidences from Aeromagnetic and Landsat-ETM data.
- Opara, A.I., (2011). Estimation of the Depth to Magnetic Basement in Part of the Dahomey Basin, Southwestern Nigeria. *Australian Journal of Basic and Applied Sciences*, Vol. 5(9), pp. 335-343.
- Opara, A.I., Udoete, R.L., Nwokocha, K.C., (2015). Structural interpretation of the Jos-Bukuru Younger Granite ring complexes inferred from landsat-TM data. *Journal of Geosciences and Geomatics*, Vol. 3(3), pp. 56-67.

- Opara, A. I., Emberga, T.T., (2015). Magnetic basement depth re-evaluation of Naraguta and environs North Central Nigeria, using 3-D Euler Deconvolution.
- Oyawoye, M.O., (1964). The geology of the Nigerian basement complex. J. Niger. Min. Geol. Metall. Soc., 1(2): pp. 87-103.
- Oyawoye, M.O., (1972). The Basement Complex of Nigeria. In: Dessauwagie, T.F.J. and A.J. Whiteman, (Eds.), Africa Geology, University of Ibadan, pp: 67-99.
- Parasnis, D. S. (1997). Principles of Applied Geophysics (5e). pp. 429
- Price, K. P., Guo, X., and Stiles, J. M. (2002). Optimal Landsat TM band combinations and vegetation indices for discrimination of six grassland types in eastern Kansas. International Journal of Remote Sensing 23, pp. 5031–5042.
- Rahaman, A. M, Breeman, V. O., Benner, J. N., and Bowden, P. (1984). Age migration of anarogenic ring complexes in Northern Nigeria. Journal Geological, 92, pp. 173 – 184.
- Raimi, J., Dewu, B. B. M. and Sule, P., (2013). An Interpretation of Structures from the Aeromagnetic field over a Region in the Nigerian Younger Granite Province. International Journal of Geosciences. pp. 313-323.
- Rashed, T., Weeks, J. R., Gadalla, M. S., and Hill, A. G. (2001). Revealing the anatomy of cities through spectral mixture analysis of multispectral satellite imagery: A case study of the greater Cairo region, Egypt. Geocarto International 16, pp. 5–15.
- Reeves, C. (2005). Aeromagnetic Survey: Principles, Practice and Interpretation
- Reid, A. B. (1990). Magnetic interpretation in three dimensions using Euler deconvolution, Geophysics, 55, pp. 80.
- Reyment, R.A. (1965). Aspects of Geology of Nigeria, Ibadan University Press, Ibadan Nigeria.106

- Reynolds, R. L., Rosenbaum, J. G., Hudson, M. R., and Fishman, N. S. (1990). Rock magnetism, the distribution of magnetic minerals in the Earth's crust, and aeromagnetic anomalies: U. S. Geological Survey Bulletin 1924, pp. 24-45
- Rothery, D. A. (1987). Improved discrimination of rock units using LANDSAT Thematic Mapper Imagery of the Oman ophiolite. *Journal. Of the Geological. Society.* 144, pp. 587-597.
- Rowan, L. C., and Kahle, A. B, (1982). Evaluations of 0.46-2.36 micrometer. Multi-spectral scanners images of the East Tintic mining district , Utah, for mapping hydro-thermally altered rocks. *Economic Geology*, 77, pp. 441-452.
- Reid, B., Allsop, J.M., Granser, H. Millet, A.J., and Somerton., I. W., (1990). Magnetic interpretation in three dimensions using Euler deconvolution., *Geophysics.* Vol. 55, No. I; P. pp. 80-91.
- Shaw, S. H.; (1951) Report on Magnetic and Resistivity Work in the Plateau Tinfield. Oversea Geological Survey Report, London.
- Spector, A. and Grant, F.S., (1970). Statistical models for interpreting aeromagnetic data. *Geophysics*, Vol.35, pp.293-302.
- Sykes, L. R.; (1978). Intraplate Seismicity, reactivation of Preexisting Zones of Weakness, Alkaline Magmatism and other Tectonism Posdating Continental Fragmentation. *Reviews of Geophysics and Space Physics*, 16(4).
- Tanaka, A., Okubo, Y., Matsubayashi, O., (1999). Curie point depth based on spectrum analysis of the magnetic anomaly data in East and Southeast Asia. *Tectonophysics* 306: pp.461-470.
- Telford, W. M., Geldart, L.P. and Sheriff, R.E. (1998). *Applied Geophysics*, (2nd Ed), Cambridge University Press, USA, pp. 113 – 114.
- Thompson, D. T. (1982). EULDPH: A new technique for making computer-assisted depth estimates from magnetic data, *Geophysics*, 47, pp. 31-37.

- Turner, D. C.; (1989): Structure and Petrology of the Younger Granite Ring Complexes. In Geology of Nigeria, Kogbe, C. A (ed), Rock View International, France, pp 175 – 190.
- Turner, D.C., (1972). Structural and Tectonic Setting of the Younger Granite Ring Complexes of Nigeria and Southern Niger. Part I: Ring Complexes and Their Component Units. Savana I, pp. 223-236.
- Van Breeman, O. and Bowden, P., (1973): Sequential Age Trend for some Nigerian Mesozoic Granites, Nature Physical Sciences, 242, pp 9 – 11.
- Whitehead, N. and Musselman, C. (2008). montaj Grav/Mag Interpretation: Processing, Analysis and Visualization System for 3D Inversion of Potential Field Data for Oasis montaj v6.3, Geosoft Incorporated, 85 Richmond St. W., Toronto, Ontario, M5H 2C9, Canada.



Interpretation of aeromagnetic and landsat-etm⁺ data over part of the younger granite complex, Nigeria: Implication for geothermal exploration. By Nwokocha, K .C. is licensed under a [Creative Commons Attribution-NonCommercial-NoDerivatives 4.0 International License](https://creativecommons.org/licenses/by-nc-nd/4.0/).